INVESTIGATION ON HOW DAYLIGHT SIMULATION SHOULD BE USED TO CHARACTERIZE DAYLIGHT-RELATED ISSUES FOR BUILDINGS IN HONG KONG

WANG JUN

PhD

The Hong Kong Polytechnic University

2021

The Hong Kong Polytechnic University
Department of Building Services Engineering

Investigation on How Daylight Simulation Should Be Used to Characterize Daylight-related Issues for Buildings in Hong Kong

WANG Jun

A thesis submitted in partial fulfilment of the requirements for the degree of Doctor of Philosophy

September 2020

CERTIFICATE OF ORIGINALITY

I hereby declare that this thesis is my own work and that, to the best of my knowledge and belief, it reproduces no material previously published or written, nor material that has been accepted for the award of any other degree or diploma, except where due acknowledgement has been made in the text.

_____(Signed)

____WANG Jun____(Name of student)

Abstract

Given the popularity of climate-based daylight modelling (CBDM) that derives various photometric quantities using space geometries and typical meteorological year (TMY) data in recent years, great efforts have been made to characterize daylight quantity and quality in different building environments. Though most of buildings in Hong Kong are expected to have sufficient daylight due to its geographical location, serious problems, such as low energy efficiency of electric lighting systems and occupants' low satisfaction with indoor and outdoor luminous environments, still exist. In this dissertation, three studies related to CBDM calculations were conducted, aiming to characterize the daylight-related issues for the buildings in Hong Kong.

The first study was carried out to quantify the difference between predicted and actual daylight quantity and quality and the performance of a closed-loop daylight-responsive dimming system in a real classroom. The predictions were made using the TMY data, while the actual performance was characterized using a real weather data. It was found that the daylight illuminance levels derived using the actual weather data were around 30% higher than those derived using the TMY data. The system was suggested to perform the calibration at the time that had similar weather conditions as the selected calibration hours in the TMY data. Otherwise, the system achieved lower energy savings and had a more frequent occurrence of over-dimming conditions, with the differences being as high as 15% and 86% respectively. A supplementary study was conducted to investigate the effect of a prismatic film on the performance of a daylight-responsive dimming system using the actual weather data. The prismatic film was found to cause the over-dimming conditions to happen more frequently in a south-facing space regardless of the calibration hours. To characterize an acceptable daylight quality for residential buildings, the second study was conducted to correlate residents'

long-term subjective evaluations on the daylight quality to the objective measures characterizing the daylight quantity and quality in their flats during a same period of time. The flats with the average $sDA_{300/50\%}$ above 66% and the maximum average daylight illuminance above 5624 lx were considered to provide an acceptable daylight quality. The final study was carried out to compare how different daylight simulation methods can be used to characterize the reflected sunlight from a curtain wall. It was found that the simulation results were significantly affected by the material specification and the luminance characterization of the sun, the ambient calculation, and the resolutions of the bidirectional scattering distribution function (BSDF) and sky patches. The forward ray-tracing method was recommended to identify the locations and directions introducing and receiving the reflected sunlight, with the backward ray-tracing method being followed to quantify the reflected sunlight illuminance.

All the three studies further our understanding about how to use daylight simulation software to characterize the daylighting performance in Hong Kong. The dissertation not only provides useful guidance to designers and engineers to better design buildings for enhancing the daylighting performance, but also allows policy makers to better evaluate the daylighting performance in buildings in Hong Kong.

Acknowledgements

I would like to acknowledge the support of the Hong Kong Polytechnic University during the period of my research work in Hong Kong. I would also like to express my sincere gratitude to the people who have helped me to complete this dissertation.

The first is my supervisor, Dr. Minchen Wei, who is quite intelligent and responsible. I have started to work with Dr. Wei since 2017. I am thankful to him for introducing me into the field of daylighting and encouraging me to do research independently. Honestly speaking, my entire researches during the last three years have benefited from his continuous inspiration, valuable advices, and careful revision. I am extremely grateful to him for offering me opportunities to publish studies and attend international conferences.

My sincere thanks also go to my co-supervisor, Prof. Cheuk-ming Mak, for the guidance and assistance in the confirmation of doctoral candidature.

I would also like to thank my colleagues: Siyuan Chen, Wenyu Bao, Yiqian Li, and Jialu Wu. It is pleased to get to know you all and work together.

A special thank goes to Meihe (Nicole) Long. Thank you for coming into my life and supporting me all the time.

Last but not least, I would like to express my huge thanks to my big family. Thank you all for always believing in me and supporting me unconditionally.

List of Contents

List of Figures

List of Tables

List of Acronyms

ASHRAE	American Society of Heating, Refrigerating and Air-conditioning Engineers
ASE	Annual Sunlight Exposure
BIPV	Building Integrated Photovoltaic
BRA	Boundary of a Reflection Area
BSDF	Bidirectional Scattering Distribution Function
CBDM	Climate-Based Daylight Modelling
cDA	Continuous Daylight Autonomy
CFD	Computational Fluid Dynamic
CFS	Complex Fenestration System
CIE	Commission Internationale de l'Eclairage
DA	Daylight Autonomy
DF	Daylight Factor
EMSD	Electrical and Mechanical Services Department
FS	Finkelstein-Schafer
IES	Illuminating Engineering Society
ISO	International Organization for Standard
IWEC	International Weather for Energy Calculation
JCIT	Jockey Club Innovation Tower
MF	Multiplication Factor
NCDC	National Climatic Data Centre
NREL	National Renewable Energy Laboratory
RGA	Reflection Glare Area
RMSE	Root Mean Square Error

sDA	Spatial Daylight Autonomy
SNL	Sandia National Laboratory
TMM	Typical Meteorological Month
TMY	Typical Meteorological Year
TRY	Test Reference Year
UDI	Useful Daylight Illuminance
WYEC	Weather Year for Energy Calculations

Chapter 1

Introduction

1.1 Research Background and General Objective

Daylight has long been considered as an integral part of building designs. The introduction of daylight into interior spaces provides a solution to reduce energy consumptions due to the excessive reliance on electric lighting systems, which account for about 30% of total energy consumption in commercial and residential buildings (Li et al., 2010; Ward, 1994; Martirano, 2011; Pandharipande et al., 2011). Apart from reducing the electricity consumption, daylight can improve luminous environmental quality, helping to enhance occupants' productivity, satisfaction, and health. Daylight performance, therefore, has a significant impact on the energy efficiency and luminous environment of the buildings. Daylight quantity, however, is not the only determinant of the daylight performance. Poor daylight quality may be counterproductive. To predict the daylight performance of the buildings, the characterizations of daylight quantity and quality are becoming more and more important, especially in a dense urban environment.

Hong Kong, which just develops 7% of total territory with 1106 square kilometres for residential buildings, is one of the largest densely-populated cities in the world. The proportion of commercial lands is even lower than that of the residences, accounting for only 2.7% of the whole territory. The number of high-rise and dense buildings, therefore, has been increasing over the past decades due to the limited developed lands and enormous population. The Electrical and Mechanical Services Department (EMSD) (2019) reported that the electric lighting systems used in the buildings account for about 20% of total electricity consumptions. Due to the fact that Hong

Kong is located in just south of the tropic of cancer, it receives a great amount of daylight. The exterior daylight levels were found to exceed 10000 lx for more than 80% of the working hours in a year (Chung, 2003), which provides great potentials to the high-rise and dense buildings in Hong Kong to receive sufficient daylight.

Serious challenges, however, are still posed to most of the buildings in such a dense urban environment, such as poor daylight performance, low energy efficiency of lighting systems, and occupants' low satisfaction with the luminous environment. For instance, as a common daylighting strategy, daylight-responsive control systems are widely applied to reduce the energy consumptions caused by the electric lighting in Hong Kong. For different control purposes, these systems switch on/off or adjust the dimming level of the electric lighting based on the amount of daylight detected by a photosensor that is commonly installed on the ceiling of a space (DiLaura et al., 2011). Although such systems were found to achieve energy savings ranging from 20% to 60% (Choi and others, 1997; Chung et al., 2001; Jennings et al., 2000; Li et al., 2006), they rarely functioned well as expected due to malfunctions caused by the inappropriate calibration time and photosensor locations (EC&M, 2007). Since these decisions are made based on the characterizations of daylight quantity and quality in a space, inaccurate characterizations can easily cause the poor performance of the systems, which affects the luminous environmental quality. The occupants may suffer visual and thermal discomforts due to the excessive amount of daylight, and have lower ability to perform visual tasks or activities due to insufficient amount of daylight. Such experiences will lower their satisfaction with the luminous environment.

Moreover, the reflected sunlight from the surrounding buildings also introduces serious challenges, such as glare, serious thermal radiation, and urban heat island phenomenon (Ichinose et al., 2017; Yuan et al., 2015; Suk et al., 2017; Danks et al.,

2016). This is mainly due to the use of glass curtain walls, which are either coated with different materials having higher reflectance and specularity or formed with specific geometry (Chow et al., 2010; Gobakis et al., 2015; DiLaura et al., 2011). For example, reflective curtain walls, especially with a concave shape, can reflect and concentrate sunlight at a single point, causing burns on pedestrians or fires on a car (Garfield, 2016; Walker, 2013).

To address various serious challenges, the prediction of daylight performance through better characterizations of daylight quantity and quality at different times is necessary and meaningful, especially given the popularity of climate-based daylight modelling (CBDM) in recent years. CBDM calculations are typically performed by taking the space information (i.e., geometry, orientation, and material) and weather conditions (i.e., sun and sky conditions) into account. Such calculations allow the predictions of different photometric quantities in a space with a certain time interval throughout a year. Based on the calculated photometric quantities, the quality and quantity of daylight, as characterized using various metrics, can be used to predict daylight performance, possible energy savings of daylight-responsive control systems, and luminous environmental quality in the space.

This dissertation aims to investigate how daylight simulation should be used to characterize different daylight-related issues for buildings in Hong Kong. Specifically, it compares the characterization of performance of a daylight-responsive dimming system using the typical meteorological year (TMY) data and the actual weather data. Then, it investigates the characterizations of daylight quality and quantity in residential buildings in Hong Kong by comparing the simulation results and questionnaire surveys. Finally, it compares how different simulation methods can be used to characterize and predict the influence of reflected sunlight from curtain walls. The investigations further

our understanding of the interaction between lighting, building and people, and help the lighting community to understand how simulation tools should be used to characterize the daylight quantity and quality in buildings in a dense urban environment.

1.2 Dissertation Layout

The dissertation is organized as follows.

Chapter 2 reviews the scientific researches about sky models, development of typical weather data, development of the CBDM, annual daylight simulation methods, daylight performance measures, evaluation of daylight-responsive dimming systems, evaluation of indoor luminous environment, and characterization of reflected sunlight.

Chapter 3 describes the research gaps that exist in the relevant works, with detailed research objectives being described.

Chapter 4 reports the investigations on the performance of a closed-loop daylight-responsive dimming control system that is calibrated based on the TMY data, with the actual performance of the system being characterized based on the actual weather data with an interval of one minute. Chapter 5 further reports how the results will be different, if a prismatic film is attached on the glazings.

Chapter 6 reports the investigations on the characterization of daylight quality in residential buildings in Hong Kong, which is based on the calculations between the calculated daylight quantities in 400 flats using the actual weather data and the collected questionnaire surveys about the residents' satisfaction with the long-term daylight quality in their flats.

Chapter 7 reports the investigations on how different daylight simulation methods can be used to characterize the negative impacts of reflected sunlight from curtain walls. Three simulation methods are used to quantify the intensities at the areas affected by the reflected sunlight from a real building in Hong Kong throughout the entire year.

Chapter 8 concludes the entire dissertation and describes the limitations that need to be addressed in future work.

Chapter 2

Literature Review

2.1 Sky Models

For daylight simulation purposes, the sun and sky are generally regarded as different sources due to their different characteristics. The sun can be regarded as a small patch of 0.5 angular diameter, having the highest luminance of approximately 1.6×10^9 cd/m^2 at noon, while the sky can be regarded as a hemispherical light source with luminance distribution that varies with solar position and climatic condition (DiLaura et al., 2011). At a given geographical location, the solar position varies with the time in a day, a season, and a year. According to the principle of apparent movement of celestial bodies, the sun generally moves 15° for each hour and arrives at its highest point at noon along a path, which is relative to the time and the geographic location of a site (DiLaura et al., 2011), as shown in Figure 2.1. The solar position can be determined by the solar altitude (θ_Z) and azimuth (θ_A) angles, with the former characterizing the vertical angular distance between the sun and a horizontal plane, and the latter characterizing the horizontal angular distance between due south and the sun projected on the ground, as shown in Figure 2.2.

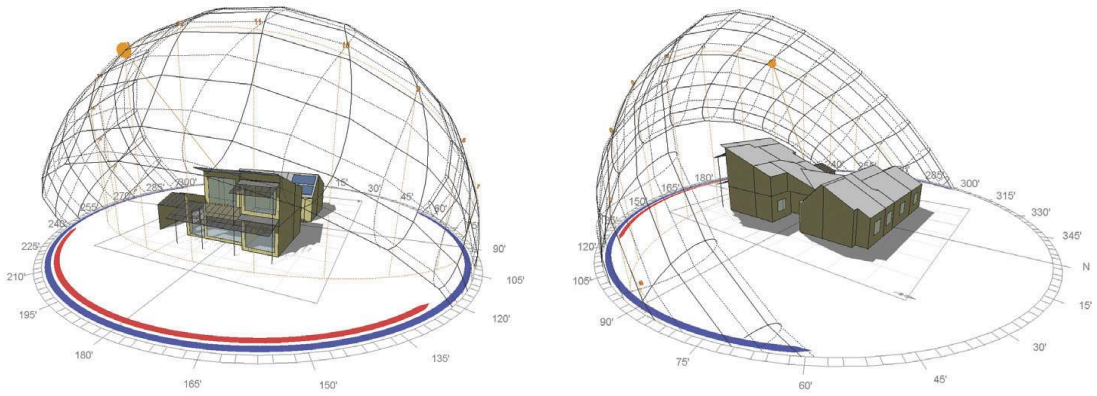

Figure 2.1 Illustration of apparent solar movement that is relative to a given site throughout the year. The arcs refer to the 21st day in each month. The highest arc refers to the solar path at the summer solstice; the lowest arc refers to the solar path at the winter solstice. Each loop refers to the solar positions at a solar time throughout the year. The middle arc crossing the centre of each loop refers to the solar path at the spring and autumn equinoxes (DiLaura et al., 2011).

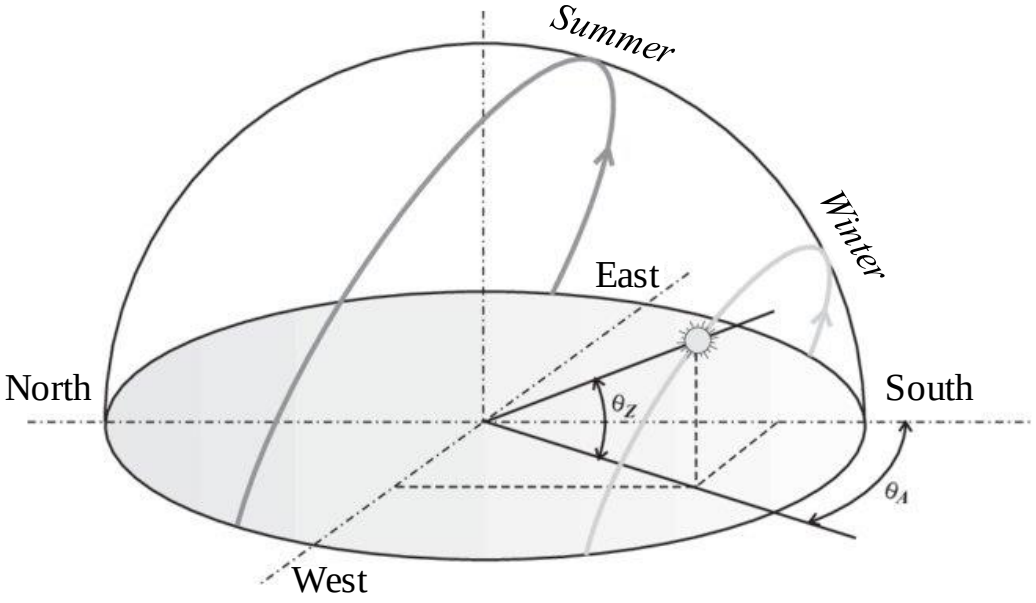

Figure 2.2 Illustration of the characterization of solar position using the solar altitude (θ_Z) and azimuth (θ_A) angles (Abu Hanieh, 2008).

Both the sun and sky luminance contributions are important to the characterizations of daylight quantity and quality. Kimball and others (1922) first summarized a systematic method to measure the sky luminance, which was referenced by the Illuminating Engineering Society (IES) (Gillette et al., 1984). Since that time, great efforts have been made to develop different sky models for better characterizing the sun and sky luminance distributions.

2.1.1 CIE Standard Sky Model

Moon et al (1942) developed an overcast sky model based on a better measurement of the sky luminance. The luminous distribution of the model is symmetrical with respect to the zenith, and the luminance increases from the horizon to the zenith with a fixed scale factor. In 1955, this model was adopted by the Commission Internationale de l'Eclairage (CIE), and it served as a standard method to characterize the luminance distribution of an overcast sky (Nakamura et al., 1985). However, a study conducted by Reinhart et al (2000) showed that the CIE overcast sky model was ineffective in characterizing daylight compared to the Perez all-weather sky model, due to its fixed sky luminance distribution. In addition, the CIE overcast sky model was found to overestimate the daylight illuminance in a dense urban environment (Ng, 2001). Mardaljevic (2004) also found that the CIE overcast sky model was unlikely to reveal the real overcast sky conditions.

To develop sky models that can characterize more realistic sky luminance distributions, Kittler (1967) proposed a clear sky model for describing the luminous distributions of clear skies, which was also defined as a CIE standard in 1973 (Kennelly et al., 2014). Both the CIE overcast and clear sky models were finally included in the relevant standards of the International Organization for Standards (ISO) in 1996 (ISO 15469:1997, 1997; Darula et al., 2002). An intermediate sky model was developed by Nakamura et al (1985), who demonstrated that the intermediate sky conditions were more likely to occur than the clear and overcast sky conditions in Japan. Igawa et al (1997) later proposed twenty sky luminance distributions, which covered a relatively wide range of luminance distributions from clear sky to overcast sky.

In order to characterize possible sky variations, Kittler et al (1998) proposed fifteen sky luminance distributions (i.e., five for overcast, five for transitional, and five for clear skies) based on the CIE clear sky model. Such a solution was found to better represent the real sky conditions, considering both the sky and sun luminance contributions. This proposal was defined as the CIE standard sky model in 2004 (ISO 15469:2004, 2004). The CIE standard sky model, however, was less representative of real skies over a long period of time, even throughout a year, except extreme conditions, such as overcast and clear skies (Enarun et al., 1995; Li et al., 2003, Li et al., 2004; Chirarattananon et al., 2007; Bartzokas et al., 2005; Wittkopf et al., 2007; Navvab et al., 2014). For daylight simulations, though the sun and sky luminance contributions can be derived using the *gensky* program in Radiance, they are unable to characterize the real sky conditions due to the use of the CIE standard sky model (Darula et al., 2002; Inanici et al., 2017).

2.1.2 Perez All-Weather Sky Model

The Perez all-weather sky model was proposed by Perez et al (1993) based on a time series of solar radiation data, which were derived from the measurements taken with a short time interval at specific locations using a sky scanner. It is actually a mathematical model predicting continuous sky luminance distributions, using geographical location, date, local time, and the measured solar radiation data, including direct normal and diffuse horizontal irradiances. It can be derived using the *gendaylit* program in Radiance (Inanici et al., 2016; Perez et al., 1993; Subramaniam, 2017). The Perez sky model was widely used to predict sky conditions at the sites where the radiation data were available. However, it was later found that this model overestimated the daylight levels under the overcast sky conditions, in comparison to the CIE overcast sky model, which was due to the failure of the Perez sky model in

deriving the sky luminance under overcast conditions (Mardaljevic, 2008; McNeil et al., 2013).

2.1.3 Tregenza and Reinhart Sky Models

These two sky models are developed by subdividing the celestial hemisphere into a series of circular or small rectangular patches. The original Tregenza sky model was developed to derive a coefficient to efficiently calculate daylight quantities under different sky luminous conditions (Tregenza, 1987). The sky was subdivided into circular patches based on the luminance measurements taken by sky scanners. One of the subdivision schemes has 145 circular patches, with each patch having an angular diameter of 10.15°, as shown in Figure 2.3(a). However, the whole sky luminance may be underestimated with such a subdivision scheme, due to the directions that are not completely covered by the sky patches (Subramaniam, 2017). To reduce the error, a refined Tregenza sky model was later proposed by averaging the measured sky luminance over rectangular patches instead of circular patches. Furthermore, Reinhart et al (2000) then subdivided the whole sky into a series of small rectangular patches using a multiplication factor (MF). Figure 2.3(b) shows the continuous sky subdivision scheme with multiple small patches.

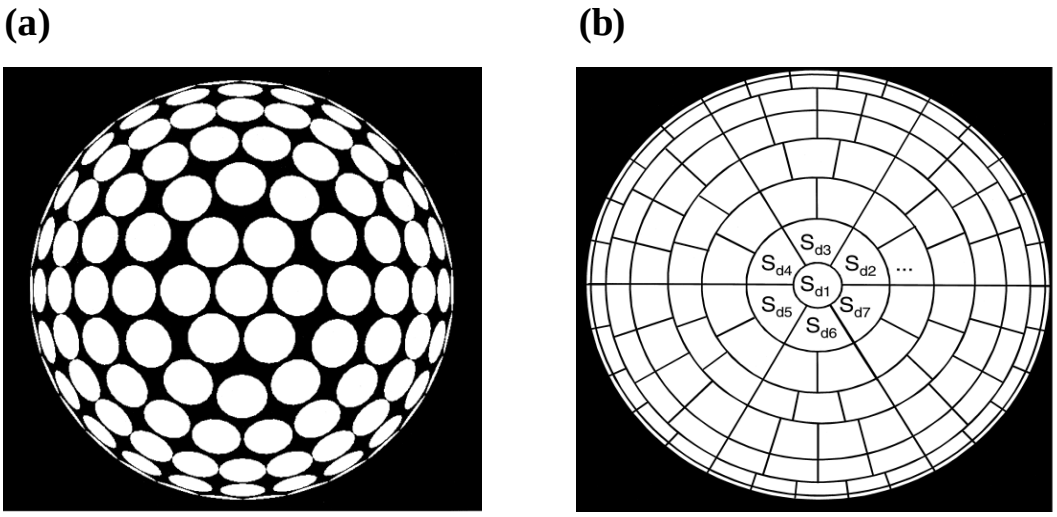

Figure 2.3 Illustration of (a) The original Tregenza sky subdivision scheme and (b) Reinhart's continuous sky subdivision scheme (Reinhart et al., 2000; Bourgeois et al., 2008).

In addition, the model can be used to approximately characterize the sun radiation. As shown in Figure 2.4, the sun at a given time is approximately represented using the three closest sky patches. Such a prediction may overestimate the sun luminance and introduce significant errors to daylight simulations, regardless of the Tregenza and Reinhart sky models. Although more subdivided patches will improve the accuracy of the sun or sky luminance characterization, it also increases the runtime and disk memory (Subramaniam, 2017).

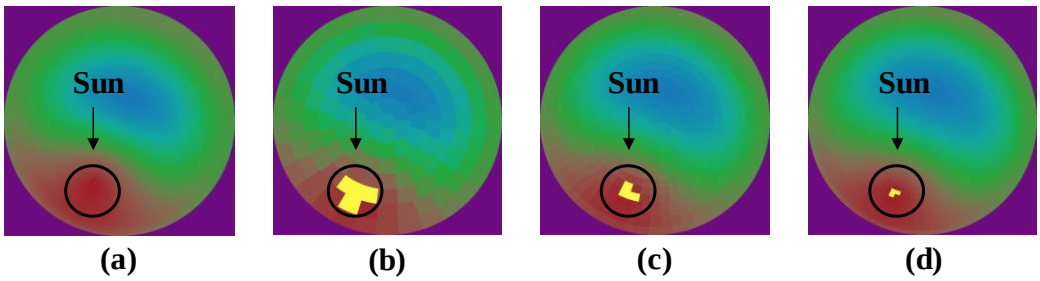

Figure 2.4 Fish-eye images of a sky model with different degrees of subdivision. (a) Continuous sky model; (b) Reinhart sky model with 145 patches; (c) Reinhart sky model with 577 patches; (d) Reinhart sky model with 2305 patches (Subramaniam, 2017).

2.2 Development of Typical Weather Data

Since the sky condition at a given site is dominated by the local climate, the climatic condition representing different sky luminance distributions will affect the characterizations of daylight quantity and quality. However, the climatic conditions vary from time to time. To represent the trends of local climate over a long period of time, measurement of weather conditions over a long time is necessary.

The long-term measured weather data can be compiled to different types for different purposes. The use of weather data in the building performance simulation became a common practice as early as the 1980s, providing the climatic conditions for the simulation models that were mainly involved in energy consumption calculations (Herrera et al., 2017). Due to the program of daylight measurement launched by the CIE (Tregenza et al., 1994), the weather data were gradually developed to include both the radiometric and photometric data (e.g., direct and diffuse radiance and irradiance data), which were expected to characterize daylight variations under different climatic conditions. In order to evaluate the daylight performance inside or outside of buildings, the weather data, especially those representing typical climatic conditions at a specific location, should be considered for daylight simulations (Hensen and others, 2019).

A variety of weather data have been developed over the last 40 years. One of the earliest representative weather data used for building performance simulation is the test reference year (TRY). It was originally developed by the National Climatic Data Centre (NCDC) and used for about 60 regions in the United States (NCDC, 1976). The measurement data used to create the TRY were collected from 1948 to 1975 (Crawley, 1998). The TRY data was a one-year duration data set initially consisting of meteorological elements, including dry bulb and wet bulb temperatures, dew point

temperature, wind direction and speed, barometric pressure, relative humidity, and cloud cover and type, among which only the dry bulb temperature was adopted as an index for selecting candidate months from the long-term measurement data (Chan, 2016, Herrera et al., 2017). During the selection process, only the candidate months with intermediate average dry bulb temperature were considered until one year remained. Due to the lack of extreme weather conditions, the TRY data was unable to comprehensively represent actual climatic conditions. In addition, the TRY data did not include solar radiance and irradiance data.

To address the limitations of the TRY data, a new weather data, also known as the typical meteorological year (TMY), was developed by the Sandia National Laboratory (SNL) in 1978 (Hall et al., 1978). The TMY data is also a one-year duration data set, consisting of 12 typical individual months selected from 1952 to 1975 (Crawley, 1998). In addition to the basic meteorological elements, the TMY data also includes the global horizontal solar radiation data. Specially, the typical meteorological months (TMMs) in the TMY data were selected by comparing the Finkelstein-Schafer (FS) indices derived for the solar radiation, dry bulb temperature, dew point temperature, and wind speed in each month of each measurement year to those in a long-term contribution of all the measurement years (Finkelstein and others, 1971; Hall et al., 1978). With different weighting factors being applied to the four elements in the selected months, those months with the lowest weighted sums were further considered as the TMMs and used to form a TMY data (Hall et al., 1978).

Many attempts were made to continuously create more typical weather data sets from 1970 to 1985. For instance, the weather year for energy calculations (WYEC) introduced by the American Society of Heating, Refrigerating and Air-conditioning Engineers (ASHRAE) (1985) was created in the TRY format using a 30-year weather

data set including solar radiations and basic meteorological elements, and widely used for predicting more typical weather conditions in North America (Crow, 1970; Crow, 1983; ASHRAE, 1985). The WYEC data was then precisely updated to WYEC2 in the TMY format in the 1990s, with a major change of using hourly solar radiation components derived from the Perez all-weather sky model, which described the sky conditions based on local time (ASHRAE, 1997a; Perez et al., 1990). In 1994, the National Renewable Energy Laboratory (NREL) created a 30-year data set using hourly solar and meteorological data derived from 239 locations during the period from 1961 to 1990 in the United States. The direct normal solar radiation was first included in the data. To distinguish it from the original TMY data, the new data set was referred to as TMY2 data (Marion and others, 1995; Maxwell et al., 1990). Several years later, ASHRAE (2002) introduced the International Weather for Energy Calculation (IWEC) data that covered 227 locations over 70 different countries. This data set was created using the TMY format, with the weather years from 1982 to 1999. However, the weighting factors given to the four meteorological elements for selecting the TMMs were different from those used in the TMY and TMY2 data, with 40% for both the solar radiation and dry bulb temperature and 10% for both the dew point and wind speed (Wilcox and others, 2008). In 2007, NREL released a set of TMY weather data that were derived using hourly measured weather data during the period from 1991-2005. This data were labelled as the TMY3 data in which the solar radiation was given the highest weight of 50%, and widely used to characterize typical weather conditions for more than 1400 locations in the United States (Wilcox and others, 2008; Chan, 2016).

Although a variety of typical weather data were developed and updated for daylight simulations at different regions, the effect of temporal weather conditions on the

prediction of the daylight performance was seldom investigated. Walkenhorst et al (2002) conducted a study to compare the energy consumption of a daylight-responsive control system calculated using a one-hour weather data with those calculated using a measured and a modelled one-minute weather data. It was found that the one-hour weather data underestimated the energy consumption. This study also suggested that the temporal daylight variations characterized by the weather conditions significantly affected the predictions of the daylight availability and electricity consumption in a building. A similar study was conducted by Iversen et al (2013), who compared the indoor daylight illuminance and the energy performance of a daylight-responsive system with different control strategies calculated using different weather data. It was found that the one-minute weather data did not introduce significant variations to the indoor daylight illuminance compared to the other hourly weather data. Also, the energy consumption of the lighting system was found underestimated when using the hourly weather data.

2.3 Climate-Based Daylight Modelling

The term climate-based daylight modelling (CBDM) was proposed in 2006 (Mardaljevic, 2006). Although there is no formal definition, CBDM can be described as a prediction of photometric quantities at given time intervals within a building environment, which is performed using realistic sun and sky contributions derived from the typical weather data through computer simulations (Brembilla et al., 2019). In effect, before CBDM was proposed, several studies were carried out to predict a point-in-time daylight condition using different lighting simulation tools.

One of the earliest studies calculating daylight illuminance in interior spaces by means of a computer program was conducted by DiLaura and others (1978), who

demonstrated the possibility of performing daylight calculations using a simulation tool. Such practices were extended by considering the space geometry, external obstructions, and CIE standard sky conditions in later studies (Bryan, 1980; Modest, 1982). The simulation tool used to calculate daylight in these studies was based on the radiosity method, assuming lights to be reflected diffusely from the surfaces. However, the radiosity method was unable to characterize specular reflections in daylight simulations, especially for those in complex geometries (Tsangrassoulis et al., 2003). Validation studies also indicated that the radiosity method had low accuracy for daylight calculations (Gibson and others, 2015). In addition, the single point-in-time daylight condition predicted in a space may be unrealistic due to the use of the CIE standard skies.

The emergence of a simulation tool named Radiance offered a great potential to realistically simulate daylight conditions under actual or typical weather conditions. Also, it was found effective and efficient for simulations involving specular reflections and complex geometries, due to the application of backward ray-tracing and Monte Carlo ambient sampling methods (Larson et al., 1998; Tsangrassoulis et al., 2003). As one of the most efficient tools used for lighting simulations, Radiance has undergone a process of development and validation for nearly 30 years (Ward et al., 1988; Ward, 2017; Geisler-Moroder et al., 2017; Mardaljevic, 1995; Mardaljevic, 1997; Mardaljevic, 2001; McNeil et al., 2013; Reinhart et al., 2001). In the meantime, the development of Radiance was accompanied by the development of annual daylight simulation methods. One of the validation studies demonstrating the accuracy of Radiance was conducted by Mardaljevic (1995), who later validated the accuracy of the annual daylight illuminance calculated using daylight coefficient method and actual local weather conditions by comparing the field measurements (Mardaljevic,

2000). Such a prediction of annual daylight illuminance in a space, by means of the daylight coefficient method and realistic sun and sky contributions, laid a foundation for the CBDM calculation.

2.4 Annual Daylight Simulation Methods

A survey conducted by Reinhart et al (2006) showed that nearly 80% of the respondents coming from the lighting research community preferred using Radiance for daylight simulations. Given the popularity of CBDM, the traditional single point-in-time daylight simulations performed under the CIE standard skies were gradually replaced with the annual daylight simulations performed using the actual or typical weather data (Brembilla et al., 2019). With the trend of characterizing daylight performance at different times in a year, different annual simulation methods were developed to improve the calculation speed and the accuracy for simulating complex fenestration systems (CFS).

2.4.1 Daylight Coefficient Method

The daylight coefficient method, which was initially proposed by Tregenza et al (1983), has been widely used for annual daylight simulations over the last few decades (Reinhart et al., 2006). It uses a coefficient to correlate the average luminance of individual sky patches to the daylight quantities at each measurement point, which improves the efficiency of the calculations under different sky conditions. Figure 2.5 shows a schematic diagram of the daylight coefficient method.

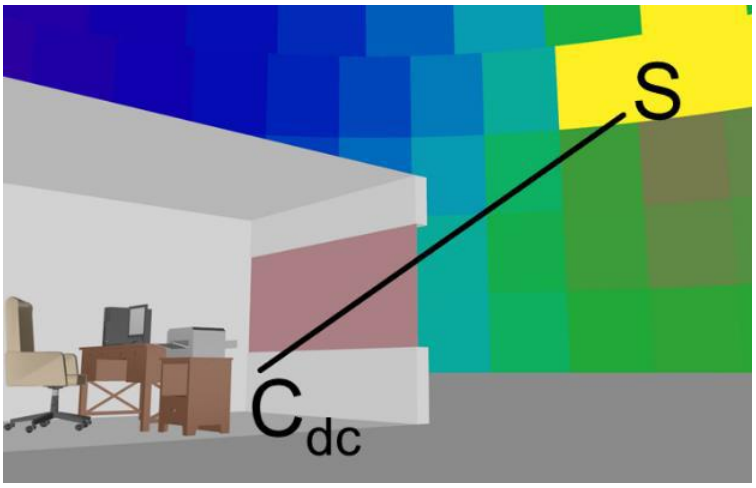

Figure 2.5 Schematic diagram of the daylight coefficient method (Subramaniam, 2017).

Since the photometric quantities at each measurement point can be correlated to the luminance of each sky patch, the quantities under the entire sky can be derived using the daylight coefficient method based on matrix-based operation, which can be expressed as Eq. (2.1) (Subramaniam, 2017):

$$E = C_{dc} \cdot s \tag{2.1}$$

Where:

E: The matrix of daylight quantities at the measurement points;

C_{dc}: The matrix of daylight coefficients;

s: The matrix of average luminance of the sky patches.

As shown in Figure 2.5, the daylight quantity at each measurement point can be derived by multiplying the daylight coefficient matrix (i.e., C_{dc}) by the sky matrix (i.e., s) containing the average luminance of the sky patches for each hour throughout a year.

The daylight coefficient method used for annual daylight simulations was validated by various studies, most of which quantified the differences between daylight simulation results and field measurements (Mardaljevic, 2000; Reinhart et al., 2001; Reinhart et al., 2006). One of the most comprehensive studies was conducted by Mardaljevic

(2000), who compared the interior daylight illuminance derived using the daylight coefficient method against those derived from field measurements, and demonstrated the reliability of the daylight coefficient method for predicting the interior daylight illuminance from a yearly perspective. It was also found that the daylight coefficient method introduced significant errors due to the characterization of the sun contributions. He then refined the daylight coefficient method by separating the daylight calculations into 4 components (i.e., direct sunlight, direct skylight, indirect sunlight, and indirect skylight) and suggested to use 2056 sun patches to characterize the direct sun luminance contributions (Mardaljevic, 2000). It was found that the simulation results were comparable to the field measurements.

Reinhart et al (2000) performed a simulation to calculate the daylight illuminance in two offices throughout a year. The annual daylight illuminance levels derived using five different simulation methods were compared against a reference case, which used a long-term local weather data to calculate the daylight illuminance. It was found that the daylight coefficient-based methods produced the smallest relative root mean square errors (RMSEs). A later study predicting the indoor daylight illuminance in an office with CFSs using the daylight coefficient method was also conducted by Reinhart et al (2001), who proposed a continuous subdivision scheme and modelled the direct sunlight contribution using 65 representative sun positions. He found a good algorithm (i.e., interpolation) for these positions in daylight simulations. In addition, the simulation results suggested that the characterization of the direct sunlight contribution significantly affected the accuracy of the illuminance calculation in the space. The method was widely used in DAYSIM and regarded as a classical DAYSIM method. It was also proposed to use 2305 direct sun positions to further improve the simulation accuracy (Bourgeois et al., 2008).

The daylight coefficient method is also known as a two-phase method, which uses the *rcontrib* program instead of the *rtrace* program in Radiance to efficiently derive the daylight coefficients in a single run (Brembilla et al., 2019). The two-phase method usually spreads out the sun luminance over three closest sky patches, which decreases the average sun luminance on the closest sky patches. To reduce the error, the sky hemisphere can be uniformly subdivided into multiple smaller patches to accurately characterize the sun luminance distribution. In addition, since a *glow* type source is used to represent the sun, the sun and sky contributions are stochastically simulated when using the two-phase method. This requires sufficient samplings that are controlled by ambient divisions parameter (i.e., -*ad*) in Radiance.

The daylight coefficient method, however, was found to fail to accurately model the optical properties when CFSs (e.g., fix or operable blinds) were used (Ward et al., 2011; Saxena et al., 2010). It was mainly due to the fact that the daylight coefficient method only calculates a single ray tracing process when daylight enters a space, making the light transfers within the fenestration systems inexplicit. Thus, a method that can accurately characterize the optical properties of CFSs is needed to improve the accuracy of the simulation results.

2.4.2 Three-phase Method

The three-phase method is an extension of the daylight coefficient method, but it addresses the challenges introduced by CFSs. It separates the daylight transfer into three independent phases (i.e., sky patches to the exterior of fenestration, transmission through fenestration, and the interior of fenestration to measurement points or specified viewing points), as shown in Figure 2.6.

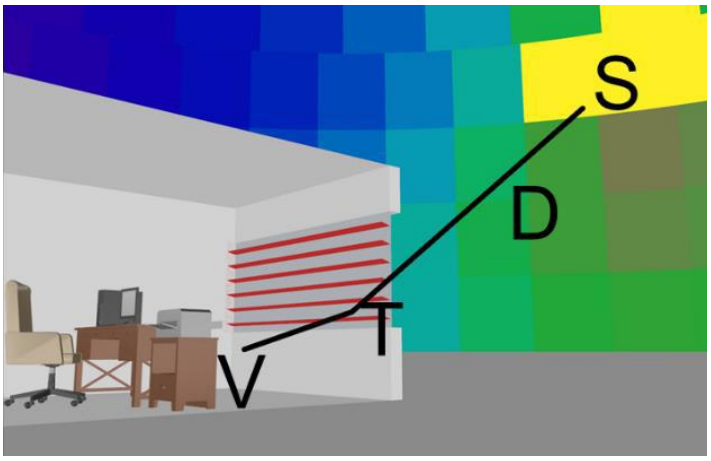

Figure 2.6 Schematic diagram of the three-phase method (Subramaniam, 2017).

The matrix-based formulation of the three-phase method can be expressed as Eq. (2.2) (Subramaniam, 2017):

$$E = VTDs \tag{2.2}$$

Where:

V: The view matrix that correlates daylight quantities at the measurement points or specified viewing points in a space to the luminance leaving from the interior side of a fenestration;

T: The transmission matrix that characterizes the reflection and transmission conditions of a fenestration;

D: The daylight matrix that correlates the luminance received at the exterior side of a fenestration to the luminance of the sky patches;

E and s are the same as described in Eq. (2.1).

As shown in Figure 2.6, the daylight quantity at each measurement point can be achieved by multiplying the three matrices (i.e., VTD) and the sky matrix (i.e., s). Similar to the two-phase method, the three-phase method also distributes the sun luminance to the closest sky patches and assigns the sun a *glow* material.

Particularly, the transmission matrix (T) is a part of a bidirectional scattering distribution function (BSDF) characterization for a fenestration. A complete BSDF comprises four components (i.e., front transmission, front reflection, back transmission, and back reflection) that characterize the transmission and reflection conditions from different directions on each side of the fenestration (Klems, 1994a; 1994b; McNeil, 2013), as shown in Figure 2.7. The BSDF can be derived either using the *genBSDF* program in Radiance or through real measurements (Mitchell et al., 2008; Grobe et al., 2015; McNeil, 2015). The three-phase method, however, only uses the front transmission component as the transmission matrix (T) in the BSDF.

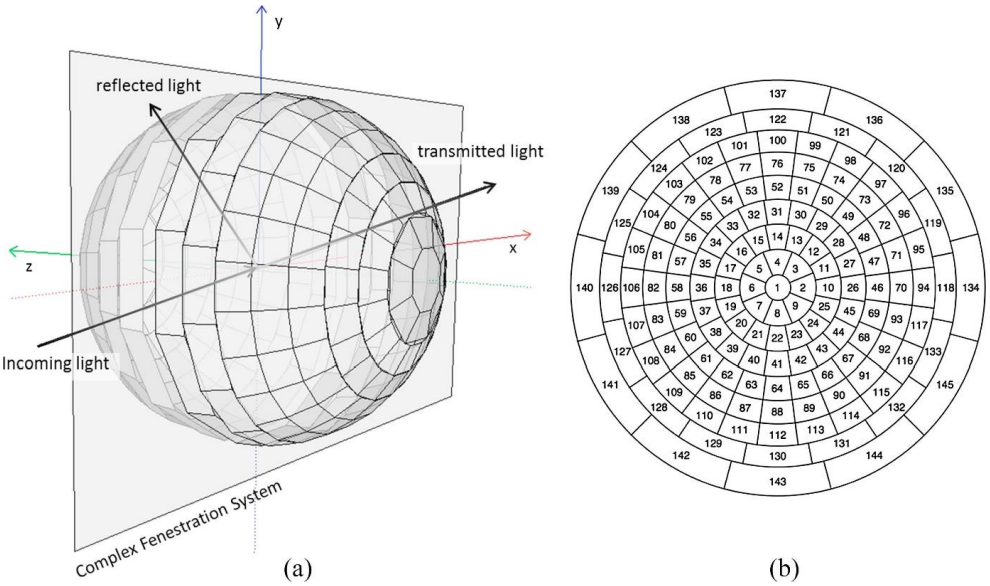

Figure 2.7 Illustration of BSDF characterization for a fenestration. (a) Schematic diagram of a BSDF representing the reflection and transmission conditions of light that happen on both the interior and exterior sides of a fenestration. (b) A standard Klems resolution of 145 patches (Sun et al., 2017).

A validation of the *genBSDF* program was performed by McNeil et al (2013), who compared the front transmission data of the BSDF derived using the *genBSDF* program against those derived using a software TracePro and a goniophotometer. The results suggested the high reliability of the *genBSDF* program. McNeil et al (2013) also carried out a validation study of the three-phase method to investigate the annual

performance of an optical light shelf in a test room. The optical light shelf was modelled using the *genBSDF* program and the actual daylight illuminance on the workplane of the test room was measured throughout a year. The results showed that the simulation results derived using the three-phase method were comparable to the actual measured data.

However, the three-phase method has some fundamental weaknesses. The errors, such as the scattered daylight distribution and missing peak intensity of daylight, were introduced by a lower resolution of the 145 patches of the Tregenza sky and Klems BSDF (Ward et al., 2011; McNeil et al., 2013). A standard Klems scheme (Klems, 1994b), with the transmission and reflection hemispheres being subdivided into 145 patches, is widely used in the lighting simulation community due to its efficiency in daylight simulations. However, it spreads out the incident light over a wide angular size, which thereby lowers the intensity of the transmitted light. In addition, the modelling of CFSs using the Klems BSDF was also found to inaccurately characterize the details and shadows due to the direct sunlight (Saxena et al., 2010; Ward et al., 2011).

2.4.3 Five-phase Method

The five-phase method is an extension of the three-phase method, but it offers a higher accuracy, especially for characterizing the direct sunlight contribution. The matrix-based formulation of the five-phase method can be expressed as Eq. (2.3) (Subramaniam, 2017):

$$E = VTDs - V_d T D_d s_d + C_{ds} s_{sun} \quad (2.3)$$

Where:

V, T, D, and s are the same as described in Eqs. (2.1) and (2.2).

V_d: The view matrix with direct sun only;

D_d: The daylight matrix with direct sun only;

s_d: The sky matrix with direct sun only;

C_{ds}: The sun coefficient matrix that correlates the luminance of the sun patches to the daylight quantities at each measurement point;

s_{sun}: The matrix containing the luminance of the sun patches.

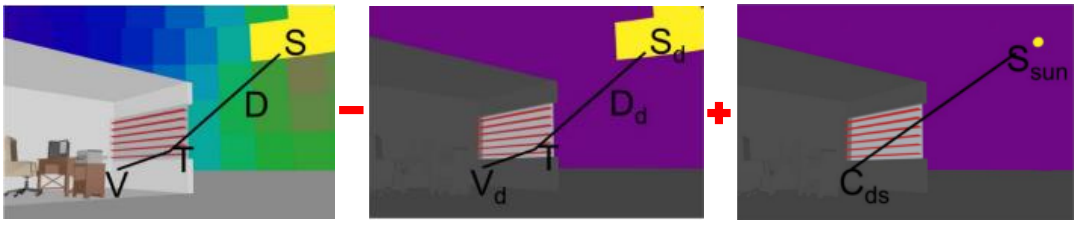

Figure 2.8 Schematic diagram of the five-phase method (Subramaniam, 2017).

As shown in Figure 2.8, the daylight quantity at each measurement point can be derived by replacing the direct solar contribution calculated using the three-phase method with a more accurate direct sunlight contribution derived using 5185 sun patches uniformly distributed on the sky vault and a high resolution tensor tree BSDF (Subramaniam, 2017).

Specifically, the third component in Eq. (2.3) is also known as the sun coefficient method. The sun is modelled as a *light* type source, with an angular diameter of approximately 0.533°, so that the direct sunlight contribution is calculated using a deterministic algorithm, rather than a stochastic algorithm as in the daylight coefficient and the three-phase methods. In addition, an insertion of a high resolution tensor tree BSDF can offer a reliable simulation of CFSs, overcoming the weakness of modelling details and shadows caused by the CFSs, in comparison to the standard Klems BSDF in the three-phase method (Ward et al., 2011). As shown in Figure 2.9, the image rendered using the five-phase method that applies a tensor tree BSDF can clearly show

the details and shadows of blinds slats, which cannot be seen when the standard Klems BSDF is used in the three-phase method. A validation of the five-phase method was carried out by Lee et al (2018), who compared the daylight illuminance on the workplane and at the vertical sensors predicted using the five-phase method against the measurement results in a test office with different CFSs, and found a good agreement between the simulation and measurement results. The study also suggested that the five-phase method was superior to the three-phase method in daylight simulations due to the use of a high resolution tensor tree BSDF.

(a) Three-phase method

(b) Five-phase method

Figure 2.9 Images rendered using (a) The three-phase method; (b) The five-phase method (Saxena et al., 2010).

2.5 Daylight Performance Measures

To better evaluate daylight performance, accurate characterizations of daylight quantity and quality are important. A traditional measure used to quantitatively characterize the daylight at any point inside a space was Daylight Factor (DF) (Walsh, 1951). DF is defined as a ratio of daylight illuminance at a point inside a space to that on an exterior horizontal surface under an unobstructed overcast sky (DiLaura et al.,

2011). It adopts the CIE standard overcast sky that was proposed in 1955. Since then, it has been widely used to evaluate the daylight performance in a space by characterizing the daylight quantity at individual points (Moon et al., 1942; Tregenza et al., 2018; Reinhart et al., 2006). Though it was later modified to characterize the daylight quantity over a space using the DF_{ave} (Lynes, 1979), these two measures are only valid under static daylight conditions (i.e., overcast). Since they ignore the temporal sun and sky luminance contributions, they cannot be used to accurately characterize the variations of daylight at a given site under different weather conditions (Reinhart et al., 2001; Reinhart et al., 2006; Nabil et al., 2006).

Given the development of CBDM, various measures, which are developed based on the CBDM simulation results, have been proposed to characterize the dynamic daylight variations under different sky conditions at given time intervals. Among these measures, daylight autonomy (DA), continuous daylight autonomy (cDA), useful daylight illuminance (UDI), spatial daylight autonomy (sDA), and annual sunlight exposure (ASE) are widely used. For example, DA is defined as the percentage of occupied hours in a year that the illuminance is higher than the target level at each measurement point (Reinhart et al., 2001). cDA is similar to DA, but gives partial credits when the illuminance is lower than the target level (Rogers, 2006). Though people had different opinions on the target illuminance for performing visual tasks, the partial contribution of daylight introduced to a space was beneficial (Reinhart et al., 2003; Jennings et al., 2000). In addition, these two measures can be used to predict the performance of different daylight-responsive control systems, in terms of potential energy saving (Reinhart et al., 2006). However, both DA and cDA were unable to indicate whether the daylight illuminance at each measurement point was too high or too low (DiLaura et al., 2011; Mardaljevic, 2015). UDI refers to determine the

percentage of occupied hours when the daylight illuminance is useful (i.e., 100-2000 lx), insufficient (i.e., less than 100 lx), or exceeded (i.e., greater than 2000 lx) for each measurement point in a year (Nabil et al., 2006). The sum of all the UDI values at a point equals to 100%.

In contrast to the measures that characterize daylight quantities at each measurement point across a space, sDA and ASE use a single value to characterize the daylight quality in a space. sDA is defined as the percentage of the workplane area in a space where the DA is higher than a target level; ASE is defined as the percentage of the workplane area in a space that the direct sunlight illuminance is higher than a certain level for more than a specified occupied hours in a year. A survey conducted by Heschong Mahone Group (2012) suggested that the occupants had a low satisfaction with the environment where the direct sunlight was higher than a certain level throughout a year. Both the sDA and ASE are included in some building standards and guidelines (e.g., IES LM-83-12 and LEED v40) (IES LM-83-12, 2013; USGBC, 2014), with the former characterizing whether the daylight is enough and the latter characterizing whether the direct sunlight is too much.

2.6 Evaluation of Daylight-responsive Dimming Systems

Daylight-responsive control systems have been widely used for several years, as they can reduce the energy consumption of electric lighting based on the amount of daylight in a space. Some codes and standards also make daylight-responsive control systems compulsory in buildings (BEC, 2015). These systems generally estimate the amount of daylight in a space using calibrated photosensors, which are typically installed on the ceiling (DiLaura et al., 2011). Dimming control, one of the most popular control strategies, adjust the dimming level of electric lighting. The higher the correlation

between the amount of daylight in a space and the signal detected by the photosensor, the better the performance of the control system. The ratio of the photosensor signal to workplane daylight illuminance (S/E) was found to be significantly affected by several factors, such as sky conditions (Rubinstein et al., 1989; Mistrick and others, 2005; Choi et al., 1998; Kim et al., 2007), space orientations (Kim et al., 2001; Mistrick and others, 1997; Ranasinghe and others, 2003), photosensor types (Mistrick and others, 1997; Choi et al., 2005), and calibration times (Park et al., 2011; Mistrick and others, 2005; Kim et al., 2001).

The performance of a daylight-responsive dimming control system is generally evaluated based on the potential energy savings. Previous studies showed that considerable energy savings could be achieved using daylight-responsive dimming control systems. Some were based on field measurements and numerical calculations (Li et al., 2003; Li et al., 2006; Chow et al., 2013; Kim et al., 2014; Choi et al., 2016). For example, Li et al (2003) carried out a field study to measure daylight and electric lighting levels, and predicted the energy savings that can be achieved by a daylight-responsive dimming system through numerical and regressive calculations. It was found that the annual energy savings can be around 70%. A similar study carried out in an open plane office found that the energy savings achieved using the dimming control system were greater than 30% (Li et al., 2006).

In contrast, some studies predicting the energy savings of daylight-responsive dimming control systems were based on computer simulations (Roisin et al., 2008; Choi and others, 1997; Mistrick and others, 2005; Li et al., 2005; Krarti et al., 2005; Mistrick et al., 2000; Kim et al., 2001). One of the earliest simulation studies was carried out by Choi and others (1997). In this study, the daylight levels were simulated using an hourly weather data derived from the standard IES sky conditions. The energy

savings achieved by the system were then predicted by considering daylight and electric light levels, determination of calibration point, S/E ratios, and over-dimming conditions. The study revealed that the energy saving achieved by a dimming system can be as high as 56%. A similar study was also conducted by Mistrick and others (2005), who compared the energy savings achieved by a daylight-responsive dimming system in five spaces with different daylight delivery systems using different dimming control strategies. The daylight illuminance level was calculated using the weather data derived from the standard CIE skies. The impact of direct sunlight on the photosensor performance was first considered. It was found that the annual energy savings of the system ranged between 40% and 50%. To improve the accuracy of predictions on the energy savings of the daylight-responsive dimming system, some studies performed daylight calculations using advanced simulation tools, such as DAYSIM and Radiance. For example, Li et al (2005) predicted the potential energy savings of a daylight-responsive dimming system based on the daylight illuminance levels derived from simulations and field measurements. The findings suggested that the energy savings of the system derived using daylight simulation results had a good agreement with those derived using the measurement results. Roisin et al (2008) carried out a study to compare the annual energy savings of a close-loop daylight dimming system in the offices with different orientations using different control strategies based on DAYSIM simulation. It was found that the annual energy saving achieved by the office rooms can be as high as 61%.

2.7 Evaluation of Indoor Luminous Environment

Though various daylight delivery systems and techniques have been developed to provide indoor spaces with sufficient daylight over the past few decades (Xue et al., 2014; Samant, 2010; Acosta et al., 2016), negative impacts caused by the excessive

daylight may be simultaneously introduced, decreasing occupants' productivity and well-beings. Therefore, it is necessary to correlate the daylight quantities with the subjective responses.

Since people usually spend nearly 45% of their time in residences, their feelings about a luminous environment of residential buildings attract researchers' attention (Klepeis et al., 2001; Xue et al., 2016). Researchers made efforts to evaluate the luminous environment through subjective evaluations, trying to reveal human responses to the luminous environment in a space and to investigate the factors affecting occupants' feelings about the luminous environment. Ng (2003) surveyed 200 individual flats in a group of high-rise and dense residential buildings in Hong Kong to investigate the residents' satisfaction with daylighting. The findings indicated that the daylight performance and the residents' satisfaction with the luminous environment of the flat had a good agreement. A similar survey was conducted by Lau et al (2010), who investigated the residents' preference of direct sunlight access in a high-rise housing estate in Hong Kong. It was found that the brightness and thermal discomforts highly affected the residents' preference of direct sunlight access in their flats. Xue et al (2014) performed a questionnaire survey to study the effects of daylight performance and human adaptive behaviours on the residents' luminous comfort in a high-rise and dense housing estate. It was found that the daylight performance was highly correlated to the residents' luminous comfort. He also studied the effects of two green building features (i.e., sunshade and balcony) on residents' luminous comfort through a questionnaire survey in high-dense residential buildings (Xue et al., 2015). The findings suggested that the sunshades and balconies directly affected the residents' luminous comfort and their adaptive behaviours.

In addition, residents were also found to take some adaptive actions in response to different luminous environments (Keyvanfar et al., 2014). The adaptive behaviours, such as adjusting shading devices, switching on/off electric lights, opening/closing windows, and moving to another seat, helped to enhance their satisfaction with the luminous environment (Schweiker, et al., 2012; Boerstra et al., 2013; Christoffersen et al., 2000; Xue et al., 2014). For example, Heydarian et al (2016) conducted a study to investigate how light settings affected the participants' performance of office-related tasks in different virtual luminous environments. It was found that the participants preferred to make use of daylight by adjusting the light settings and worked efficiently in an environment with sufficient amount of daylight.

Though the subjective evaluations help to reflect the residents' feelings about a luminous environment, they cannot reveal how the occupants' feelings are affected by the daylight quality, which cannot help to create a better luminous environment at the early stage of building designs. To address the challenges, some researchers tried to investigate occupants' feelings about a luminous environment by correlating the subjective evaluations to the objective measures. Reinhart et al (2012) carried out a study to investigate the relationship between the objective daylight performance measures and the subjective evaluations made by the students in a studio. It was found that the values of $sDA_{300/50\%}$ of the studio were highly correlated to the students' subjective evaluations. However, the subjective evaluations were made based on students' short-term opinions about the daylight performance in the space, which was not consistent with the period considered for daylight calculations. Xue et al (2016) also conducted a study to characterize the residents' long-term feelings about the luminous environment in their residences using the objective daylight performance measures. It was found that the values of DA_{300} and uniformity were highly correlated

to the residents' evaluations on the luminous comfort. However, the daylight performance was characterized using a Perez sky model and a daylight coefficient method, which was not comparable to the real conditions experienced by the residents.

2.8 Characterization of Reflected Sunlight

Sunlight reflected from building facades has been found to introduce negative impacts on the surrounding areas of a building, such as glare disability and discomfort, urban heat island, severe thermal effects (e.g., fires). To reduce the negative impacts, many attempts have been made to optimize the optical property of materials for the building facades, including solar reflectance, solar transmittance, solar absorptance, and infrared emittance (Gobakis et al., 2015; Ichinose et al., 2017; Yuan et al., 2015; Santamouris et al., 2011; BCA, 2016). However, the orientation and geometry of the building facades should also be considered to reduce the negative impacts caused by reflected sunlight, especially at the early stage of building designs. Given the development of computer-based simulations, different methods were developed to characterize reflected sunlight.

Shih et al (2001) proposed a Boundary of a Reflection Area (BRA) concept to characterize reflected sunlight caused by glass curtain walls by means of a computer-based visualization. The BRA represented using a test cube with reflective materials was regarded as a reference to identify the boundaries affected by the reflected sunlight. However, this method ignored the reflectance of the materials, shapes or orientations of the building geometry, and the spatial distribution of the reflected sunlight. A similar concept was also proposed by Brzezicki (2012), who introduced a Reflection Glare Area (RGA) to predict the areas that were affected by the reflected sunlight and to emphasize the shapes of the boundaries. Four different geometries were used to

predict the RGA areas, in which the luminous intensity of the reflected sunlight was also characterized. However, the reflectance of the material and the duration of the reflections were not taken into account.

Besides the geometric methods, Danks (2014) proposed a simple analytical method to predict reflected sunlight in an urban environment by only considering one mirror-like reflection. This method was coded into a computational fluid dynamic (CFD) simulation suite to derive the accumulative illuminance of reflected sunlight from a concave façade, which was found to have a good agreement with the measured results (Danks et al., 2016). However, these two studies ignored the optical properties of the building façade materials.

Though the simple geometric and analytical methods provided a solution to study the reflected sunlight, they had several limitations that affected the accuracy, especially for complex geometries and specular reflections. In contrast, Yang et al (2013) conducted a study to efficiently predict the potential areas receiving reflected sunlight around a building using a forward ray-tracing and a simplified density estimation method. However, the scattering and specular properties of the building façade surfaces were not specified in the simulation. A similar work based on the workflow of Yang's study was carried out by Schregle et al (2018), who performed a time-series simulation to predict the areas affected by reflected sunlight from a building integrated photovoltaic (BIPV) using a photon mapping method, which considered the diffuse scattering and specular reflections of the materials used in the simulation.

Chapter 3

Research Gaps and Objectives

3.1 Research Gaps

As a sustainable resource, daylight plays an important role in improving energy efficiency and luminous environment of buildings. Thus, the effect of daylight on the energy performance of electric lighting systems and the occupants' feelings about the luminous environment attract many researchers' attention. Due to the development of CBDM, which can derive daylight quantities at measurement points in a building using validated daylight simulation methods and the TMY data, the daylight quantities can be summarized and presented from different perspectives using various measures to characterize the daylight quality.

Based on the literature review of previous studies, the TMY data is believed to represent the typical weather conditions of a local climate, and is widely used in CBDM calculations to characterize the daylight quantity and quality. Few study, however, investigated whether the daylight quantity and quality and the performance of a daylight-responsive dimming system predicted using the TMY data were accurate, especially the temporary daylight variations are not revealed by the hourly TMY data. In addition, little effort has been made to evaluate the daylight quantities in a space and the residents' feelings about the luminous environment during a same period of time, which made it impossible to correlate the subjective evaluations on the daylight quality and the objective measures characterizing the daylight quantity.

Moreover, the popularity of curtain walls introduces serious problems to the surrounding areas due to reflected sunlight. Though previous studies proposed several

methods to characterize the effect of reflected sunlight, they rarely investigated the effect of the highly specular reflected sunlight from building facades using different matrix-based simulation methods throughout a year.

3.2 Research Objectives

This dissertation includes three studies to address the above research gaps.

The first study aimed to comprehensively quantify the difference of daylight quantity and quality and the performance of a closed-loop daylight-responsive dimming system between the prediction and the real condition for a real classroom equipped with four different fenestration systems (i.e., clear glazing, 0°, and ±45° venetian blinds) in Hong Kong. The investigations were performed using two weather data (i.e., the TMY data and the actual weather data with a one-minute interval) and three simulation methods (i.e., the daylight coefficient, three-phase, and five-phase methods) from a yearly perspective. Specifically, the simulation results derived using the TMY weather data were regarded as the prediction, while the simulation results derived using the one-minute interval weather data that were measured at a weather station in Hong Kong throughout an entire year were regarded as the real condition. The investigation was also performed to see how an additional prismatic film on the glazing would affect the performance of a daylight-responsive dimming system.

The second study aimed to characterize the acceptable daylight quantity and quality for high-rise and dense residential buildings in Hong Kong by correlating the subjective evaluations to the objective measures. The subjective evaluations were collected through a questionnaire survey on the residents' long-term opinions about luminous environment in their residences. The objective measures characterizing the daylight quantity and quality were derived using three different simulation methods

(i.e., the daylight coefficient, three-phase, and five-phase methods) and the actual local weather data measured at a weather station in Hong Kong. Both the subjective evaluations and the objective measures focused on a same period of time.

The third study aimed to compare how the matrix-based simulation methods (i.e., the two-phase, three-phase, and sun coefficient methods) could be used to characterize the effect of the reflected sunlight, in terms of illuminance, from curtain walls of a real building in Hong Kong throughout an entire year.

Chapter 4

Study 1-1: Does Typical Weather Data Allow Accurate Predictions of Daylight Quality and Daylight-responsive Control System Performance

4.1 Methodology

4.1.1 Space and Modelling

A real east-facing classroom in Hong Kong (22°17′ N, 114°9′ E), with dimensions of 8.35 m (depth) × 11.8 m (width) × 2.6 m (height), and the adjacent buildings were modelled using SketchUp and imported into Radiance. The classroom was located on the 5^{th} floor, with the height of about 20 m above the ground. Four windows of the classroom, with each size of 1.6 m (width) × 2.04 m (height) and a distance of 2.7 m between each other, were located at 0.56 m above the floor. The interior floor, ceiling, and walls of the classroom were modelled with a reflectance of 20%, 70%, and 50%. The exterior ground and the adjacent buildings were considered as the obstructions, with the reflectance being set as 10% and 30% respectively. A grid of 359 calculation points, with a spacing of 0.5 m for each other, was uniformly placed on a workplane which was 0.75 m above the floor. Figure 4.1 shows the layout of the classroom and the arrangements of the calculation points.

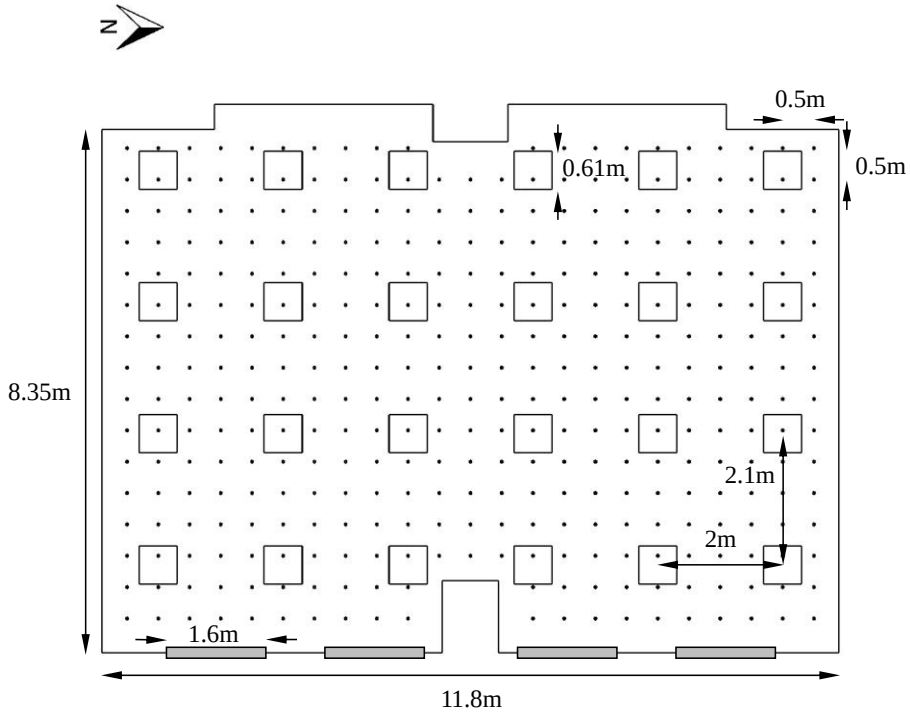

Figure 4.1 Layout of the classroom and the arrangements of the calculation points and luminaires.

A clear glazing and three types of internal venetian blinds were modelled for the classroom and imported into Radiance. The transmittance of the clear glazing was set as 80%. For setting up the venetian blinds, 68 pieces of blinds slats, with dimensions of 1.6 m (width) × 0.03 m (depth) and reflectance of 65%, were modelled with three different tilt angles, including 0° (i.e., horizontally placed), +45° (i.e., 45° downwards towards the inside), and -45° (i.e., 45° downwards towards the outside). The gap size of the slats with ±45° and 0° tilt angles was 0.021 m and 0.03 m respectively.

4.1.2 Daylight Simulation and Weather Data

The daylight illuminance at each of the 359 calculation points on the workplane was derived using three simulation methods, including the daylight coefficient, three-, and five-phase methods. By setting the *MF* to 5, the 3601 sky and 3601 sun patches plus one patch for the ground were generated for the simulations. It is worthwhile to mention that the 3601 sun patches were used for the sun coefficient calculation in the

five-phase method. The ambient divisions (*-ad*) and ambient bounces (*-ab*) were set as 10000 and 5 respectively. When using the three-phase method, the BSDF characterizing the transmittance of four different fenestrations was generated using the *genBSDF* program in Radiance based on a standard Klems scheme, which resulted in an average transmittance value of 72.9%, 71.2%, and 60% for the clear glazing, 0°, and ±45° blinds. When using the five-phase method, a high resolution tensor tree BSDF was generated for the four different fenestrations respectively, and used in the sun coefficient calculation.

The daylight simulation was performed based on two sets of Hong Kong weather data, including the TMY data and the actual weather data with a one-minute interval. The TMY data, which were downloaded from the EnergyPlus website, were used to characterize the daylight quantity and quality of the classroom under typical weather conditions in Hong Kong, to design a daylight-responsive dimming control system for the classroom, and to predict the performance of the system. The actual weather data, which were measured at the Hong Kong King's Park Meteorological Station from Dec 1st 2014 to Nov 30th 2015 with a one-minute interval, were used to investigate the actual daylight quantity and quality of the classroom and the actual performance of the daylight-responsive dimming control system. Specifically, the direct normal solar irradiance was measured using a EKO MS-54 pyrheliometer integrated with a STR sun tracker, the diffuse horizontal solar irradiance was measured using a EKO MS-802 pyranometer, and the global horizontal solar irradiance was measured using a Kipp & Zonen CM5 pyranometer. The average difference between the measured global irradiance data and the sum of the measured direct and diffuse irradiance data was only 56.2, which suggested a high reliability of the measured data. The occupied period was

set to 8 AM-6 PM, so that the TMY and actual weather data resulted in 3650 and 219000 illuminance values for each calculation point from a yearly perspective.

4.1.3 Design of Electric Lighting

An electric lighting system in the classroom was designed to provide a target illuminance of 500 lx on the workplane (DiLaura et al., 2011). The luminaires were selected and arranged by considering the daylight on the workplane. Twenty-four ceiling-mounted 26 W LED luminaires, with dimensions of 0.61 m × 0.61 m, were arranged as six columns and four rows. The spacings between the luminaires were 2 m for each column and 2.1 m for each row. The arrangement of the luminaires is shown in Figure 4.1. Furthermore, the luminaires, with a total light loss factor of 0.75, were able to provide an average maintained illuminance of 505 lx to the 359 calculation points on the workplane. Based on the daylight illuminance derived on the workplane, the first two rows of the luminaires in the vicinity of the windows were functioned as the dimmed lighting zone, while the other two rows were functioned as the non-dimmed lighting zone.

4.2 Difference between the TMY Data and Actual Weather Data

Since the TMY data was developed based on the TMMs, as described in Section 2.2, which represented the most typical weather conditions over a long period of time (i.e., 30 years), it was expected to be different from the actual weather data that characterized the temporal daylight variations with a one-minute interval. The difference between the two weather data will affect the daylight quantity and quality and the performance of the daylight-responsive dimming control system. To quantify the difference, the two weather data within the occupied period were compared from different perspectives.

Within the occupied period, 3.1% and 28.43% of the recorded direct solar irradiance values were zero in the TMY data and the actual weather data. In addition, the actual weather data was found to have higher frequencies with the ratio of the direct normal to the global horizontal irradiance beyond 0.9 and below 0.1, which suggested that overcast and sunny sky conditions happened more frequently, as shown in Figure 4.2. To more directly quantify the difference between the two weather data for the daylight availability of the classroom, vertical daylight illuminance on the four windows was calculated throughout an entire year. A grid of 300 calculation points, with a spacing of 0.1 m, was placed on the exterior side of each window equipped with a clear glazing. The average vertical daylight illuminance derived using the actual weather data in a year was 15582 lx, which was about 30% higher than that derived using the TMY data (i.e., 12120 lx). In addition, the actual weather data had larger variations in the diffuse horizontal, direct normal, and global horizontal solar irradiance levels, as suggested in Figure 4.3, which may affect the actual performance of the daylight-responsive dimming control system.

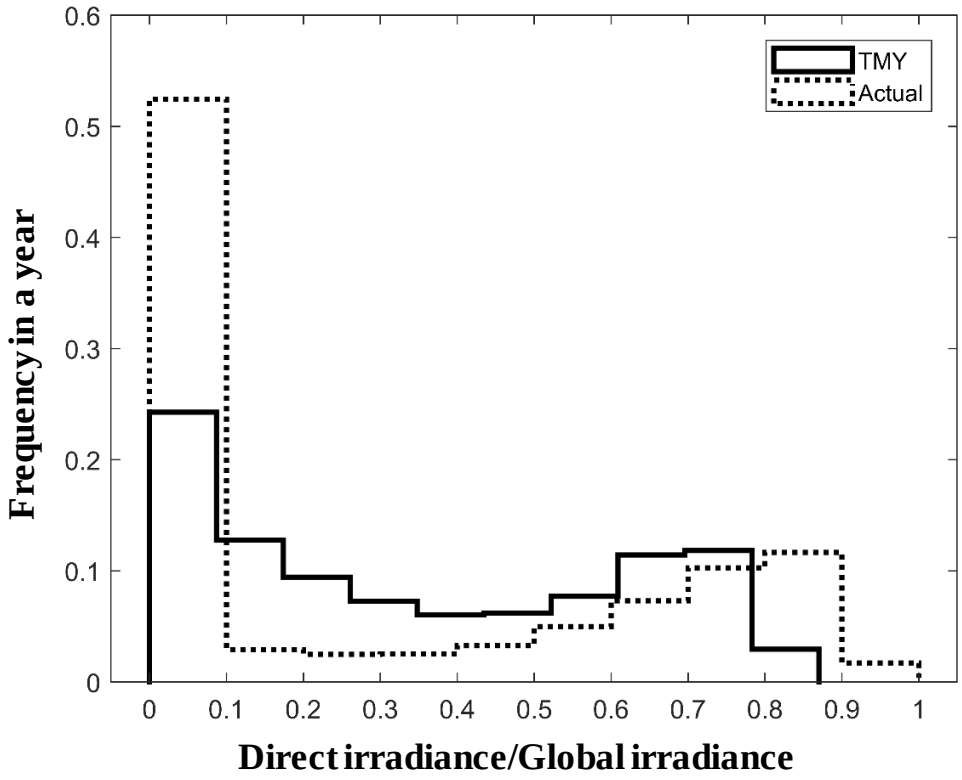

Figure 4.2. Histogram of the ratio of the direct normal irradiance to the global horizontal irradiance within the occupied period for the two weather data, with a lower value for an overcast sky and a higher value for a sunny sky.

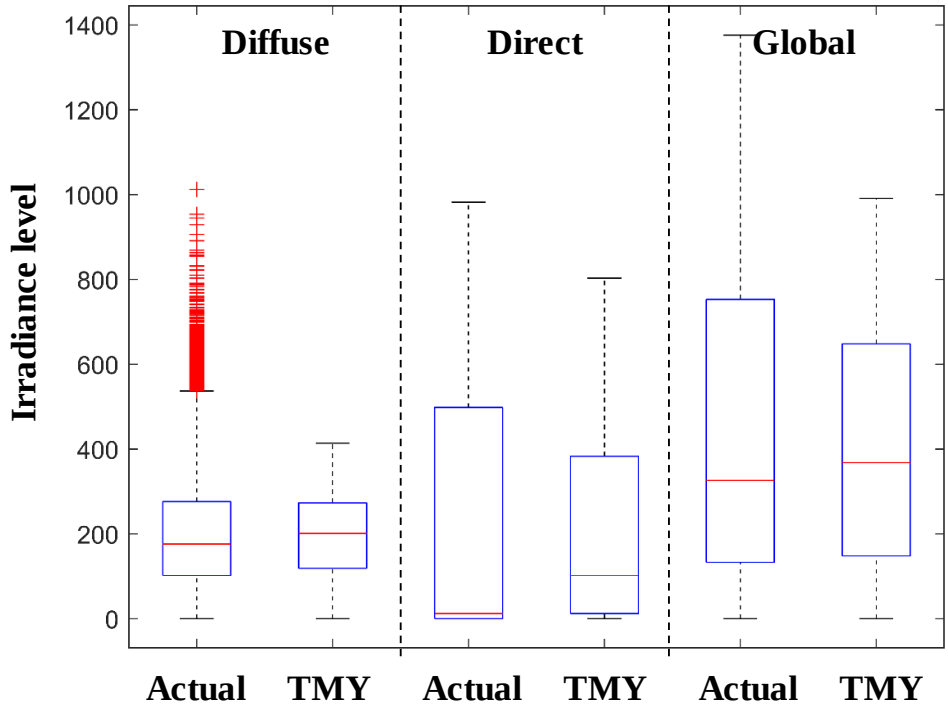

	Actual	TMY	Actual	TMY	Actual	TMY
Mean	197.10	196.63	231.60	208.03	428.70	404.66
Std. dev.	124.25	100.25	299.20	227.81	331.85	281.47

Figure 4.3 Boxplots of the diffuse horizontal, direct normal, and global horizontal solar irradiance levels of the two weather data.

4.3 Daylight Quantity and Quality in the Classroom

The daylight illuminance values at each of the 359 calculation points in the classroom were calculated using the three different simulation methods and the two weather data for the four different fenestrations during the occupied period throughout an entire year. The annual daylight illuminance values, as characterized using different measures, were then used to evaluate the daylight quality in the classroom.

4.3.1 $sDA_{300/50\%}$ and $ASE_{1000h,\ 250h}$

As recommended in both LEED v4 and IES LM-83-12, two measures—$sDA_{300/50\%}$ and $ASE_{1000,\ 250h}$—can be used to characterize the daylight sufficiency and the potential visual discomfort caused by direct sunlight (USGBC, 2014; IES LM-83-12, 2013).

The former is defined as the percentage of the areas in a space that the daylight illuminance is higher than 300 lx for more than 50% of the occupied period in a year; the latter is defined as the percentage of the areas that the direct sunlight illuminance is beyond 1000 lx for more than 250 hours of the occupied period in a year. Both measures were calculated and summarized in Figures 4.4 and 4.5. As shown in Figure 4.4, the three- and five-phase methods resulted in similar values of $sDA_{300/50\%}$, which were around 5% higher than those calculated using the daylight coefficient method, regardless of the different fenestrations. The comparisons of the $ASE_{1000,\ 250h}$ values were made based on the TMY data and the actual weather data that averaged the irradiance levels within each hour using the five-phase method, since the ASE evaluated on a basis of one minute was impractical. As shown in Figure 4.5, the $ASE_{1000,\ 250h}$ values derived using the actual weather data that contained hourly averaged irradiance levels were slightly lower than those derived using the TMY data for the clear glazing. However, the two weather data did not introduce differences to the $ASE_{1000,\ 250h}$ values derived for the +45° blinds and the direct sunlight was effectively blocked by the other two fenestrations.

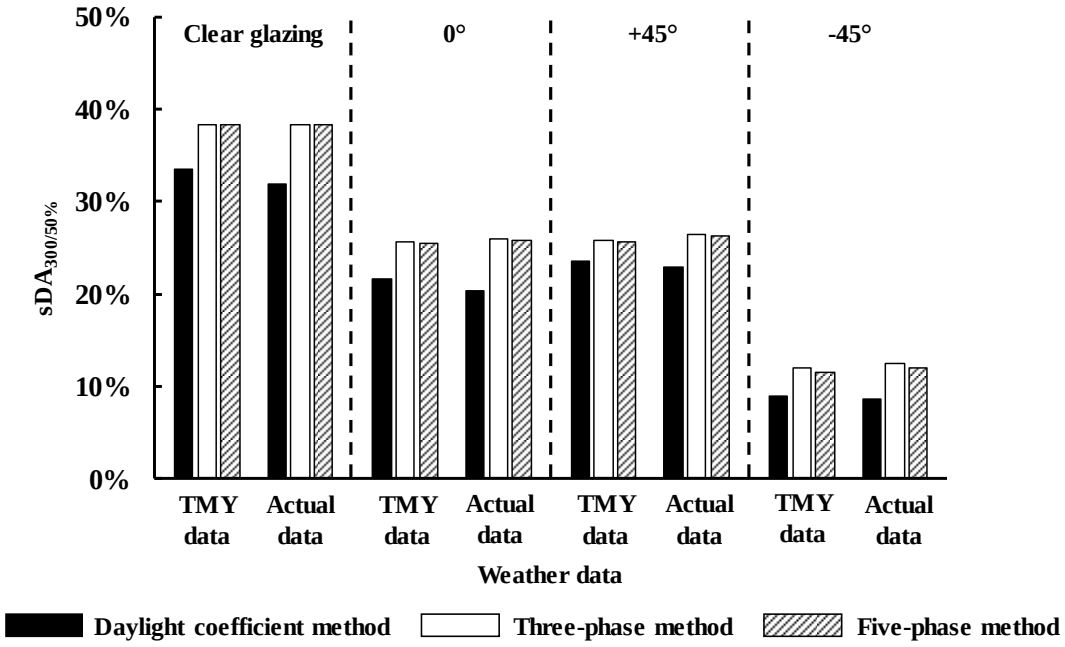

Figure 4.4 Comparison of the $sDA_{300/50\%}$ values that were derived using the different simulation methods and the two weather data for each of the four fenestration systems.

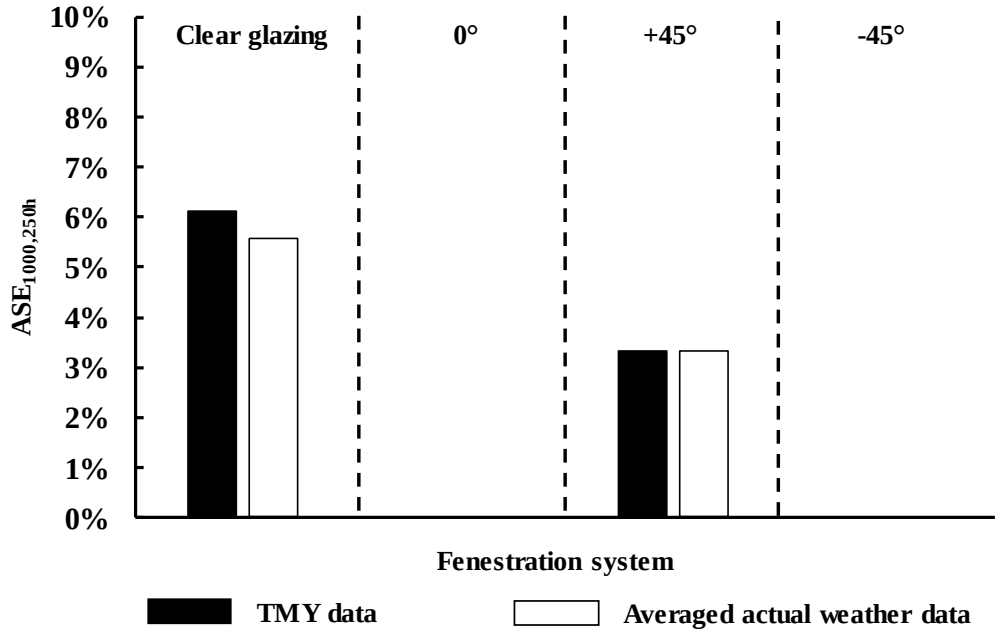

Figure 4.5 Comparison of the $ASE_{1000,\ 250h}$ values based on the two different weather data, both of which were derived using the direct sunlight contribution in the five-phase simulation method. (note: both 0° and -45° blinds were effective in blocking the direct sunlight).

4.3.2 UDI

The average UDI values that characterized daylight quantity in the three categories—insufficient (i.e., <100 lx), useful (i.e., 100 lx—2000 lx), and exceeded (i.e., >2000 lx)—were calculated using the different simulation methods and weather data, as summarized in Figure 4.6. It was found that the two weather data introduced a slight difference to the average UDI values for the three categories. However, the simulation methods had a significant influence on the average UDI values. For example, the daylight illuminance calculated using the daylight coefficient method was more frequently classified as “insufficient” compared to those derived using the three- and five-phase methods.

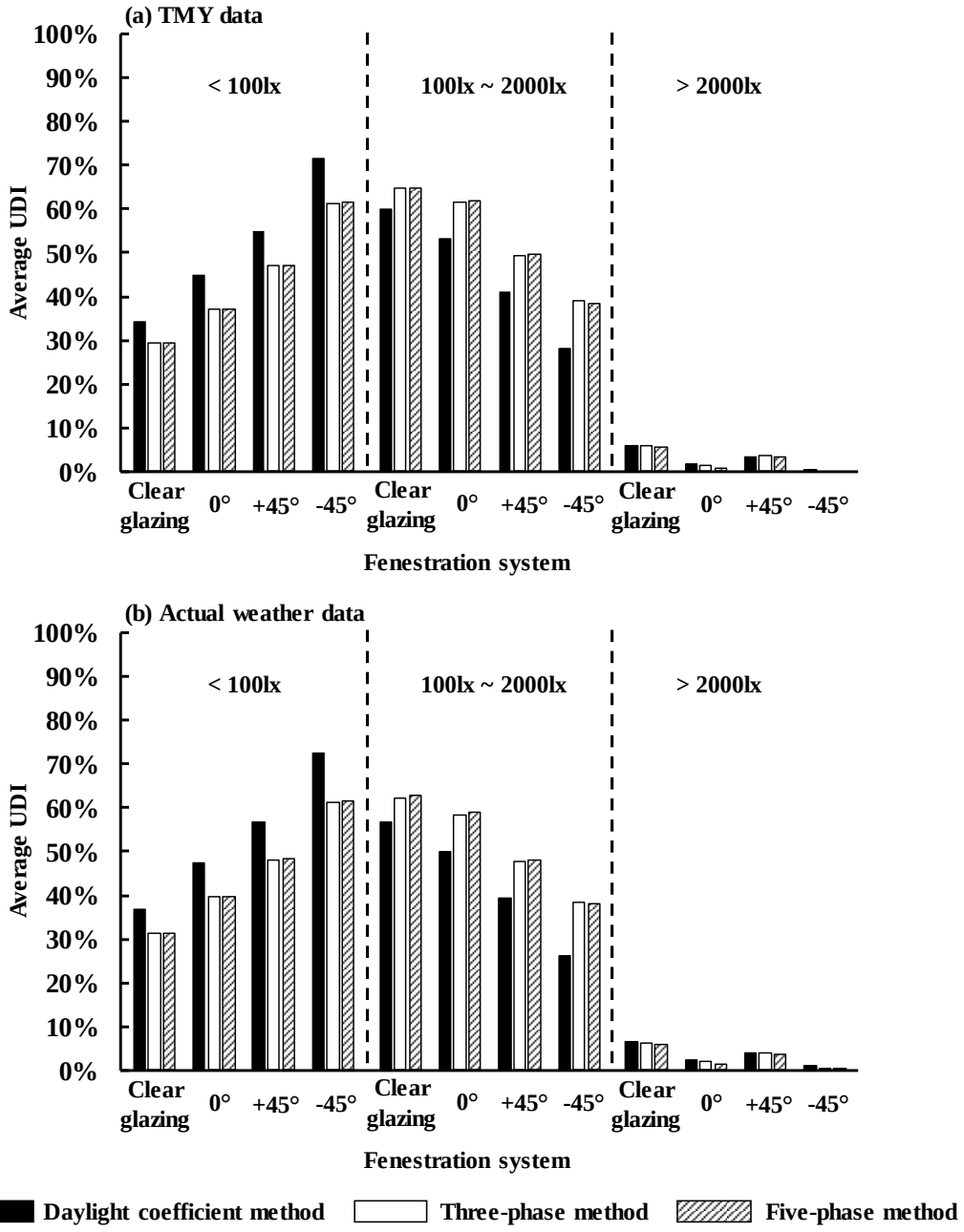

Figure 4.6 Comparison of the average UDI values of all the calculation points that were calculated using the three different simulation methods and the two weather data for each of the four fenestration systems. (a) Average UDI values based on the TMY data; (b) Average UDI values based on the actual weather data.

4.3.3 cDA_{500} and Possible Energy Saving of A Daylight-responsive Dimming Control System

Since the target illuminance was set to 500 lx for the classroom, cDA_{500} at each calculation point was calculated using the three different simulation methods and two

weather data. Similar to the averaged UDI values, the cDA_{500} values were not affected by the two weather data but the different simulation methods. As shown in Figure 4.7, the daylight coefficient method always resulted in lower daylight illuminance values in the areas that were further away from the windows. Though the cDA_{500} generally characterized the frequency of the daylight illuminance at each calculation point beyond 500 lx, it gave partial credits to the calculation points when the daylight illuminance was lower than 500 lx, which correlated well to the potential energy savings of the daylight-responsive dimming control system (DiLaura et al., 2011).

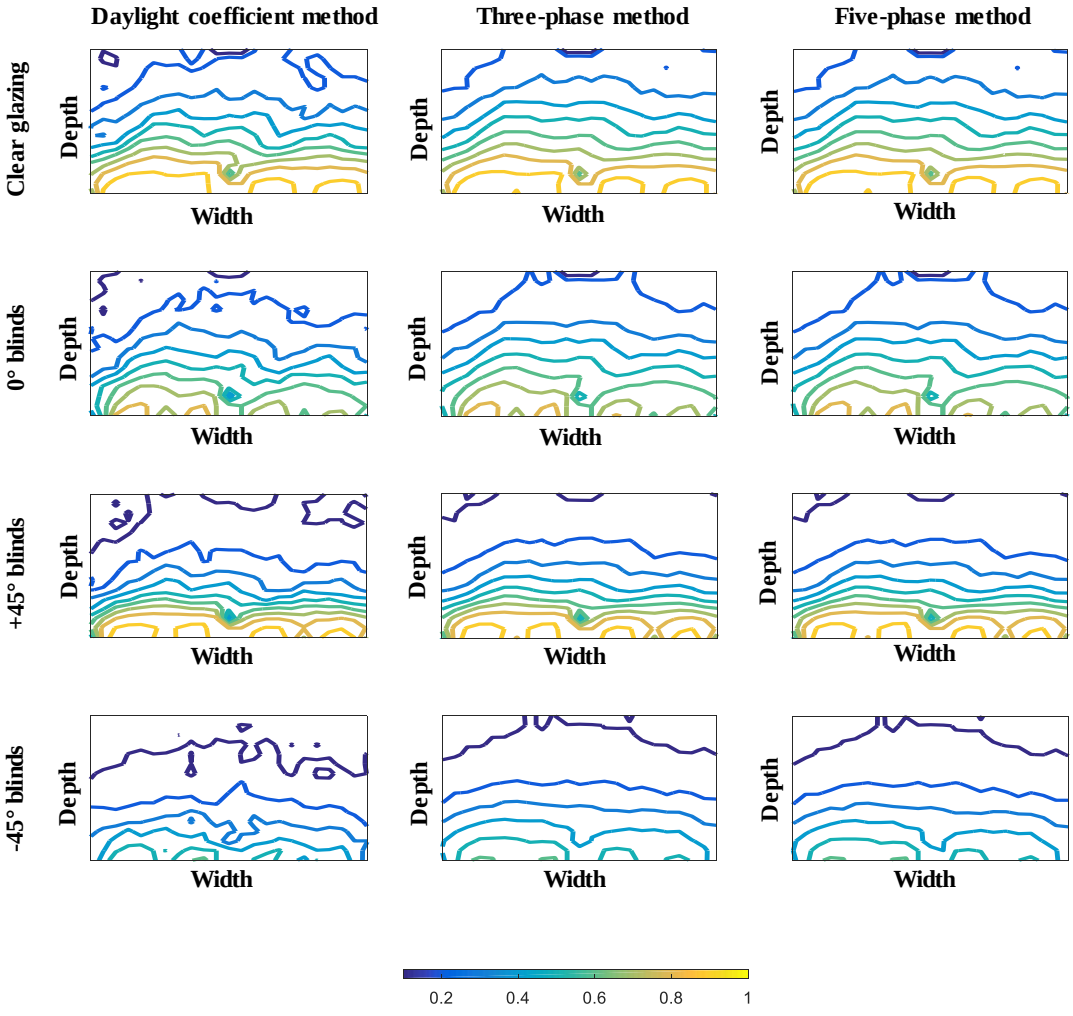

(a) TMY data

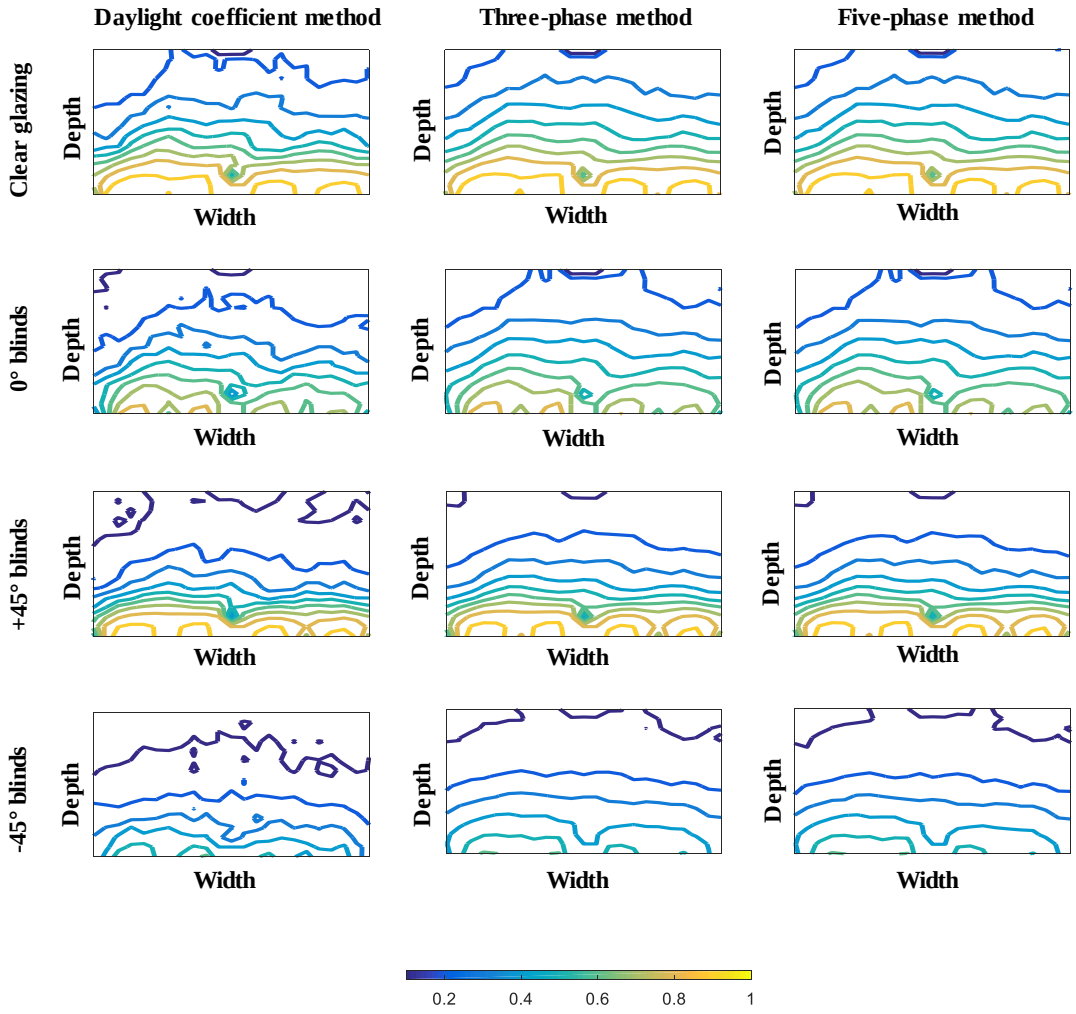

(b) Actual weather data

Figure 4.7 Comparison of the cDA_{500} values across the workplane of the classroom that were calculated using the three different simulation methods and the two weather data for each of the four fenestration systems. (a) TMY data; (b) Actual weather data.

4.3.4 Average Daylight Illuminance

The average daylight illuminance on the workplane was derived using the different simulation methods and weather data for the different fenestrations throughout an entire year. As shown in Figure 4.8, the daylight illuminance derived using the daylight coefficient method was generally lower than those using the three- and five-phase methods, which also explained why the $sDA_{300/50\%}$ and UDI values were lower. Such a lower illuminance was more obvious to the calculation points that were further away from the windows when a CFS (e.g., 0° blinds) was used, as shown in Figure 4.9. This

was because the three- and five-phase methods were more efficient to characterize the transmitted daylight from the blinds to the calculation points compared to the daylight coefficient method by considering more light bounces.

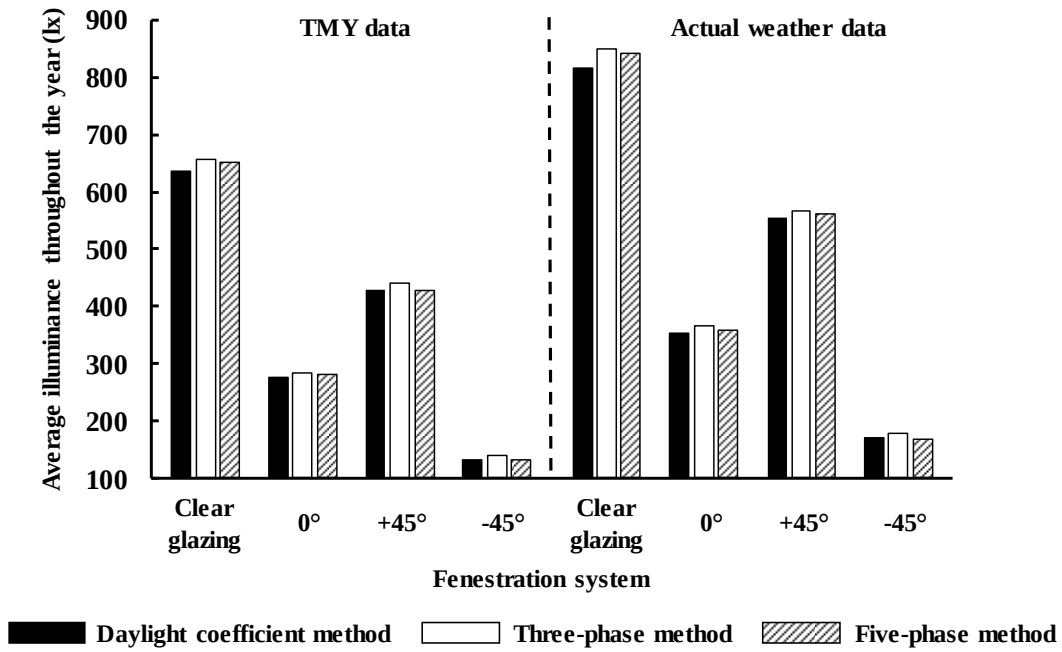

Figure 4.8 Comparison of the average daylight illuminance that was calculated using the different simulation methods and the two weather data throughout the entire year for each of the four fenestration systems.

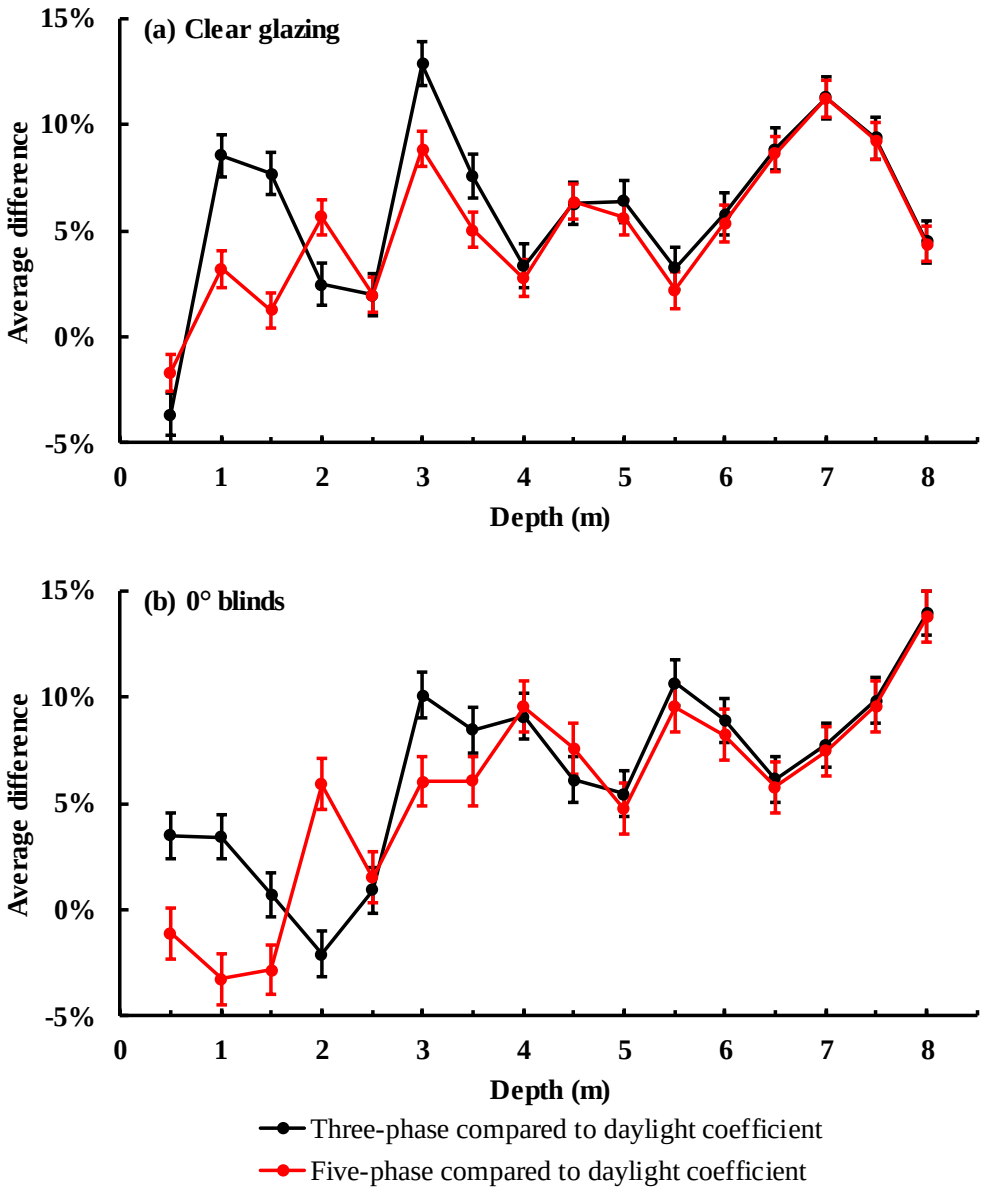

Figure 4.9 Comparison of the average difference of illuminance throughout the entire year at different room depths between the different simulation methods (i.e., the daylight coefficient method versus the three-phase method, and the daylight coefficient method versus the five-phase method) for the two fenestration systems. (a) Clear glazing; (b) 0° blinds.

Though the two weather data did not produce a large difference to the measures, such as $sDA_{300/50\%}$, $ASE_{1000,\ 250h}$, UDI, and cDA_{500}, the average daylight illuminance of the classroom derived using the actual weather data was around 30% higher than that using the TMY data, which was consistent with the difference between the vertical daylight illuminance on the exterior of the windows derived using the two weather data. Such a difference suggested that the TMY data may underestimate the amount of daylight

in the classroom. Thus, a daylight-responsive dimming control system was likely to achieve a greater energy saving in the real conditions than the predictions based on the TMY data.

4.4 Design of A Closed-loop Daylight-responsive Dimming Control System

A closed-loop daylight-responsive dimming control system was designed for each of the four fenestration systems (i.e., clear glazing, 0°, and ±45° blinds) in the classroom. According to a common practice in industry, the TMY data was used to select the important parameters of the system, such as the workplane calibration point, photosensor location, and calibration hours, and to predict the performance of the system.

4.4.1 Selection of A Calibration Point on Workplane and A Photosensor Location on Ceiling

The illuminance at any calculation point at any time is the sum of daylight illuminance and the illuminance of the electric light from the non-dimmed and dimmed zone, which can be expressed as Eq. (4.1) (Mistrick et al., 2015):

$$E = E_{daylight} + E_{non-dimmed\ zone} + E_{dimmed\ zone} \times DL \quad (4.1)$$

Where:

E: The illuminance at each point;

$E_{daylight}$: The daylight illuminance at each point;

$E_{non\text{-}dimmed\ zone}$: The electric light illuminance from the non-dimmed zone at each point;

$E_{dimmed\ zone}$: The electric light illuminance from the dimmed zone with a dimming level of 100% at each point;

DL: The dimming level of the dimmed zone.

A daylight-responsive dimming control system adjusts the dimming level of electric light from the dimmed zone based on the amount of daylight detected by the photosensor installed on the ceiling, so that the light level can reach the target illuminance level (Mistrick et al., 2005; Mistrick et al., 2015). Therefore, the optimal dimming level of the dimmed zone at a certain time was calculated for each calculation point by replacing E with E_{target} (i.e., 500 lx) in Eq. (4.1). The calculation point that had the highest optimal dimming level of the dimmed zone was selected as the *critical point* at that time, since the illuminance at all the other calculation points would be higher than the target illuminance level (i.e., 500 lx) with such a dimming level. Though the location of the *critical point* varies with times, the system calibration is typically performed at a single point. Thus, the calculation point, which was the point being most frequently selected as the *critical point* throughout the entire year, was selected as the *workplane calibration point*. Figure 4.10 shows the locations of the *workplane calibration point* that was derived using the different simulation methods for the four different fenestration systems (note: since the *workplane calibration point* derived using the daylight coefficient method for the -45° blinds setting was out of the dimmed lighting zone, requiring a higher dimming level to achieve the target illuminance level at this *workplane calibration point*, only the three- and five-phase methods were used to derive the *workplane calibration point*).

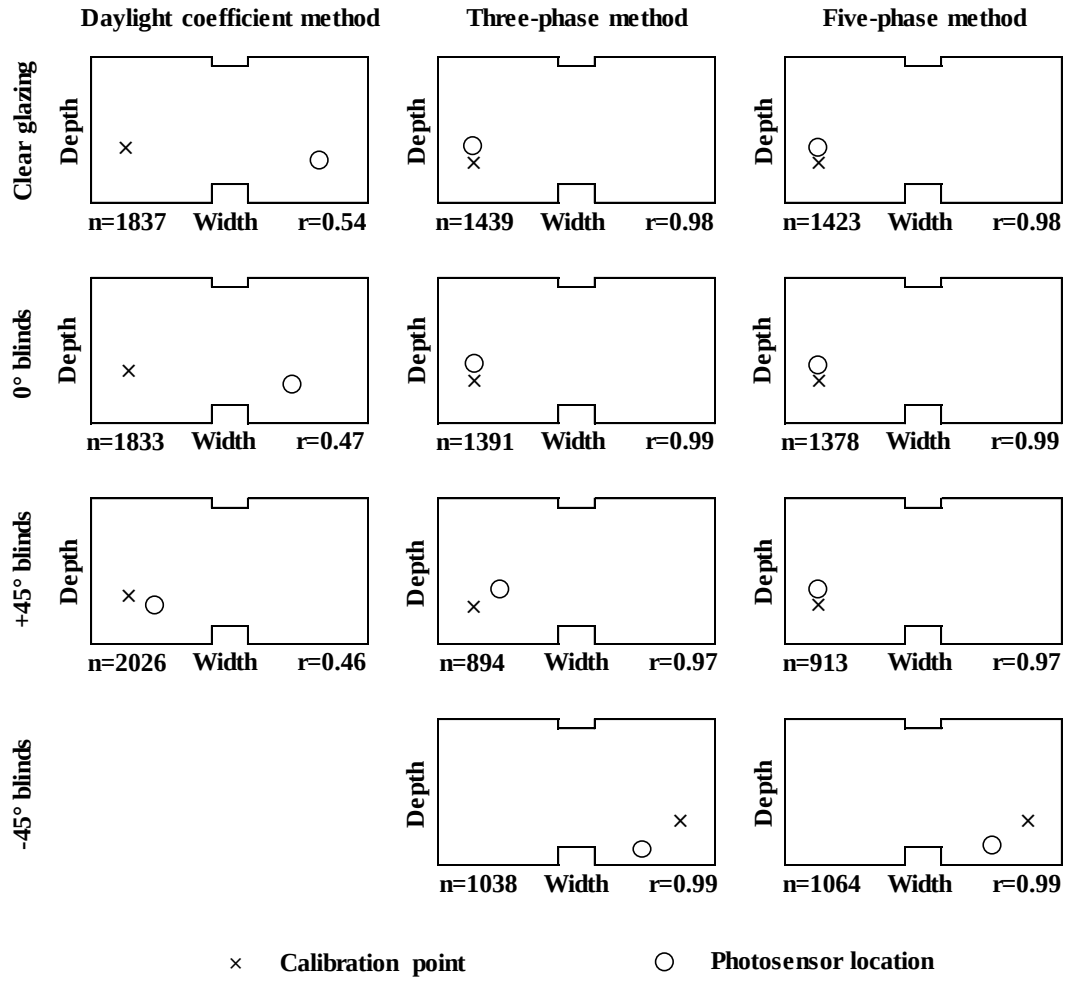

Figure 4.10 Locations of the workplane calibration point and the ceiling-mounted photosensor based on the different simulation methods for each of the four fenestration systems, with n indicating the frequency that this location was the critical point and r indicating the correlation between the illuminance at the photosensor and that at the workplane calibration point throughout the entire year.

Since a photosensor detecting the amount of light directly decides the actual dimming level of the dimmed zone, the placement of the photosensor significantly affects the performance of a daylight-responsive dimming control system (Kim et al., 2001; Doulos et al., 2014). Though it is ideal that a photosensor can be installed at the calibration point on a workplane, it is always installed on the ceiling in practice. For determining the photosensor location, a grid of points facing down, with a spacing of 0.25 m, was placed 0.02 m below the ceiling. The point where the daylight illuminance values had the highest correlation to those at the *workplane calibration point* was

selected as the photosensor location. Figure 4.10 shows the photosensor locations that were derived using the different simulation methods for the four different fenestrations. It can be seen that the daylight coefficient method caused much lower correlations than the other methods. Coupled with the significant difference introduced in the daylight calculation results, as shown in Figure 4.9, the daylight coefficient method was not used in the following analyses.

4.4.2 Selection of System Calibration Time

Figure 4.11 shows an example of a scatter plot of the optimal dimming level calculated using Eq (4.1) versus the signal detected by a photosensor. The signal values are the sum of the signals due to the daylight and the electric light in both the dimmed (with the optimal dimming level) and the non-dimmed zones. The daylight-responsive dimming control system, however, does not work optimally in reality. It follows a calibration line to adjust the dimming level proportionally based on the photosensor signal, with the calibration line being decided based on the two calibration conditions. The night-time calibration typically happens with the maximum dimming level when there is no daylight; the day-time calibration happens when the dimming level is low. Therefore, the day-time calibration significantly affects the performance of the system. Those points above the calibration line represent the over-dimming conditions that the actual dimming level is below the optical dimming level, while those below the calibration line represent the under-dimming conditions that the actual dimming level is higher than the optical dimming level.

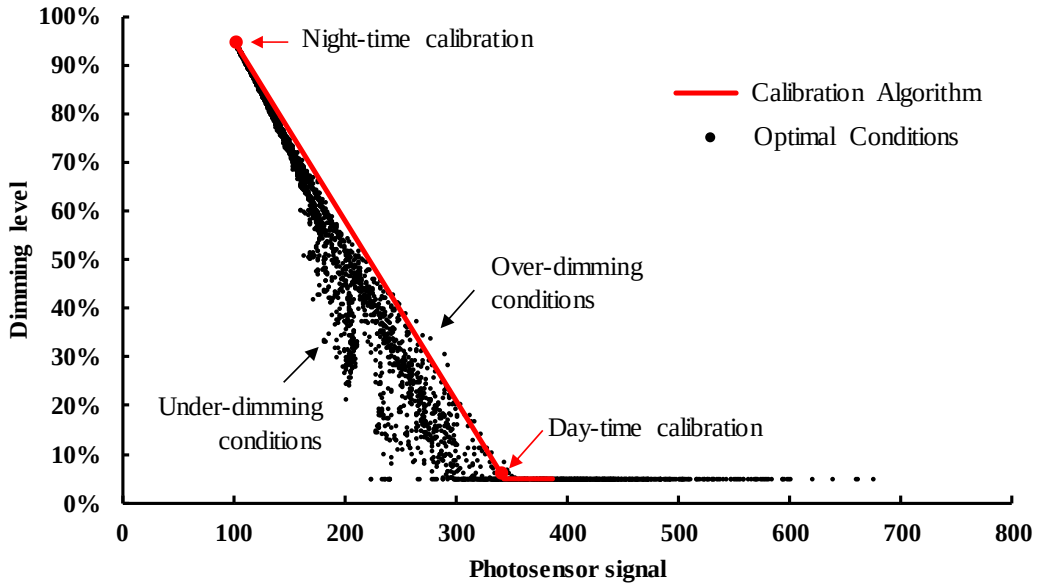

Figure 4.11 Illustration of a closed-loop daylight-responsive dimming control algorithm. The scattered points represent the optimal dimming levels that were calculated based on the illuminance at the workplane calibration point; the red line represents the algorithm which the dimming control actually follows. The points above the calibration line are the over-dimming conditions when the actual illuminance is lower than the target illuminance; the points below the calibration line are the under-dimming conditions when the actual illuminance is higher than the target illuminance.

Two criteria were adopted for selecting the day-time calibration time. One is to limit the occurrence of over-dimming conditions below 2% of the occupied period, and the other is to minimize the difference between the actual and optimal dimming levels, as characterized using the root mean square error (RMSE) (Mistrick et al., 2000; Chen, 2013; Subramaniam et al., 2013). Table 4.1 summarizes the day-time calibration times that were selected for each fenestration system using the three- and five-phase methods, together with the corresponding RMSE values, the percentage of the over-dimming conditions, and dimming levels at the calibration time. It is worthwhile to mention that it was difficult to limit the percentage of the over-dimming condition below 2% for the -45° blinds, since the blinds frequently reflected daylight to the photosensor. Thus, only two day-time calibration times were selected with the minimal occurrence of the over-dimming conditions for the -45° blinds. As shown in Table 4.1, the different

simulation methods and fenestration systems required different day-time calibration times.

Table 4.1 Summary of the day-time calibration times selected for the four fenestration systems using the two simulation methods, together with the RMSE values, the percentage of the over-dimming conditions, dimming levels at the calibration time, the photosensor illuminance, the average predicted dimming levels throughout the entire year, and the average optimal dimming levels, which were all selected and calculated using the TMY data.

	Clear glazing			**0° blinds**			**+45° blinds**			**-45° blinds**	
Calibration Time	25-Mar 9:30 AM	14-Apr 9:30 AM	5-Jul 9:30 AM	16-May 11:30 AM	19-Sep 12:30 PM	20-Sep 12:30 PM	7-Jan 9:30 AM	23-Dec 9:30 AM	24-Dec 9:30 AM	29-Apr 2:30 PM	8-Oct 2:30 PM
RMSE	9.3%	9.2%	9.2%	6.6%	6.6%	6.5%	9.6%	9.8%	9.9%	12.1%	12.0%
Over-dimming	1.67%	1.77%	1.67%	1.79%	1.88%	1.98%	1.85%	1.70%	1.62%	5.30%	5.68%
DL @ Calibration Time	7.55%	6.15%	7.09%	6.10%	8.47%	9.39%	9.62%	5.74%	5.67%	7.03%	5.33%
Photosensor Illuminance	332.06	334.94	332.56	319.67	313.54	310.63	368.92	383.41	384.61	311.78	274.33
Average Predicted DL*	51.64%	51.56%	51.57%	58.02%	57.99%	57.92%	70.25%	70.41%	70.47%	65.25%	65.16%
Average Optimal DL*		46.19%			53.89%			63.74%			61.26%
Calibration Time	9-Jan 9:30 AM	25-Mar 9:30 AM	27-Sep 8:30 AM	8-Jan 9:30 AM	16-May 11:30 AM	16-Jul 11:30 AM	10-Apr 9:30 AM	15-Apr 9:30 AM	27-Apr 8:30 AM	8-Oct 2:30 PM	11-Nov 2:30 PM
RMSE	9.4%	9.3%	9.4%	6.7%	6.7%	6.7%	10.4%	10.3%	10.4%	11.2%	11.3%
Over-dimming	1.90%	1.97%	1.52%	1.87%	1.87%	1.93%	1.18%	1.21%	1.15%	5.22%	5.08%
DL @ calibration time	9.04%	7.67%	5.10%	6.45%	6.54%	6.45%	9.32%	7.56%	5.33%	5.33%	6.45%
Photosensor Illuminance	382.52	331.91	339.67	322.00	321.64	321.76	348.18	351.60	359.24	244.53	249.40
Average Predicted DL*	51.69%	51.67%	51.75%	58.23%	58.21%	58.20%	70.73%	70.61%	70.70%	61.43%	61.48%
Average Optimal DL*		46.27%			54.04%			63.90%			62.07%

4.4.3 Prediction of Potential Energy Savings of the System

Ideally, the maximal potential energy savings achieved by the daylight-responsive dimming system throughout the entire year can be predicted based on the difference between the 100% dimming level and the average optimal dimming level of a year. The former can be calculated when the electric lights are set to 100% output, the latter can be calculated when the target illuminance (i.e., 500 lx) at the *workplane calibration point* is maintained throughout the entire year, as listed in Table 4.1. However, the illuminance at the *workplane calibration point* cannot always be maintained in reality, since the dimming level is decided by the calibration line (Eq. (4.2)) and the signal received by the photosensor (Eq. (4.3)).

$$DL = S_{photosensor} \cdot k + b \tag{4.2}$$

$$S_{photosensor} = S_{daylight} + S_{non-dimmed\ zone} + S_{dimmed\ zone} \times DL \tag{4.3}$$

Where:

DL: The dimming level of the dimmed zone;

$S_{\text{photosensor}}$: The photosensor signal, with the sum of the daylight illuminance (S_{daylight}), the illuminance from the non-dimmed zone ($S_{\text{non-dimmed zone}}$), and the illuminance from the dimmed zone with the dimming level *DL* ($S_{\text{dimmed zone}} \times DL$);

k and *b*: Two parameters for describing the slope and intercept of the calibration line.

The actual dimming level at a certain time can be calculated by solving Eqs. (4.2) and (4.3) simultaneously. The predicted dimming levels, as listed in Table 4.1, were calculated using the illuminance values derived based on the TMY data. It can be seen that the average predicted dimming levels were slightly higher than the average optimal dimming levels, which suggested that the target illuminance (i.e., 500 lx) at the *workplane calibration point* was not always be maintained throughout the entire year.

Thus, the potential energy savings achieved by the daylight-responsive dimming control system throughout the entire year were predicted based on the average predicted dimming levels, with around 48%, 42%, 30%, and 38% for the clear glazing, 0°, and ±45° blinds systems, as shown in Figure 4.12. It was found that the two simulation methods and the calibration times had little impact on the energy saving prediction.

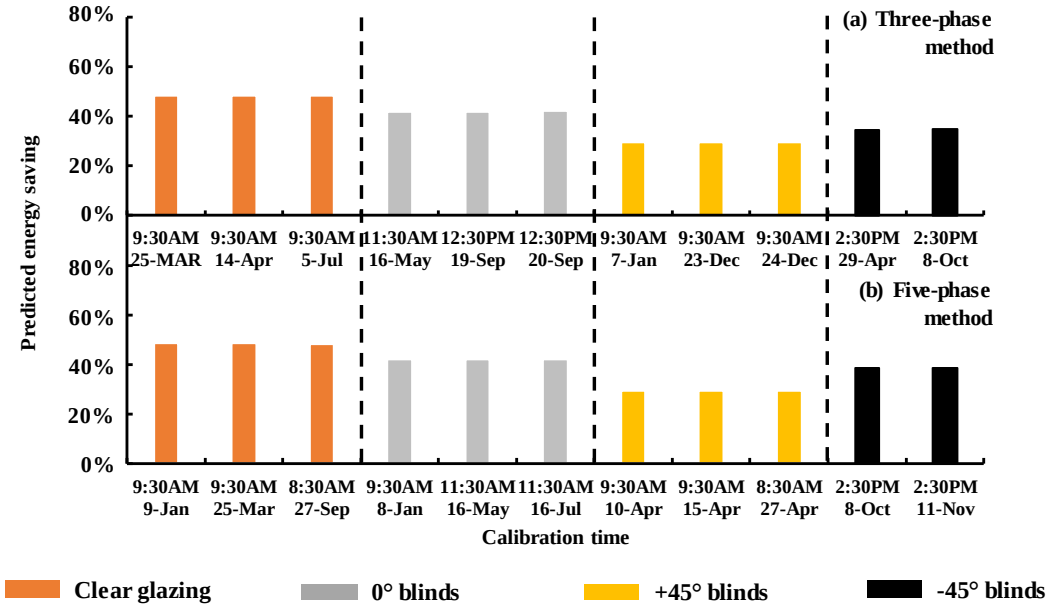

Figure 4.12 Predicted energy savings achieved by the closed-loop daylight-responsive dimming system throughout the entire year for the different fenestration systems using the different simulation methods. The predictions were made based on the illuminance values derived using the TMY data and the calibration conditions selected based on the TMY data. (a) Three-phase method; (b) Five-phase method.

4.5 Actual Performance of the Closed-loop Daylight-responsive Dimming Control System

The actual performance of the system was investigated using the actual weather data with a one-minute interval. Though the TMY data is commonly used to select the calibration times, which are considered to have appropriate daylight conditions for performing the calibration, the actual calibration can be performed at any time within the selected calibration hour without considering the actual weather condition in practice. At a certain time within the selected calibration hour, the dimming level is adjusted to achieve the target illuminance (i.e., 500 lx) at the *workplane calibration point*. Therefore, the dimming level was calculated based on the illuminance at the *workplane calibration point* for each minute within each selected calibration hour, as if the system was calibrated at that specific time.

As shown in Figures 4.13-4.16, the dimming levels for calibrating the system were found to have large variations within each selected calibration hour. Due to the excessive amount of daylight, some periods within the selected calibration hours or even the entire hours were found not appropriate for calibrating the system, as shown in Figure 4.17.

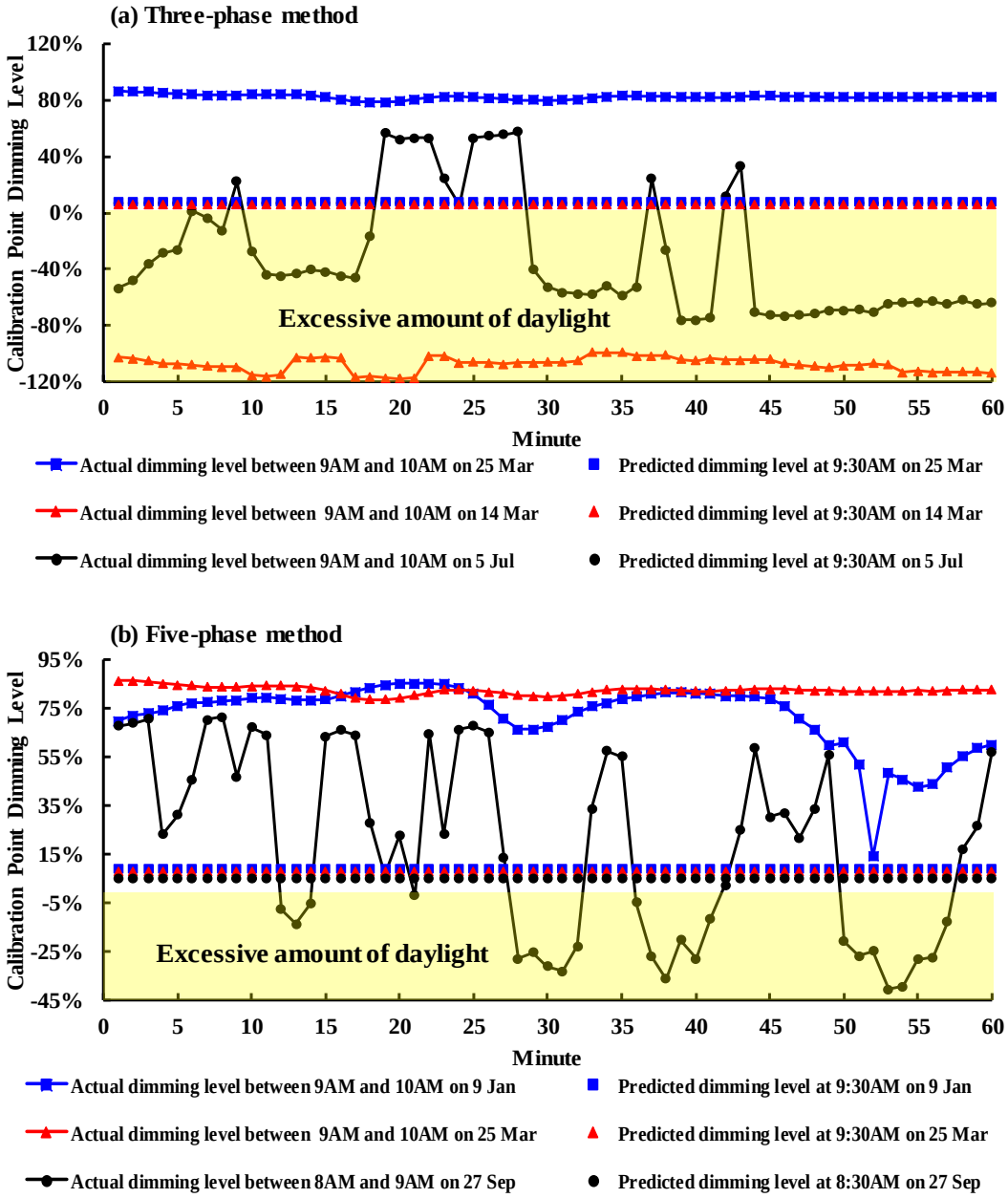

Figure 4.13 Predicted dimming levels and the actual dimming levels for performing the system calibration with the clear glazing. The predicted dimming levels were calculated using the TMY data at the calibration hour that was selected using the TMY data; the actual dimming levels were calculated using the actual weather data at each minute within the calibration hour that was selected using the TMY data. (note: the yellow region indicates that the daylight illuminance was too high so that the calibration cannot be performed). (a) Three-phase method; (b) Five-phase method.

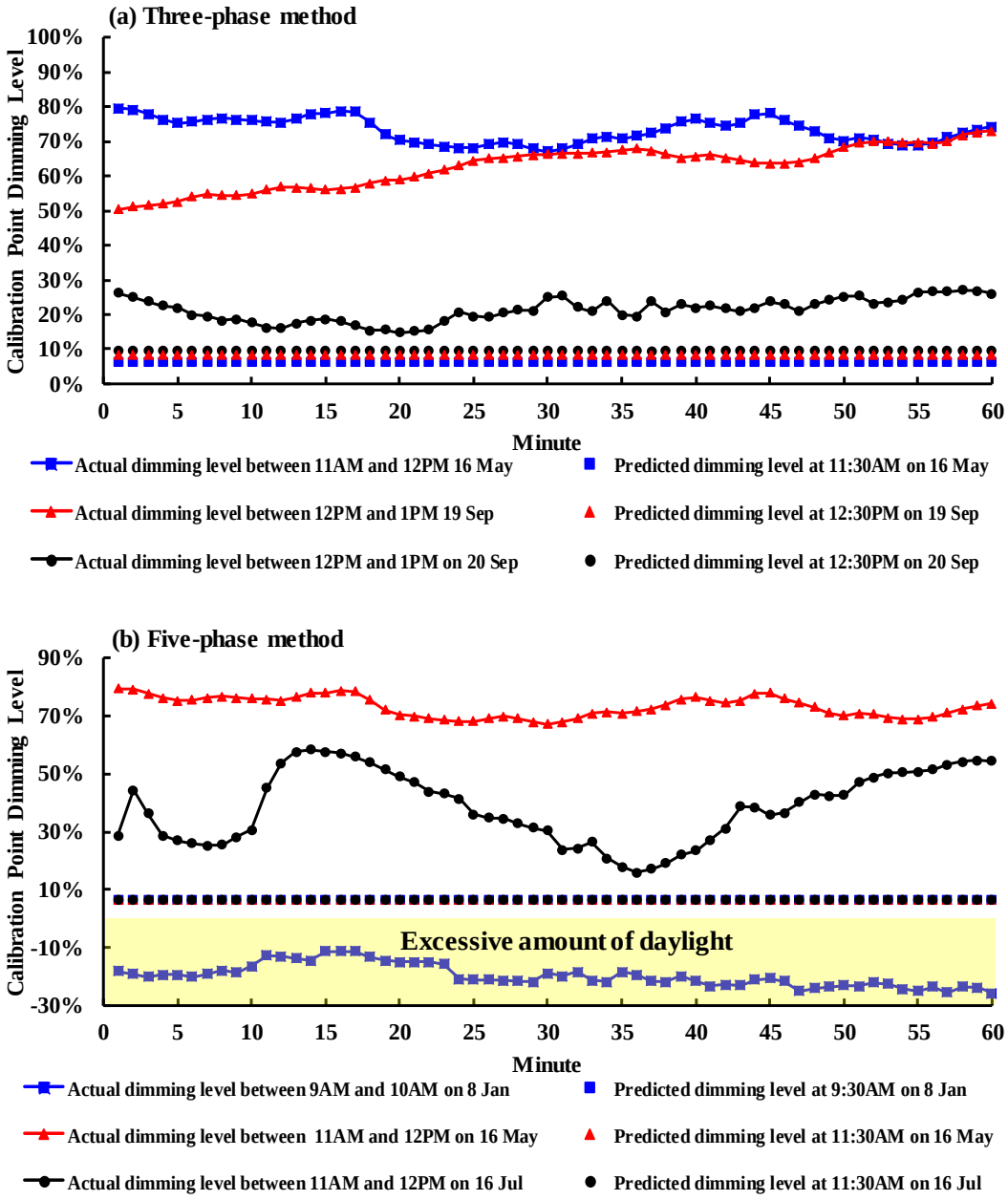

Figure 4.14 Predicted dimming levels and the actual dimming levels for performing the system calibration with the 0° blinds. The predicted dimming levels were calculated using the TMY data at the calibration hour that was selected using the TMY data; the actual dimming levels were calculated using the actual weather data at each minute within the calibration hour that was selected using the TMY data. (note: the yellow region indicates that the daylight illuminance was too high so that the calibration cannot be performed). (a) Three-phase method; (b) Five-phase method.

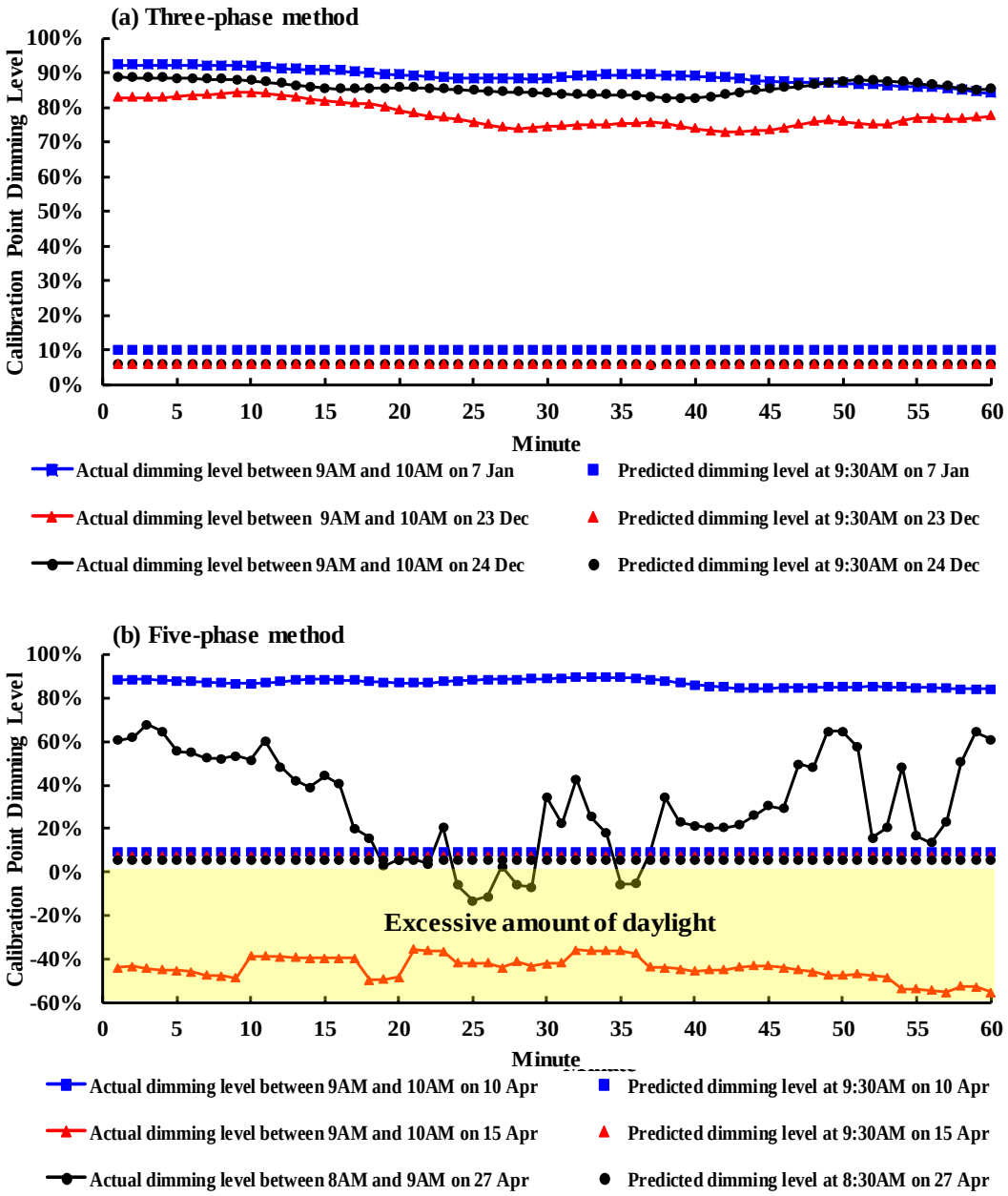

Figure 4.15 Predicted dimming levels and the actual dimming levels for performing the system calibration with the +45° blinds. The predicted dimming levels were calculated using the TMY data at the calibration hour that was selected using the TMY data; the actual dimming levels were calculated using the actual weather data at each minute within the calibration hour that was selected using the TMY data. (note: the yellow region indicates that the daylight illuminance was too high so that the calibration cannot be performed). (a) Three-phase method; (b) Five-phase method.

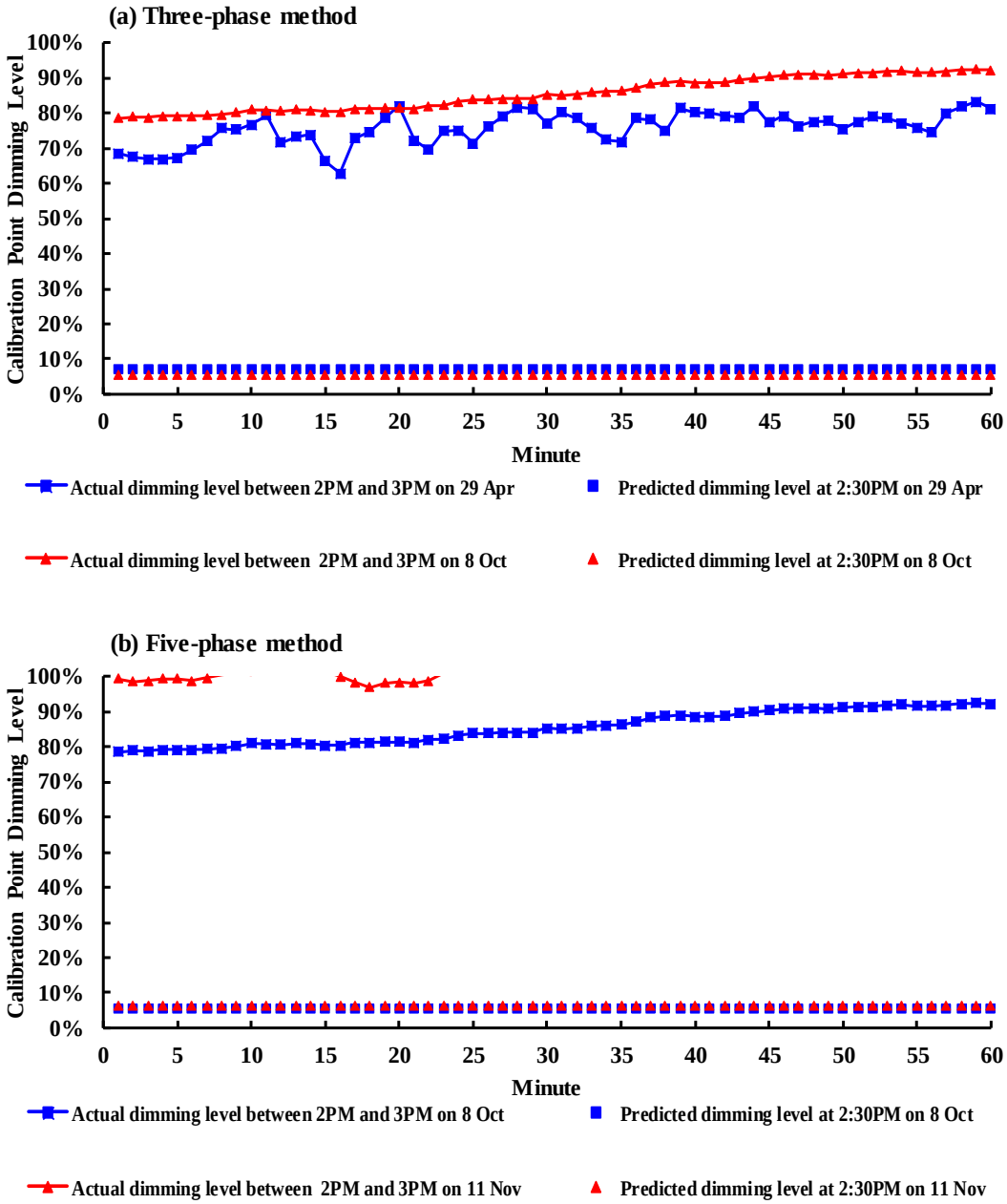

Figure 4.16 Predicted dimming levels and the actual dimming levels for performing the system calibration with the -45° blinds. The predicted dimming levels were calculated using the TMY data at the calibration hour that was selected using the TMY data; the actual dimming levels were calculated using the actual weather data at each minute within the calibration hour that was selected using the TMY data. (a) Three-phase method; (b) Five-phase method.

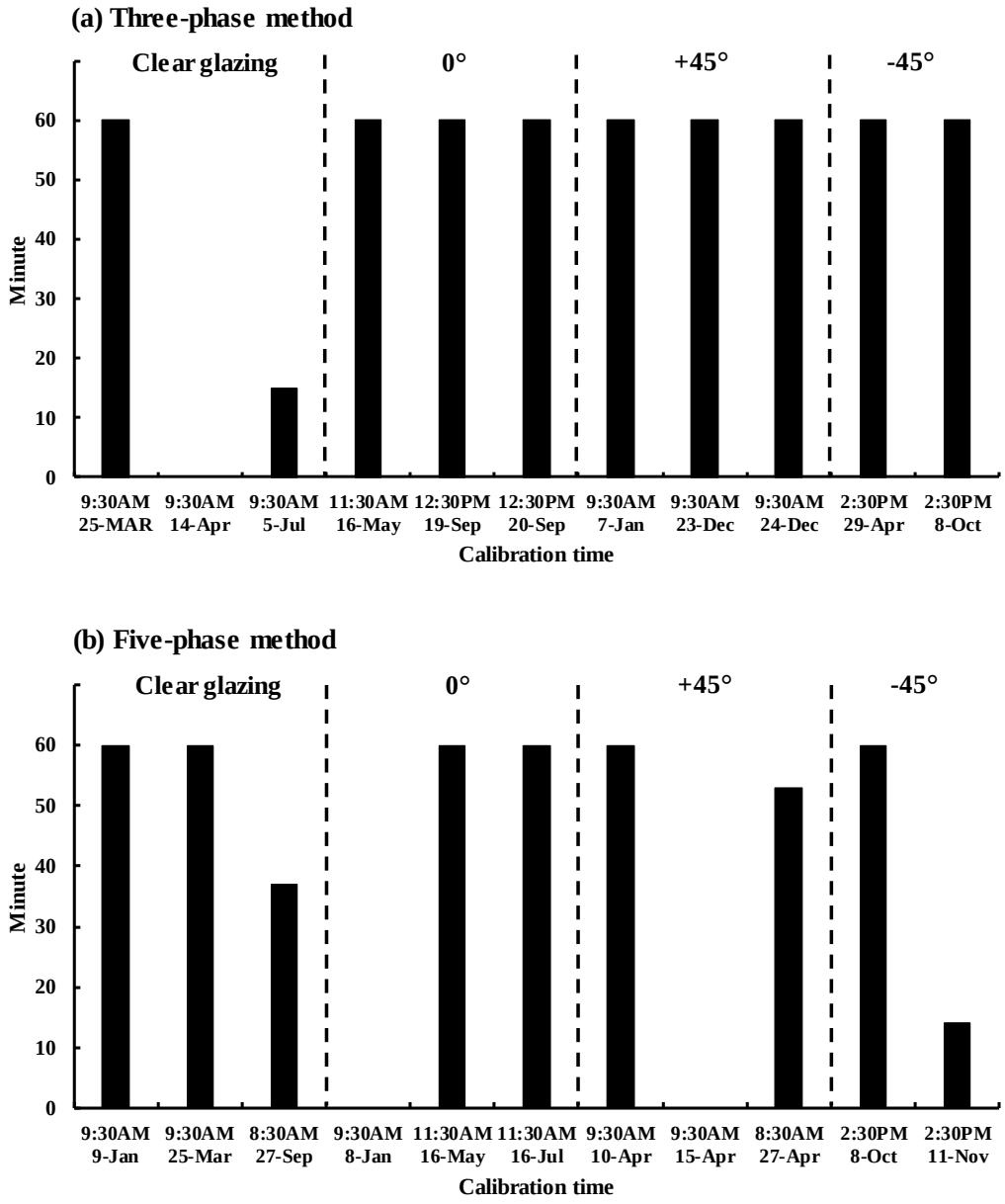

Figure 4.17 Number of minutes within each selected calibration hour that were appropriate for performing system calibration. (a) Three-phase method; (b) Five-phase method.

For each minute within the selected calibration hours that allowed the calibration of the system, the corresponding calibration line correlating the dimming levels and the photosensor signals derived using Eq. (4.2), as if the system was calibrated at that minute. The actual dimming level at each minute throughout the entire year was then calculated by solving Eqs. (4.2) and (4.3) simultaneously, as described in Section 4.4.3, which allowed to calculate the actual energy savings achieved by the system and the occurrence of actual over-dimming conditions throughout the entire year.

As shown in Figure 4.18, the actual energy savings calculated based on the actual calibration minutes within the selected calibration hours, in comparison to the predicted energy savings calculated based on the selected calibration hours, were found to have large differences, which can be as high as 15%. In addition, the occurrence of the over-dimming conditions was significantly affected by the actual calibration minutes within the selected calibration hours, as shown in Figure 4.19. For example, the frequency of the over-dimming conditions varied a lot when performing the calibration of the system between 8 and 9 AM on Sep 27th, ranging from 17.2% to 71.1%. More importantly, though the calibration hours were selected to limit the frequency of the over-dimming conditions below 2% in the entire year, the over-dimming conditions were found to happen much more frequently. This was especially more serious to the case using the -45° blinds system, since the blinds reflected daylight to the ceiling and increased the photosensor signals.

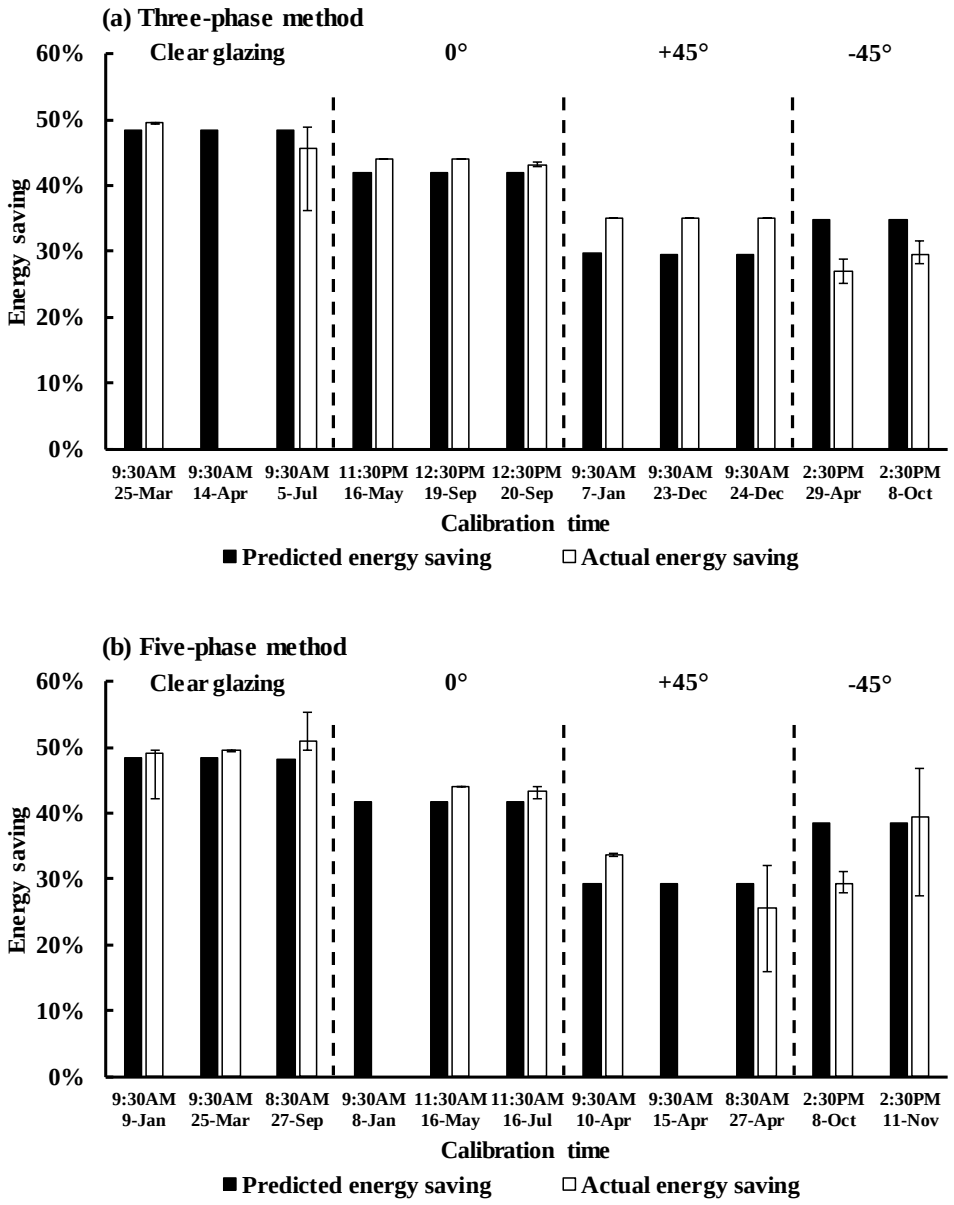

Figure 4.18 Differences between the energy saving predicted using the TMY data and the actual energy saving calculated using the actual weather data with the system being calibrated at different minutes within the calibration hours. The error bars represent the variations that were caused by performing the calibration at different minutes within the calibration hours. The two empty bars suggest that the entire 60 minutes within these two hours were not appropriate for performing system calibration due to the excessive amount of daylight at the workplane calibration points. (a) Three-phase method; (b) Five-phase method.

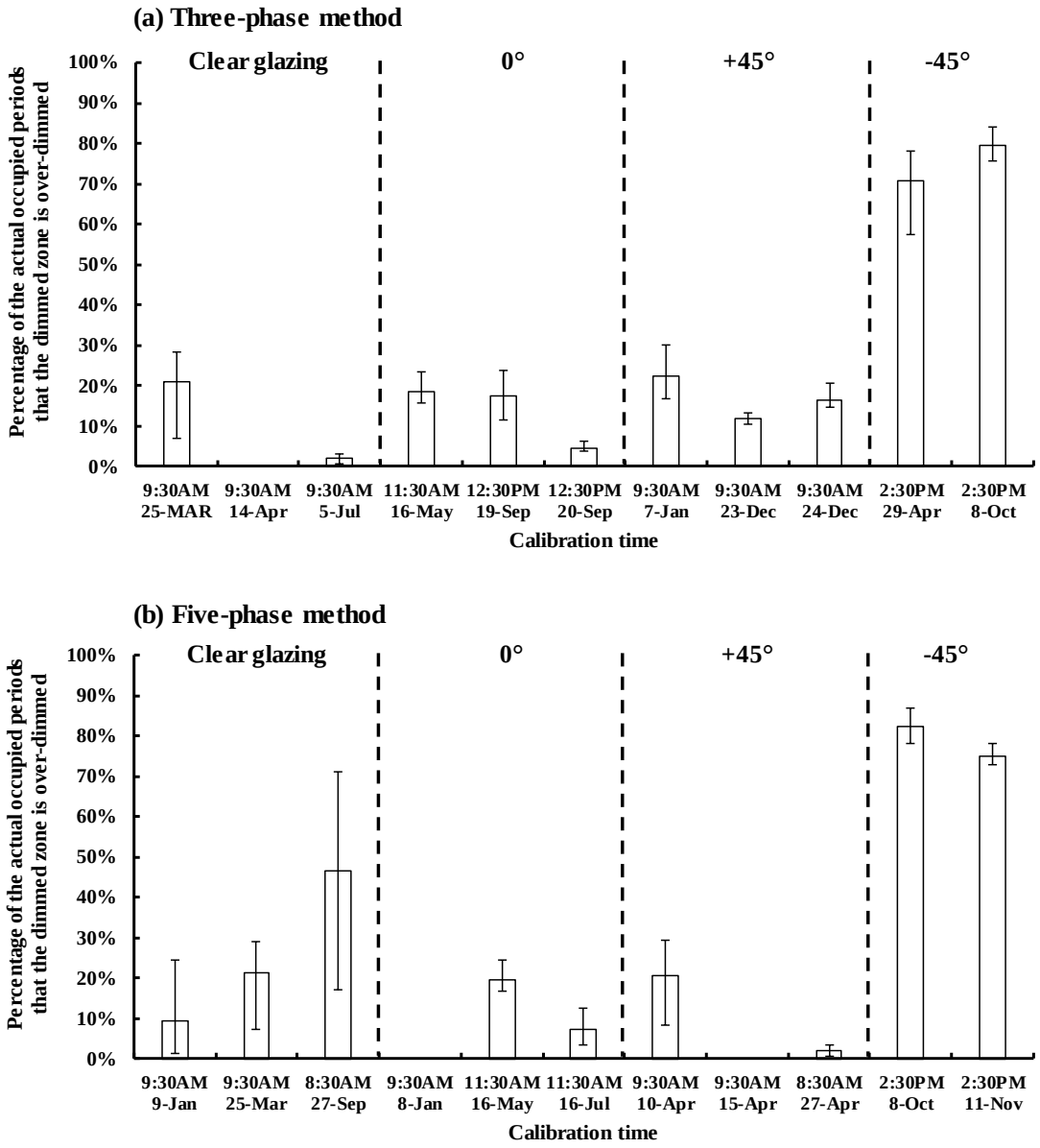

Figure 4.19 Frequencies of the over-dimming conditions calculated using the actual weather data with the system being calibrated at different minutes within the calibration hours. The error bars represent the variations that were caused by performing the calibration at different minutes within the calibration hours. The calibration hour was selected to limit the frequency of the over-dimming conditions to below 2% in the entire year using the TMY data (See Table 4.1). (a) Three-phase method; (b) Five-phase method.

The differences between the predicted and actual performance of the system were likely due to the different weather conditions, since the weather conditions at the actual calibration minutes within the selected calibration hours were different from those at the selected calibration hours in the TMY data. As shown in Figure 4.20, the actual weather conditions during the two hours were found not appropriate for performing

the system calibration due to the sunny skies that had high direct solar irradiance levels. Though the actual weather conditions during the 2 to 3 PM on Oct 8th were also sunny skies, they would not cause problems to the calibration of the system due to the direct sunlight blocked by the -45° blinds.

In addition, since the S/E ratio directly determines the slope of the calibration line as shown in Figure 4.11, it is important to investigate the relationship between the weather conditions and the S/E ratio (Mistrick et al., 2015; Chen, 2013). The S/E ratios derived at the selected calibration hours and at the actual calibration minutes within the selected calibration hours are shown in Figure 4.21. It was found that the calibration hours selected based on the TMY data generally had similar S/E ratios. Though nine of the eleven actual calibration minutes had similar S/E ratios as the selected calibration hours, the actual performance of the system was still not as good as the predicted performance.

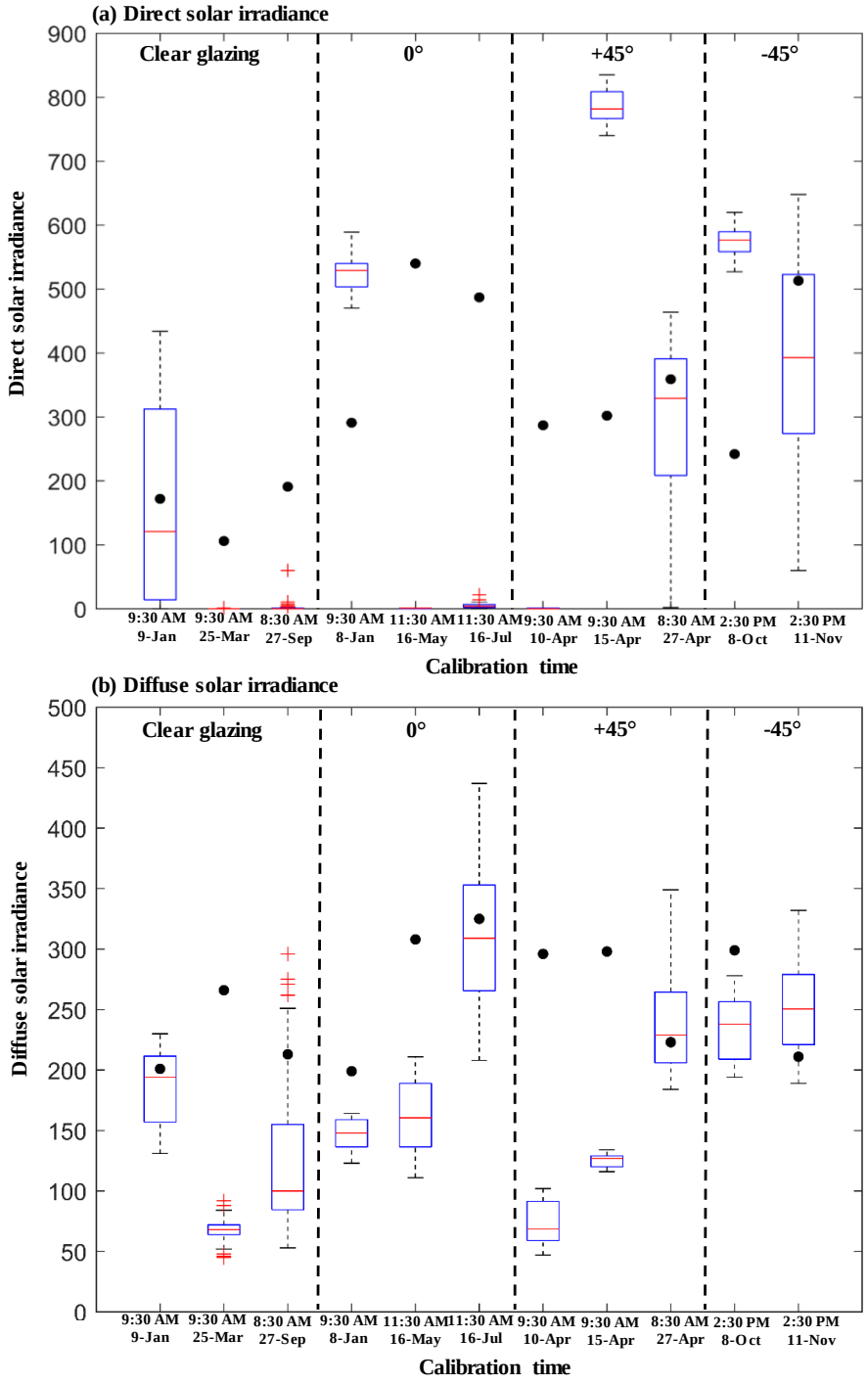

Figure 4.20 Comparisons of the weather conditions between the calibration times in the actual weather data and the calibration hours selected using the TMY data. The circles represent the weather conditions at the selected calibration hours in the TMY data; the boxplots represent the weather conditions at the minutes within the selected calibration hours in the actual weather data. (a) Direct solar irradiance; (b) Diffuse solar irradiance.

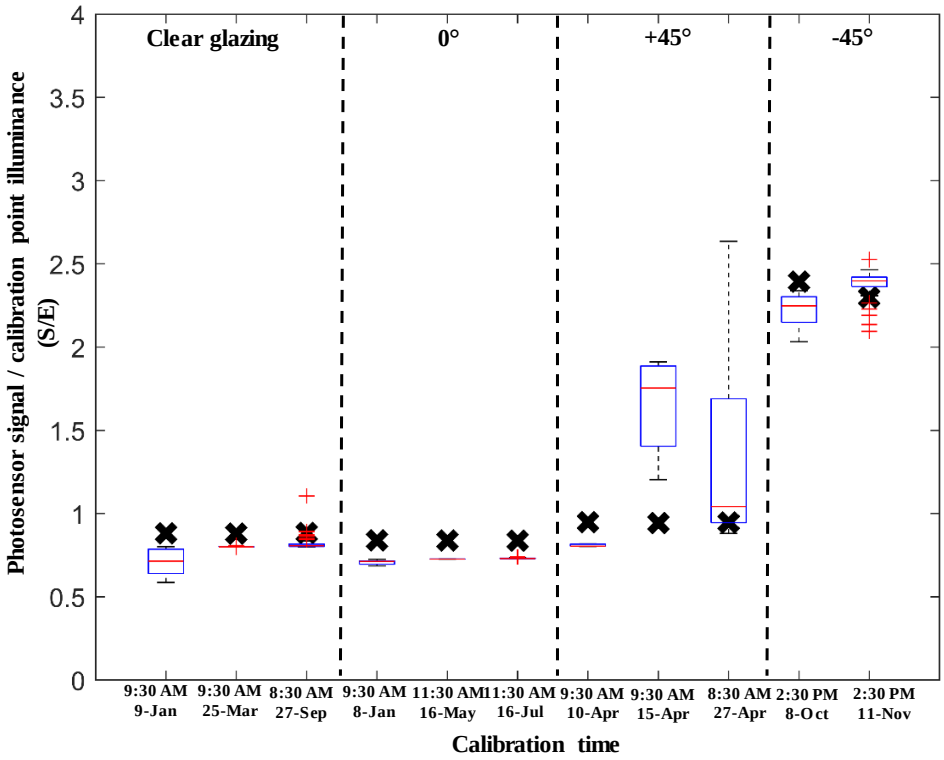

Figure 4.21 Comparison of the S/E ratios between the minutes within the selected calibration hours in the actual weather data and the selected calibration hours in the TMY data. The crosses represent the TMY calibration time; the boxplots represent the actual weather data.

Therefore, the differences between the predicted and actual performance of the system are mainly due to the variations of the weather conditions within each selected calibration hour. As shown in Figure 4.22 (a) and (b), though the boxplots of the S/E ratios were generally similar between the TMY data and the actual weather data with a one-minute interval, regardless of the fenestration systems, the actual weather data had a lot more outliers that could not be captured by the hourly data in the TMY data. The S/E ratios of these outliers were much higher than those at the calibration hours selected using the TMY data, which caused the over-dimming conditions due to the higher signals detected by the photosensor installed on the ceiling.

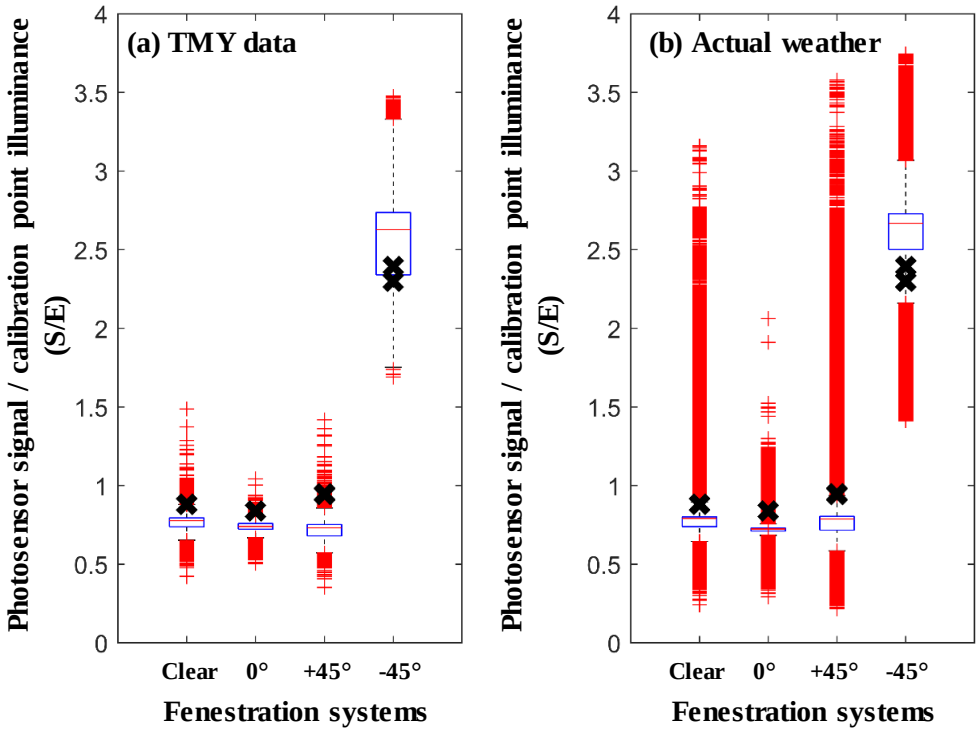

Figure 4.22 Comparisons of the S/E values throughout the entire year between the TMY data and the actual weather data. The crosses represent the values at the hours in the TMY data; the boxplots represent the values in the entire year. (a) TMY data; (b) Actual weather data.

Coupled with the comparisons between the predicted and actual energy savings, the results clearly suggested that the actual calibration of the system should be performed when the actual weather conditions were similar to those at the selected calibration hours in the TMY data. In addition, performing the calibration under the weather conditions that produced higher S/E ratios may be helpful to reduce the frequency of the over-dimming conditions.

4.6 Summary

This study aimed to investigate whether the daylight quantity and quality and the performance of a daylight-responsive dimming control system predicted using the TMY data were comparable to those happened in the real condition. The investigation was performed on a real east-facing classroom equipped with four different

fenestration systems (i.e., clear glazing, 0°, and ±45° venetian blinds) in Hong Kong throughout an entire year. Three daylight simulation methods (i.e., the daylight coefficient, three-phase, and five-phase methods) and two sets of weather data (i.e., the TMY data and the actual weather data with a one-minute interval) were used in the annual daylight simulation.

The two weather data did not introduce significant differences to the daylight quantity and quality of the classroom that were characterized using different CBDM-based measures, such as $sDA_{300/50\%}$, UDI, and cDA_{500}. The average daylight illuminance derived using the actual weather data throughout the entire year, however, were found around 30% higher than those derived using the TMY data, which suggested a possibility to achieve a greater energy saving of a closed-loop daylight-responsive dimming control system.

For the design of the closed-loop daylight-responsive dimming control system, the TMY data was used to select the workplane calibration point, ceiling-mounted photosensor location, and calibration hours. The calibration hours were selected to limit the frequency of the over-dimming conditions below 2% of the occupied period throughout the entire year and to maximize the potential energy savings. The actual energy savings were calculated at every minute within the selected calibration hours derived using the TMY data. It was found that the actual energy savings had large variations compared to the predicted energy savings, which was dependent on the actual calibration times.

In addition, larger variations of the weather conditions in the actual weather data suggested the necessity to perform the calibrations under the weather conditions that were similar to those at the selected calibration hours in the TMY data. Otherwise, the

calibration performed under inappropriate weather conditions would cause lower energy savings (e.g., as high as 15% compared to the predicted energy saving based on the TMY data) and a much higher frequency of the over-dimming conditions (e.g., as high as 86% of the occupied period in a year). It was found beneficial to perform the calibrations under the weather conditions having high S/E ratios, which can help to reduce the frequency of the over-dimming conditions.

Chapter 5

Study 1-2: Impact of A Prismatic Film on the Actual Performance of A Closed-loop Daylight-responsive Dimming System

5.1 Methodology

5.1.1 Space Modelling

The space with four windows described in Chapter 4 (Section 4.1.1) was employed in this study, with its orientation being changed to south-facing. The interior walls, ceiling, and floor of the space were modelled with a reflectance of 50%, 70%, and 20% respectively; the exterior ground and surrounding buildings were modelled with a reflectance of 10% and 30% respectively. In this study, two types of fenestration systems—a clear glazing and a clear glazing with a prismatic film being attached to the interior side—were considered. Specifically, the prismatic film was attached to the upper part (i.e., 0.51 m) of the glazing that had a total height of 2.04 m. A grid of 359 calculation points were uniformly distributed on the workplane that was 0.75 m above the floor, with a spacing of 0.5 m between each other, as shown in Figure 5.1.

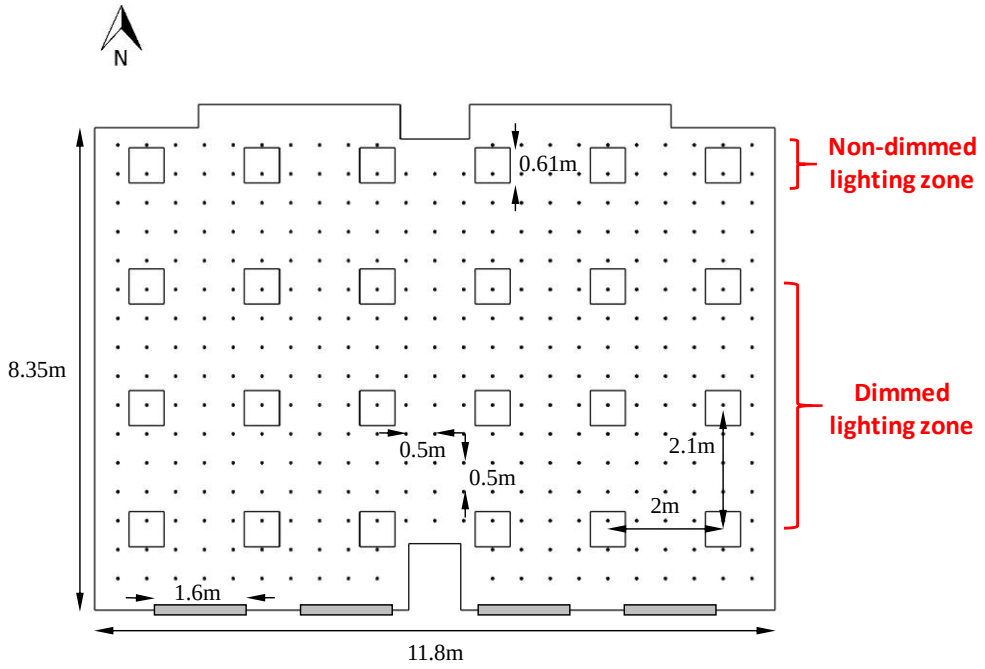

Figure 5.1 Arrangements of the electric lighting system and the calculation points in the space.

5.1.2 Daylight and Electric Lighting Simulations

The daylight illuminance at each of the 359 calculation points on the workplane was derived using the five-phase method. Since the *MF* value was set to 5, the 3601 sky and 3601 sun patches plus a ground patch were generated for the daylight simulation. The ambient bounces (*-ab*) and ambient divisions (*-ad*) were set to 5 and 10000 respectively. Two BSDF files were generated based on the standard Klems scheme using the *genBSDF* program in Radiance to characterize the transmittance of the fenestration systems, with one for the clear glazing and one for the clear glazing with the prismatic film. Figure 5.2 shows the BSDF results of the two fenestration systems. The actual weather data with a one-minute interval, as described in Chapter 4 (Section 4.1.2), were used with the average of the direct normal and diffuse horizontal irradiance levels within each hour being used in the daylight simulations. Therefore, the actual weather data resulted in 8760 hourly data in the entire year. Since the

occupied hours were set to between 8AM and 6PM, 3650 illuminance values were calculated at each calculation point.

(a) A clear glazing

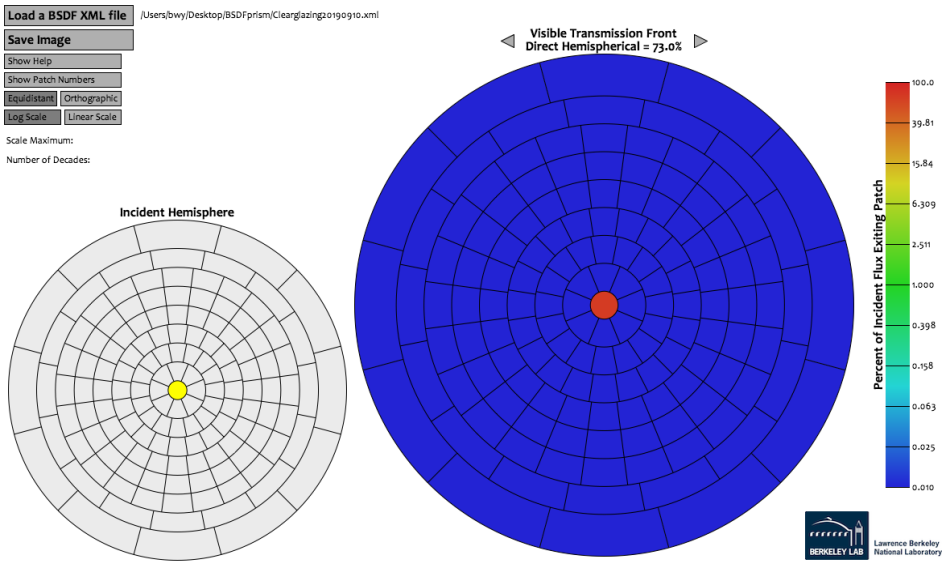

(b) A clear glazing equipped with a prismatic film

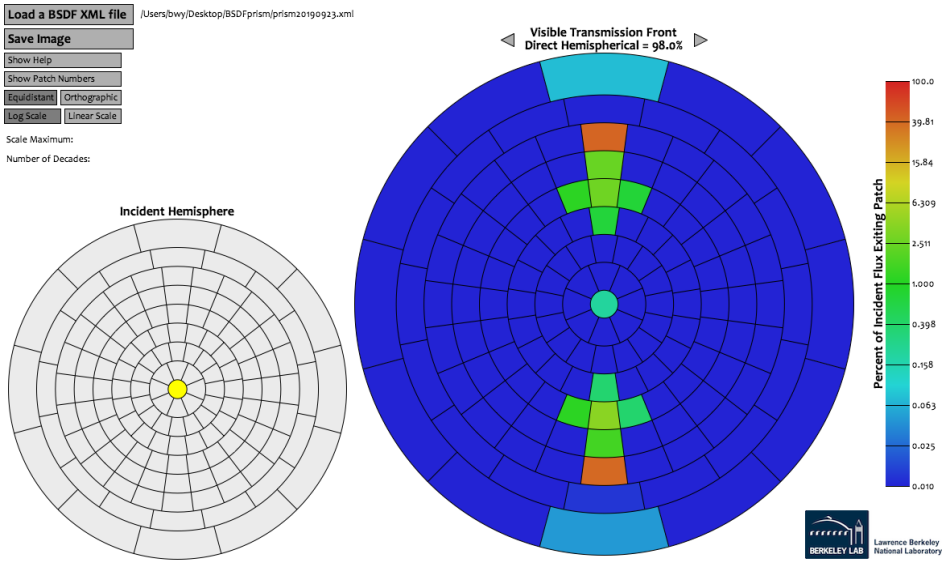

Figure 5.2 Screenshot of the BSDF generated based on the standard Klems scheme with 145 × 145 patches for the two different fenestration systems. The left figure refers to incident hemisphere, the right figure refers to transmitted hemisphere showing the front transmission conditions. (a) A clear glazing; (b) A clear glazing with a prismatic film being attached to the interior side of the upper part of the glazing.

The electric lighting system described in Chapter 4 (Section 4.1.3) was used in this study to achieve the average maintained illuminance of 505 lx at each of the 359 calculation points, which met the target illuminance (i.e., 500 lx) for performing visual tasks in a typical classroom (DiLaura et al., 2011). Based on the daylight quantity derived on the workplane in the space, the first three rows of the luminaires near the windows were functioned as the dimmed lighting zone, while the last row was functioned as the non-dimmed lighting zone, as shown in Figure 5.1.

5.2 Determinations of A Workplane Calibration Point and A Photosensor Location

The optimal dimming levels at each calculation point during the occupied hours throughout the entire year were calculated according to Eq. (4.1). As mentioned in Chapter 4 (Section 4.4.1), a *critical point* at a certain hour is defined as the calculation point that has the highest optimal dimming level, which ensures that the illuminance levels at all the other calculation points can achieve the target illuminance level with such a dimming level. Thus, the calculation point that had the highest frequency to be the *critical point* throughout the entire year was selected as the *workplane calibration point*. Figure 5.3 illustrated the frequency of each calculation point that was considered as the *critical point* throughout the entire year. It can be seen that the point shaded in red had the highest frequency to be the *critical point* on the workplane throughout the year, reaching up to 989 and 839 times for the reference and test cases respectively. The two cases thus had the same location of the *workplane calibration point*, as shown in Figure 5.4, suggesting that the prismatic film did not significantly affect the daylight distribution on the workplane.

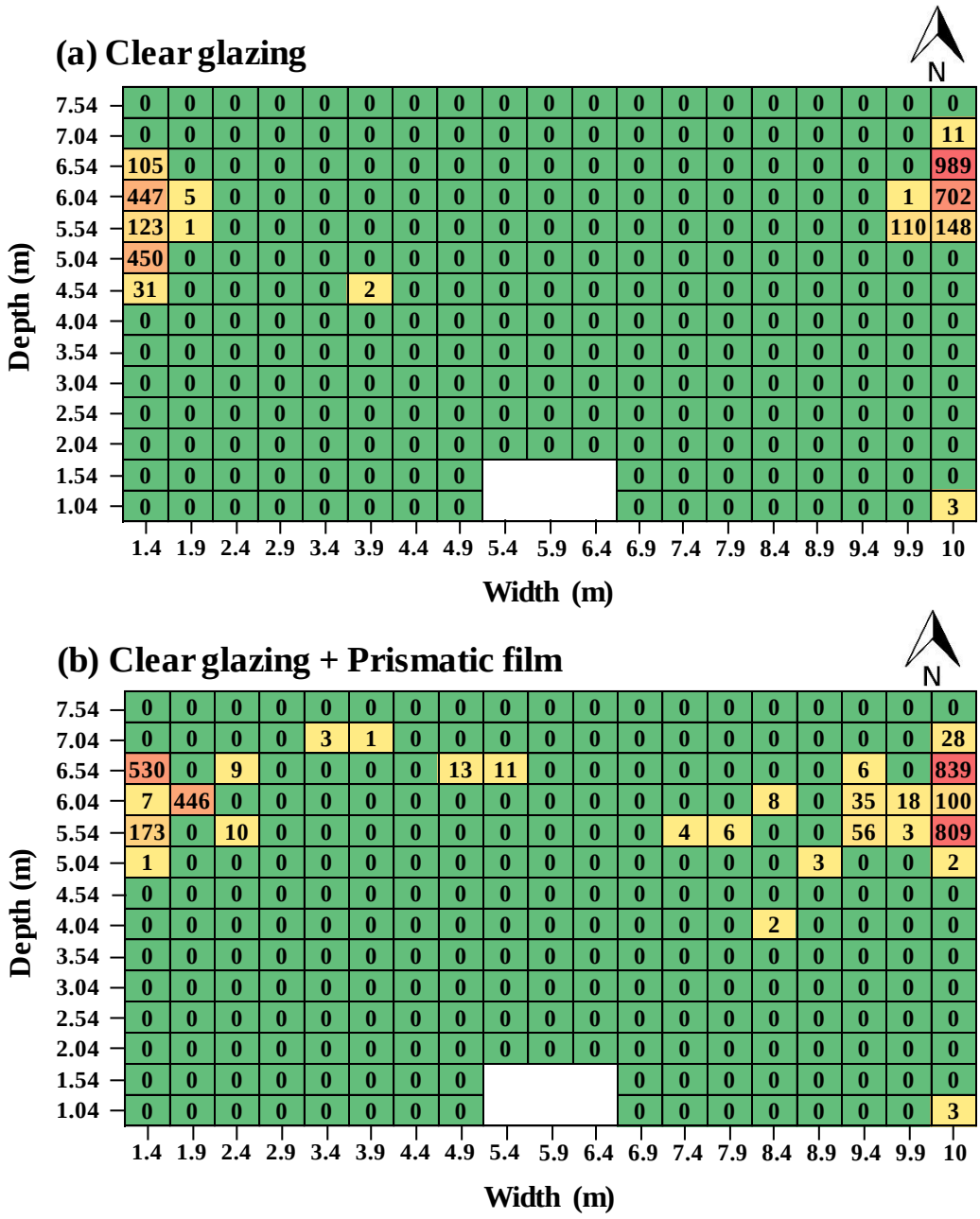

Figure 5.3 Illustration of the critical points for the two cases throughout the entire year. The number represents the number of hours that the calculation point was selected to be the critical point throughout the entire year. (a) The space that is only equipped with the clear glazings (i.e., the reference case); (b) The space that is equipped with the clear glazings and the prismatic films (i.e., the test case).

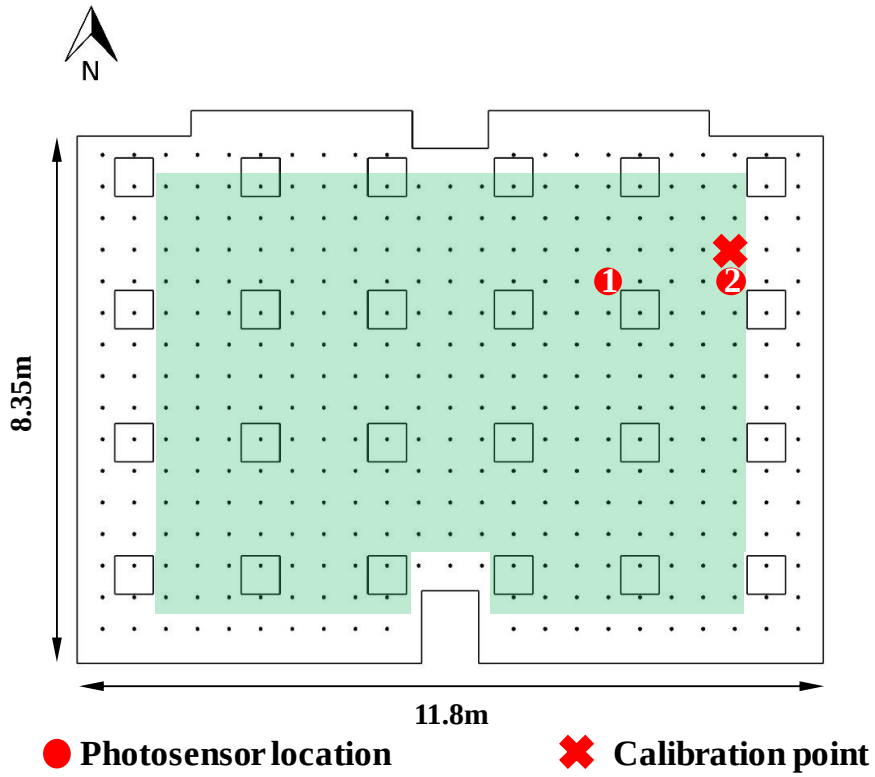

Figure 5.4 Locations of the workplane calibration point and the ceiling-mounted photosensor location for the two cases. The area shaded with green includes 260 calculation points that were considered for the critical points throughout the entire year. The location labelled with "1" represents the photosensor location for the reference case; the location labelled with "2" represents the photosensor location for the test case.

A similar grid of ceiling calculation points, as described in Chapter 4 (Section 4.4.1), was used to derive photosensor signals in this study. The photosensor location was then determined by considering the correlation between the photosensor signal and the illuminance at the *workplane calibration point* throughout the entire year. The ceiling calculation point that had the highest correlation between the photosensor signal and the illuminance at the *workplane calibration point* was used as the photosensor location. Figure 5.4 shows the photosensor locations of the reference and test cases, with the correlation coefficients of 0.97 and 0.63. It is obvious that the prismatic film significantly affected the light to the ceiling and the signals received by the photosensor.

5.3 Determination of Calibration Time and Algorithm Line

As shown in Figure 4.11 (Chapter 4, Section 4.4.2), the daylight-responsive dimming system never functions optimally, since it adjusts the dimming level proportionally based on the photosensor signal by following the calibration algorithm line. The calibration algorithm line is decided by the conditions at two calibration times (i.e., night- and day-time calibrations). It can be seen that the S/E ratios at the two calibration times determine the slope of the algorithm line.

Based on the two criteria to select the best day-time calibration hour as described in Chapter 4 (Section 4.4.2), three calibration hours were selected for each case, as summarized in Table 5.1. The corresponding RMSE values, frequency of actual over-dimming conditions, dimming levels at the calibration time, photosensor signals, and the S/E ratios are also listed in Table 5.1.

Table 5.1 Three day-time system calibration hours selected for each fenestration system using the five-phase method, together with the RMSE values, the frequency of actual over-dimming conditions, dimming levels at the calibration hour, S/E ratios, the photosensor illuminance, the average actual dimming levels throughout the entire year, and the average optimal dimming levels, which were all calculated using the actual weather data.

		Clear glazing			**Clear glazing + Prismatic film**		
Five-phase Method	Calibration Time	22-Apr 12:30 PM	14-May 14:30 PM	27-Jul 14:30 PM	4-Feb 9:30 AM	14-Aug 10:30 AM	9-Sep 9:30 AM
	RMSE	11.19%	10.99%	11.01%	8.90%	9.58%	9.46%
	Actual over-dimming	1.37%	1.63%	1.54%	5.96%	4.86%	5.15%
	DL @ Calibration Time	8.20%	8.50%	8.76%	9.16%	6.98%	8.23%
	Photosensor Illuminance	286.15	284.81	284.43	248.07	253.37	251.21
	S/E ratio	1.07	1.05	1.06	0.93	0.93	0.93
	Average Actual DL*	39.21%	39.08%	39.09%	36.83%	37.20%	37.14%
	Average Optimal DL*	33.40%			32.14%		

5.4 Prediction of Actual Energy Savings of the System

Since the average optimal dimming level maintains the target illuminance level (i.e., 500 lx) on the workplane, it can be used to predict the maximal potential energy

savings. However, the actual performance of the dimming system depends on the signals detected by the ceiling-mounted photosensor, instead of the illuminance value at the *workplane calibration point*. When the calibration hour was determined, a calibration algorithm line was set up to derive the actual dimming levels for different photosensor signals, which were used to predict the actual performance of the system. Figure 5.5 shows the optimal conditions and the calibration line based on one selected calibration hour for each case.

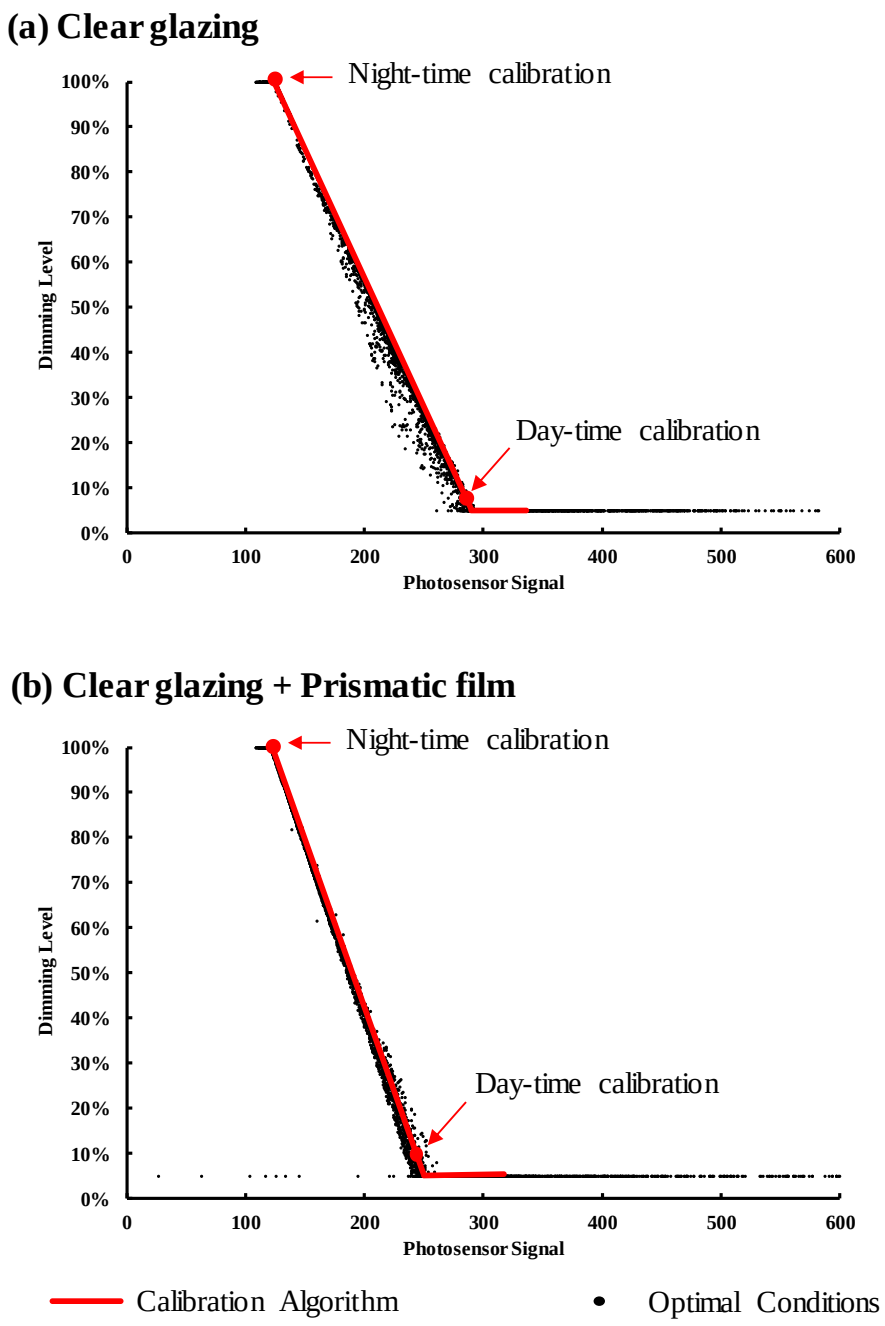

Figure 5.5 Illustration of the daylight-responsive dimming control algorithm. The scattered points represent the optimal dimming levels that were calculated based on the illuminance at the workplane calibration point; the red line represents the calibration algorithm which the dimming control actually follows. The points above the calibration line indicate the over-dimming conditions that the actual illuminance was lower than the target illuminance; the points below the calibration line indicate the under-dimming conditions that the actual illuminance was higher than the target illuminance. (a) The space equipped with the clear glazings (i.e., the reference case) and the system day-time calibration hour was selected at 12:30PM on Apr 22nd; (b) The space equipped with the clear glazings and the prismatic film (i.e., the test case) and the system day-time calibration hour was selected at 9:30AM on Feb 4th.

The average actual dimming levels at each calibration hour derived by solving the Eqs. (4.2) and (4.3) simultaneously for the two fenestration systems were described in Table 5.1. The average actual dimming levels were found slightly higher than the average optimal dimming levels, which suggested that the target illuminance (i.e., 500 lx) could not always be maintained at the *workplane calibration point* throughout the year in reality. Moreover, the average actual dimming levels derived for the reference case were always higher than those for the test case, which suggested that a higher illuminance may be needed to maintain the target illuminance (i.e., 500 lx) on the workplane in the reference case. This was mainly due to the reflected daylight to the photosensor on the ceiling due to the prismatic film. In addition, the average actual dimming levels also allowed a prediction of actual energy savings of the system throughout the entire year. As shown in Figure 5.6, it was found that the actual energy savings for the test case were slightly higher than those for the reference case, suggesting little impact of the two fenestration systems on the prediction of the actual energy savings.

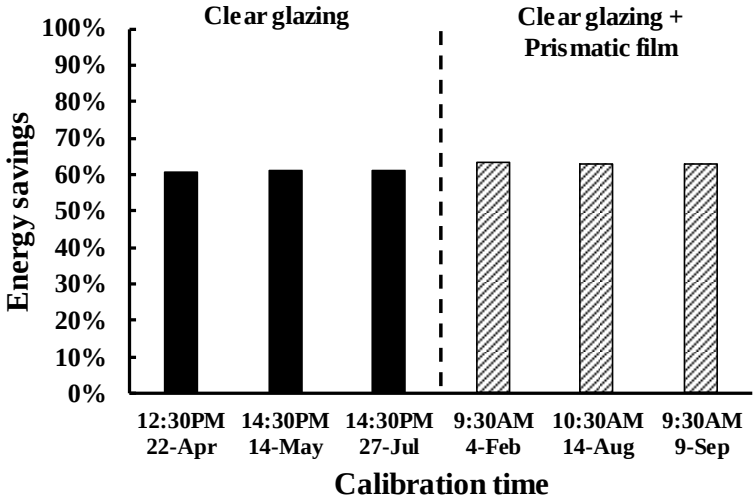

Figure 5.6 Actual energy savings that were achieved by the closed-loop daylight-responsive dimming system throughout the entire year for the two different fenestration systems.

5.5 Actual Dimming Conditions at the Calibration Hours

As shown in Table 5.1, it was found that the actual over-dimming conditions for the test case happened more frequently than those for the reference case, although the calibration hours were selected for the test case by lowering the RMSE values and limiting the frequency of over-dimming conditions below 2% throughout the year. This was probably due to the prismatic film used in the test case, which introduced daylight into the deeper areas of the space. Since the prismatic film was used on the upper part of the glazing, it would reflect daylight to the ceiling where the photosensor was installed. As a result, the photosensor frequently detected a greater amount of daylight than the amount of daylight on the workplane, leading to a decrease in the dimming levels and a higher frequency of over-dimming conditions. Such a problem may be serious in December and January when the solar altitude was lower, since Hong Kong is located in just south of the tropic of cancer. Figure 5.7 shows the daylight distributions in the space for the two different fenestration systems at 12:30 PM on Dec 21st. It can be seen that the daylight was introduced to the deeper areas and reflected to the ceiling of the space using the prismatic film.

(a) A clear glazing **(b) A clear glazing equipped with a prismatic film**

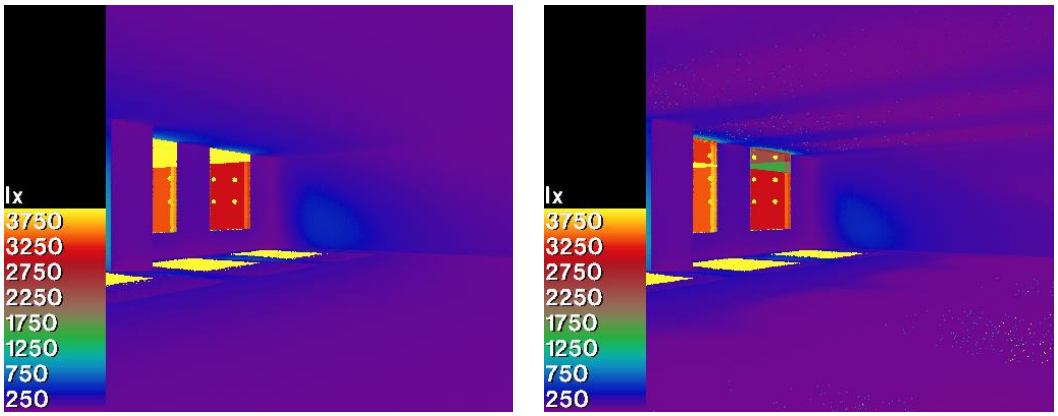

Figure 5.7 Comparison of the daylight distributions in the space at 12:30 PM on Dec 21st. (a) The space equipped with the clear glazings; (b) The space equipped with the clear glazings and the prismatic films.

5.6 Summary

This supplementary study was carried out to investigate the impact of the prismatic film on the actual performance of a closed-loop daylight-responsive dimming system. The investigation was performed on a real south-facing space equipped with two different types of fenestration systems (i.e., the clear glazing and the clear glazing with the prismatic film) in Hong Kong throughout an entire year, with the former being regarded as a reference case and the latter being regarded as a test case. The annual daylight simulation was performed using the five-phase method and the one-year duration actual weather data measured at a station in Hong Kong. It was found that the different fenestration systems did not have significant impacts on the actual energy savings of the dimming system. However, the over-dimming conditions happened more frequently for the test case, which was likely due to the reflected daylight to the photosensor on the ceiling due to the prismatic film. More importantly, such a problem caused by the prismatic film cannot be solved by changing the day-time calibration time.

Chapter 6

Study 2: Characterization of the Acceptable Daylight Quality in Typical Residential Buildings in Hong Kong

6.1 Methodology

6.1.1 Simulation Setup

- **Space Modelling**

The residential buildings in Bauhinia Garden in Hong Kong (22°17′ N, 114°9′ E), with a site area of around 13770 m^2, were modelled using SketchUp, as shown in Figure 6.1. The site and floor plans of the residential buildings were derived from Hong Kong Housing Authority and Independent Checking Unit. The residential buildings have eight blocks, with each block having 40 floors. On each floor, there are 10 flats with different orientations and there are three to four windows around 1.3 m above the floor in each flat.

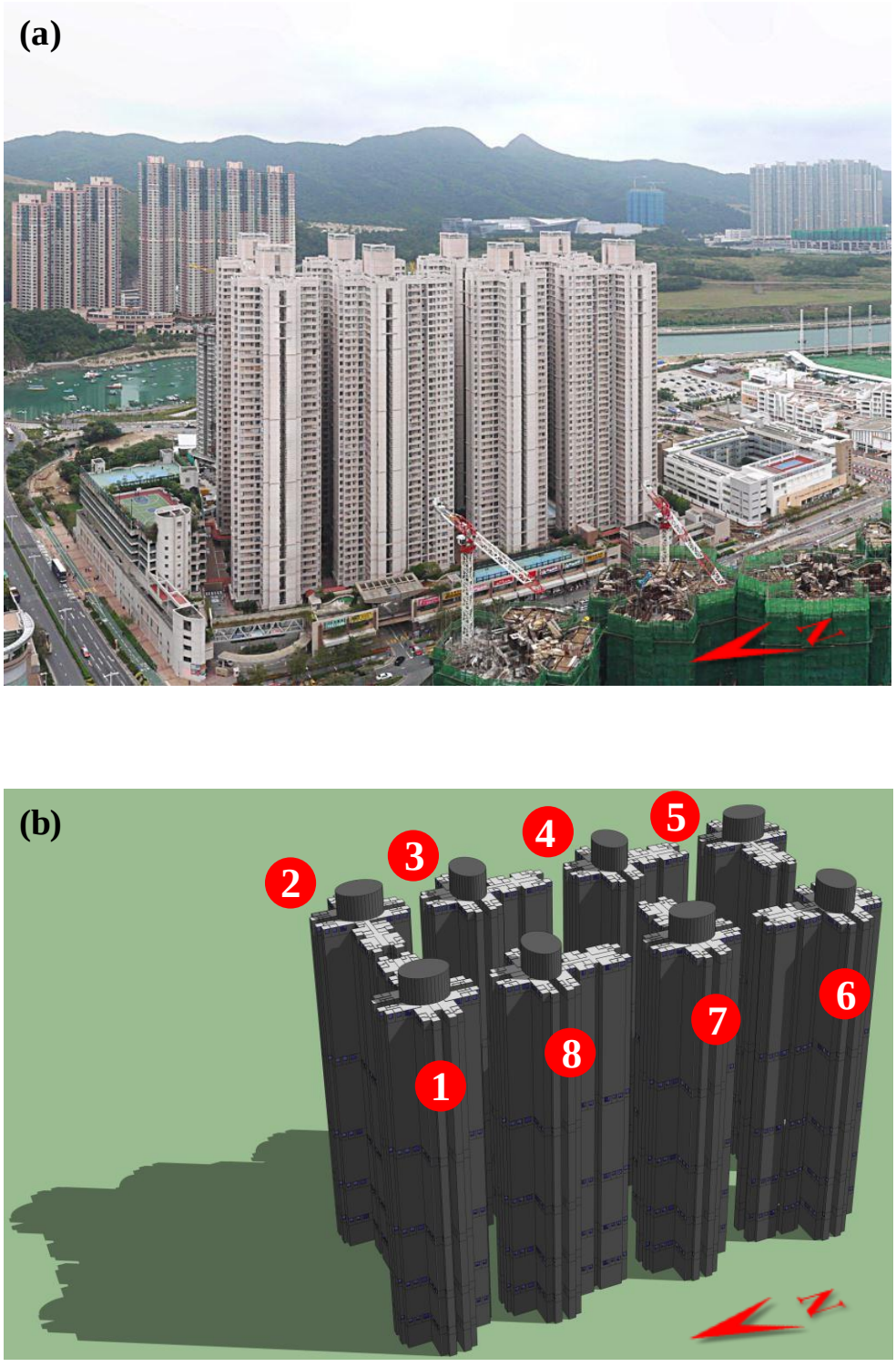

Figure 6.1 Airscape of the residential buildings in Bauhinia Garden. (a) Photograph (Billy, 2012); (b) SketchUp model.

Since the eight blocks have the same layout of the flats, the 10 flats on each of selected five floors (i.e., 4th, 8th, 15th, 25th, and 40th) in each block were modelled, as shown in Figure 6.1(b). Thus, a total of 400 flats were used for the daylight simulation. To

achieve accurate simulation results, the interior ceiling, floor, and walls of each flat were modelled with the reflectance values of 70%, 20%, and 50% respectively. The ground and surrounding blocks were modelled with the reflectance values of 10% and 30%. A clear glazing was modelled for the windows using the *genBSDF* program in Radiance, with the transmittance value of 80%. A horizontal grid of 1412 calculation points, with a spacing of 0.4 m, was placed on the workplane that was 0.8 m above the floor, as shown in Figure 6.2.

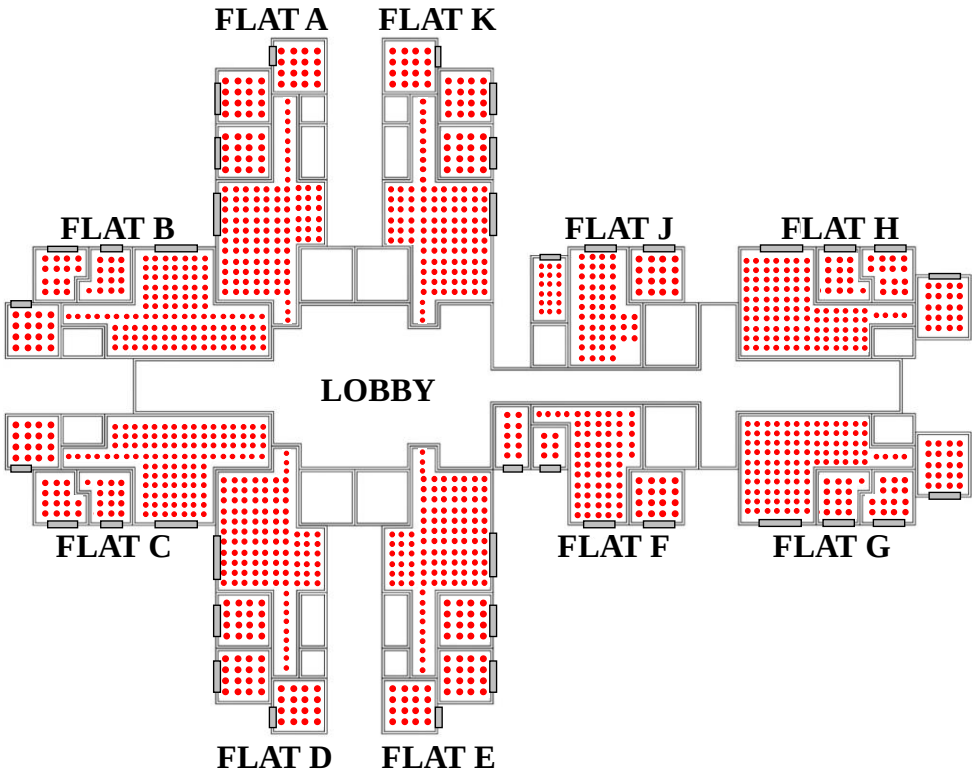

Figure 6.2 Layout of a selected floor and the arrangement of the measurement points.

- **Daylight Simulation**

Daylight illuminance values at the 1412 calculation points at each selected floor were derived using three different simulation methods (i.e., the daylight coefficient, three-, and five-phase methods). In total, the 3601 sky and 3601 sun patches plus a ground patch were used for the daylight simulation in Radiance, with the *MF* value being set

to 5. The ambient bounces (*-ab*) and ambient divisions (*-ad*) were set to 5 and 5000 for the simulations. The daylight simulation was performed using the TMY data and the actual weather data of Hong Kong. The TMY data were downloaded from the EnergyPlus website; the actual weather data were measured from Dec 1st 2014 to Nov 30th 2015 with a one-minute interval at the Hong Kong's Kings Park Meteorological Station, with the global horizontal, direct normal, and diffuse horizontal solar irradiance values being measured using a Kipp&Zonen CM5 pyranometer, a EKO MS-54 pyrheliometer integrated with a STR sun tracker, and a EKO MS-802 pyranometer. The data measured with a one-minute interval were then averaged in each hour, with the averaged data being centred on half-hour, which was how the hourly TMY data were derived. Since the occupied hours were set from 8AM to 6PM, the TMY data and the actual weather data resulted in 3650 illuminance values for each of the calculation points from a yearly perspective.

6.1.2 Questionnaire Survey and Data Analyses

A questionnaire survey was carried out to ask residents to subjectively evaluate their long-term feelings about the luminous environment in their flats in Bauhinia Garden. The questions were classified into five categories, including background information, façade features, feelings towards daylight, human adaptive behaviours, and satisfaction with luminous environment, as shown in Figure 6.3. In particular, the background information included residents' age and gender. The façade features included floor level, orientation of the flat, living room area, window area, and external obstructions, all of which were considered as key factors affecting the daylight quantity and quality (Li et al., 2006). To evaluate the residents' long-term opinions about the daylighting in their flats from different perspectives, the feelings towards daylight included the duration of daylight, perception of uniformity, (expected) hours

of sunlight entering the living room in summer and winter, potential problems caused by sunlight (i.e., thermal discomfort, glare, and fading objects), and satisfaction with daylighting. To evaluate how the residents respond to the luminous environment, the human adaptive behaviours included questions about the types of indoor activities, status of internal shading devices, reasons of adjusting shadings, hours of opening electric lights. The satisfaction with luminous environment aimed to evaluate the residents' overall satisfaction with the daylighting and the electric lighting in their flats. The items, such as perception of uniformity, satisfaction with daylighting, and satisfaction with luminous environment, were evaluated using a Likert 5-point scale, with "1" indicating "strongly dissatisfied" and "5" indicating "strongly satisfied" (Masters, 1985). The residents were reminded to answer the questions based on their long-term feelings during the past one year instead of answering the question at the time or during a specific short period. In total, 340 completed surveys were collected.

Questionnaire Survey of Luminous Environment in Residential Buildings

Category 1. General Information

1. Age

≤25	26-35	36-45	46-55	≥56

2. Gender

Male	Female

Category 2. Façade Features

3. Which floor do you live on?

≤5	6-10	11-20	21-30	≥31

4. Which way does the flat face?

North	East	West	South

5. How large is the living room? (ft^2)

≤50	51-100	101-200	201-300	≥301

6. How large is the window of the living room? (ft^2)

≤10	11-20	21-30	31-40	≥41

7. How much of the sky is obstructed when you are looking out of windows in the flat?

All	Most	A half	Less than a half	None

Category 3. Feelings towards Daylight

8. What is the duration of daylight in the flat during the daytime?

<1	1-2	2-3	3-4	>4

9. Do you agree that the uniformity of the daylight distribution in the flat is satisfactory?

Strongly disagree	Disagree	Just right	Agree	Strongly agree

10. How many hours do you expect when the sunlight enters the flat in summer?

<1	1-2	2-3	3-4	>4

11. How many hours will the sunlight enter the flat in summer?

<1	1-2	2-3	3-4	>4

12. How many hours do you expect when the sunlight enters the flat in winter?

<1	1-2	2-3	3-4	>4

13. How many hours will the sunlight enter the flat in winter?

<1	1-2	2-3	3-4	>4

14. How often do you think the sunlight bring about the following problems ?

(1) Thermal discomfort

Always	Often	Sometime	Rarely	Never

(2) Glare

Always	Often	Sometime	Rarely	Never

(2) Fading objects

Always	Often	Sometime	Rarely	Never

15. Do you agree that the daylighting in the flat is satisfactory?

Strongly disagree	Disagree	Just right	Agree	Strongly agree

Category 4. Human Adaptive Behaviors

16. What kind of activities do you usually have in the flat?

Relaxing	Watching	Eating	Chatting	Reading

17. What is the status of the internal shading devices in the flat?

All drawn	Drawn more than a half	Drawn a half	Drawn less than a half	Not drawn

18. What is main reason for you to adjust the internal shading devices?

No shading	Prevent direct sunlight	Prevent reflected sunlight	Protect private	Prevent heat

19. How many hours is the electric light switched on in the flat during the daytime?

<1	1-3	3-5	5-7	>7

Category 5. Satisfaction with Luminous Environment

20. Do you agree that the overall luminous environment in the flat is satisfactory?

Strongly disagree	Disagree	Just right	Agree	Strongly agree

Figure 6.3 A questionnaire survey that was distributed to the Bauhinia Garden to collect the residents' subjective evaluations about the luminous environment in their flats.

Since the survey included questions about the psychological responses, the reliability of the survey data was validated. The Cronbach' s alpha was used to test the internal

consistency of two categories, including “the feelings towards daylight” and “the human adaptive behaviours”. The Spearman’s rank correlation, known as a non-parametric measure of a correlation, is used to evaluate the similarity between the two variables. In this study, the relationships between the residents’ satisfaction with daylighting and the potential factors were investigated using the Spearman’s rank correlation. To figure out the major determinant for the residents’ satisfaction with daylighting, a stepwise regression analysis was performed to fit a regression model that revealed the best correlation between the residents’ satisfaction with daylighting and the factors. The Kruskal-Wallis test, also known as a non-parametric measure characterizing the dominant relationship between each sample, was used to investigate how the residents’ satisfaction with daylighting influenced their satisfaction with the luminous environment. The survey data were analysed using SPSS 25.

6.2 Results

6.2.1 Simulation Results of Daylight Quantity and Quality

The daylight illuminance values at each calculation point during the occupied hours throughout the entire year, which were calculated using the three different simulation methods and the two weather data, were used to calculate the various CBDM-based measures for characterizing the daylight quantity and quality in the 400 flats.

- **$sDA_{300/50\%}$ and $ASE_{1000,\ 250h}$**

To quantify the daylight sufficiencies and the possibilities of visual discomfort caused by direct sunlight in the flats, two CBDM-based measures—$sDA_{300/50\%}$ and $ASE_{1000,\ 250h}$—were calculated as recommended in both IES LM-83-12 and LEED v4 (IES LM-83-12, 2013; USGBC, 2014). The $sDA_{300/50\%}$ characterizes the percentage of the areas

in a flat that the daylight illuminance achieve 300 lx for more than 50% of the occupied hours for a year; the $ASE_{1000,\,250h}$ characterizes the percentage of the areas in a flat that the illuminance values provided by direct sunlight exceed 1000 lx for more than 250 hours of the occupied time for a year. The results of the average $sDA_{300/50\%}$ and $ASE_{1000,\,250h}$ are summarized in Figures 6.4 and 6.5. It was found that the two weather data did not produce large differences to the average $sDA_{300/50\%}$ values. Both the three- and five-phase methods produced similar results, which were around 5% higher than that derived using the daylight coefficient method. This may be due to the limited number of ambient bounces (i.e., *-ab*) being calculated using the daylight coefficient method. In addition, a better daylight sufficiency could be found in the flats on the higher floors than those on the lower floors, as shown in Figure 6.4. Moreover, the lower average $sDA_{300/50\%}$ values that were derived in the north-facing flats below the 15^{th} floor suggested that these flats were difficult to receive sufficient daylight throughout the entire year. In contrast, the daylight sufficiency was always acceptable in west-facing flats, regardless of the floors.

Figure 6.5 shows the average $ASE_{1000,\,250h}$ values derived using the five-phase method and the two weather data. Since the north-facing flats did not receive any direct sunlight, the average $ASE_{1000,\,250h}$ values were only calculated for the flats with the other orientations (i.e., south, west, and east). It can be observed that the average $ASE_{1000,\,250h}$ values derived using the TMY data were higher than those derived using the actual weather data, with the largest difference around 16% in the south-facing flats on the lowest floor in Block 6.

In addition, the average $ASE_{1000,\,250h}$ values were found to vary with the orientations of the flats, regardless of the weather data. For example, the west-facing flats in the blocks on the west side (i.e., Blocks 1, 6, 7, and 8 as shown in Figure 6.1) resulted in

higher average $ASE_{1000,\ 250h}$ values than the other sides, with the values ranging from 40% to 67%. Such higher values indicated a more frequent occurrence of the visual discomfort caused by the direct sunlight in the late afternoon. Due to the movement of the sun, the east-facing flats in the blocks on the east side (i.e., Blocks 2, 3, 4, and 5 as shown in Figure 6.1) were mostly affected by the direct sunlight in the early morning, with the average $ASE_{1000,\ 250h}$ values being greater than 30%. The higher average $ASE_{1000,\ 250h}$ values achieved in the east- and west-facing flats also suggested a necessity of vertical shading devices. Though the south-facing flats in Blocks 5 and 6 also resulted in higher average $ASE_{1000,\ 250h}$ values, the application of adjustable horizontal blinds or an overhang would be helpful to reduce the visual discomfort caused by the direct sunlight.

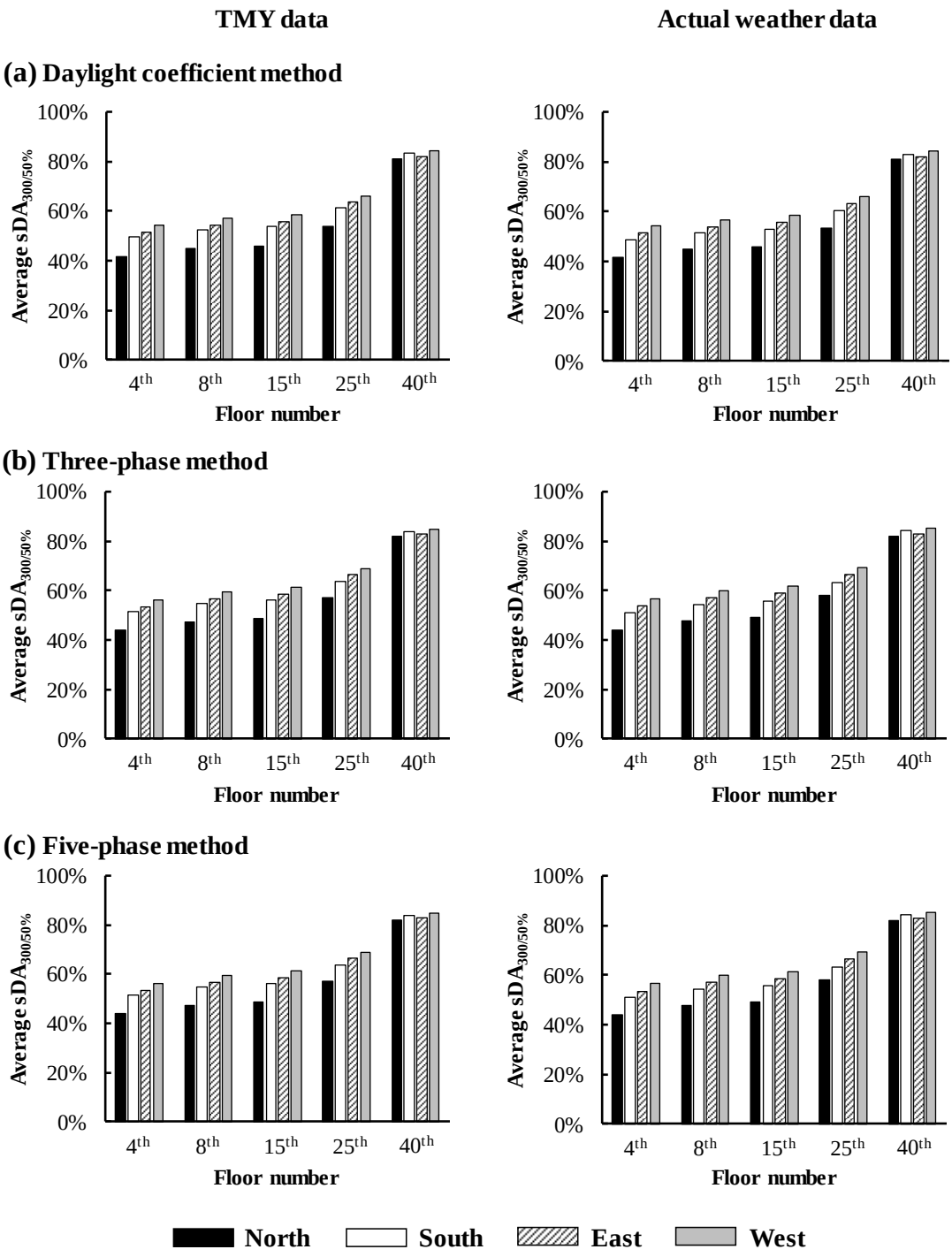

Figure 6.4 Comparisons of the average $sDA_{300/50\%}$ values that were derived using the three simulation methods and the two weather data throughout the entire year.

(a) South

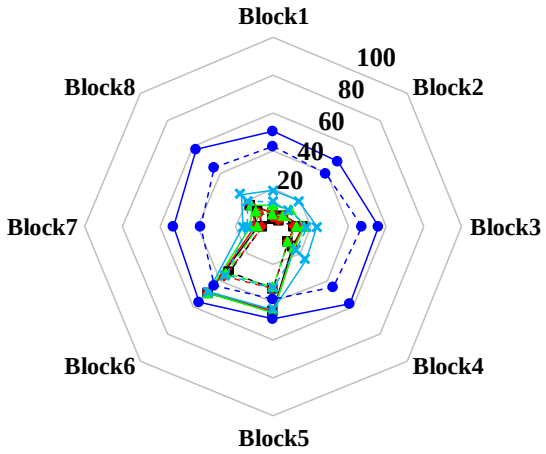

(b) East

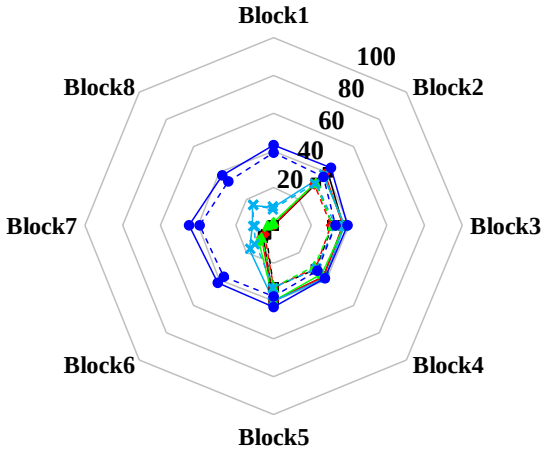

(c) West

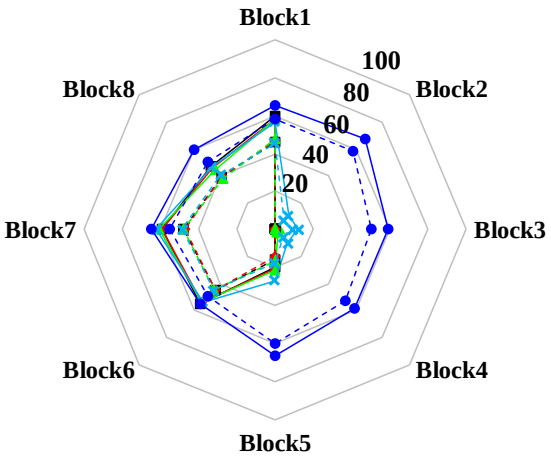

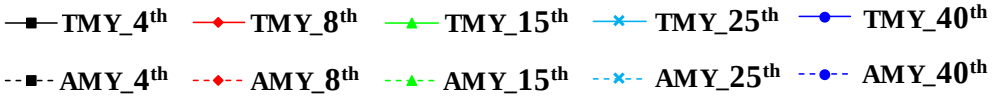

Figure 6.5 Comparisons of the average $ASE_{1000,\ 250h}$ based on the two different weather data for the flats on different floors in the 8 blocks. (note: the north-facing flats received no direct sunlight).

- **UDI and DA_{300}**

The average UDI values of the flats were derived using the three simulation methods and the two weather data. It was found that the two weather data did not produce large differences to the average UDI values in the three categories (i.e., "insufficient", "useful", and "exceeded"), with Fig 6.6 using the average UDI values in the "useful" category as an example. The different simulation methods, however, had a significant impact on how frequently the daylight received in the flats could be classified into three categories, with the amount of daylight derived using the three- and five-phase methods being frequently considered as "useful" in the flats. Similar findings due to the simulation methods and the weather data were also found in the average DA_{300}, as shown in Figure 6.7.

To provide a direct insight into the daylight availability in the flats, four identical living rooms facing different orientations on three floors were selected to characterize an annual spatial distribution of the UDI values, which were calculated using the five-phase method and the actual weather data, as shown in Figures 6.8 and 6.9. It was found that the UDI values in the three categories were slightly affected by the floor levels, but little difference was found in the spatial distribution of the UDI values. However, the orientation of a flat was found to have a significant impact on the spatial distribution of the UDI values. For example, the south-facing living room more frequently received "exceeded" amount of daylight than the rooms facing the other orientations, with some flats on the highest floor (i.e., the 40^{th} floor) having the "exceeded" amount of daylight for more than 75% of the occupied time. In contrast, the north-facing flats had the least frequencies to receive the "exceeded" amount of daylight, and more frequently received the "useful" amount of daylight, especially to those on the highest floor (i.e., the 40^{th} floor).

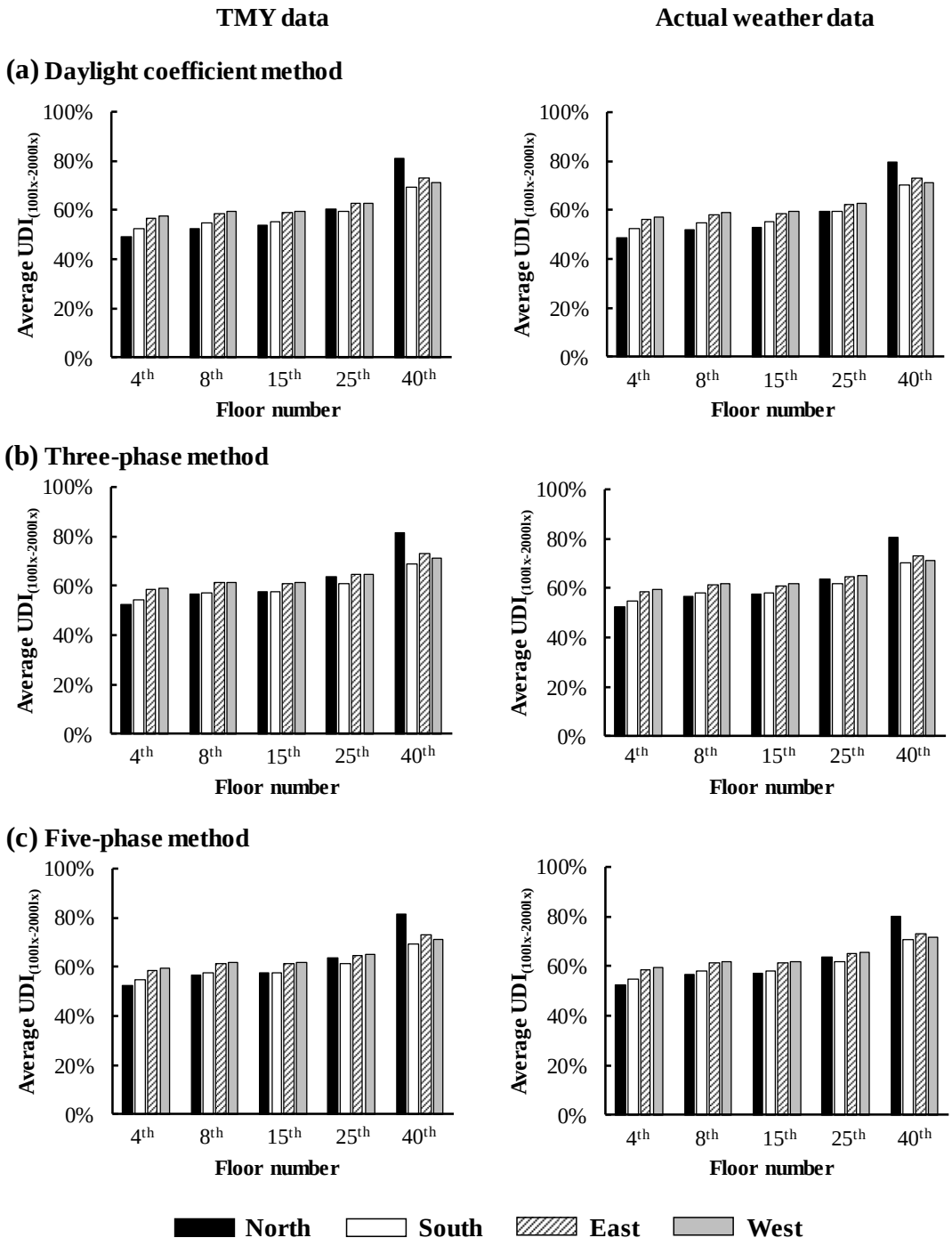

Figure 6.6 Comparisons of the average useful UDI values (i.e., 100 lx-2000 lx) that were derived using the three simulation methods and the two weather data throughout the entire year.

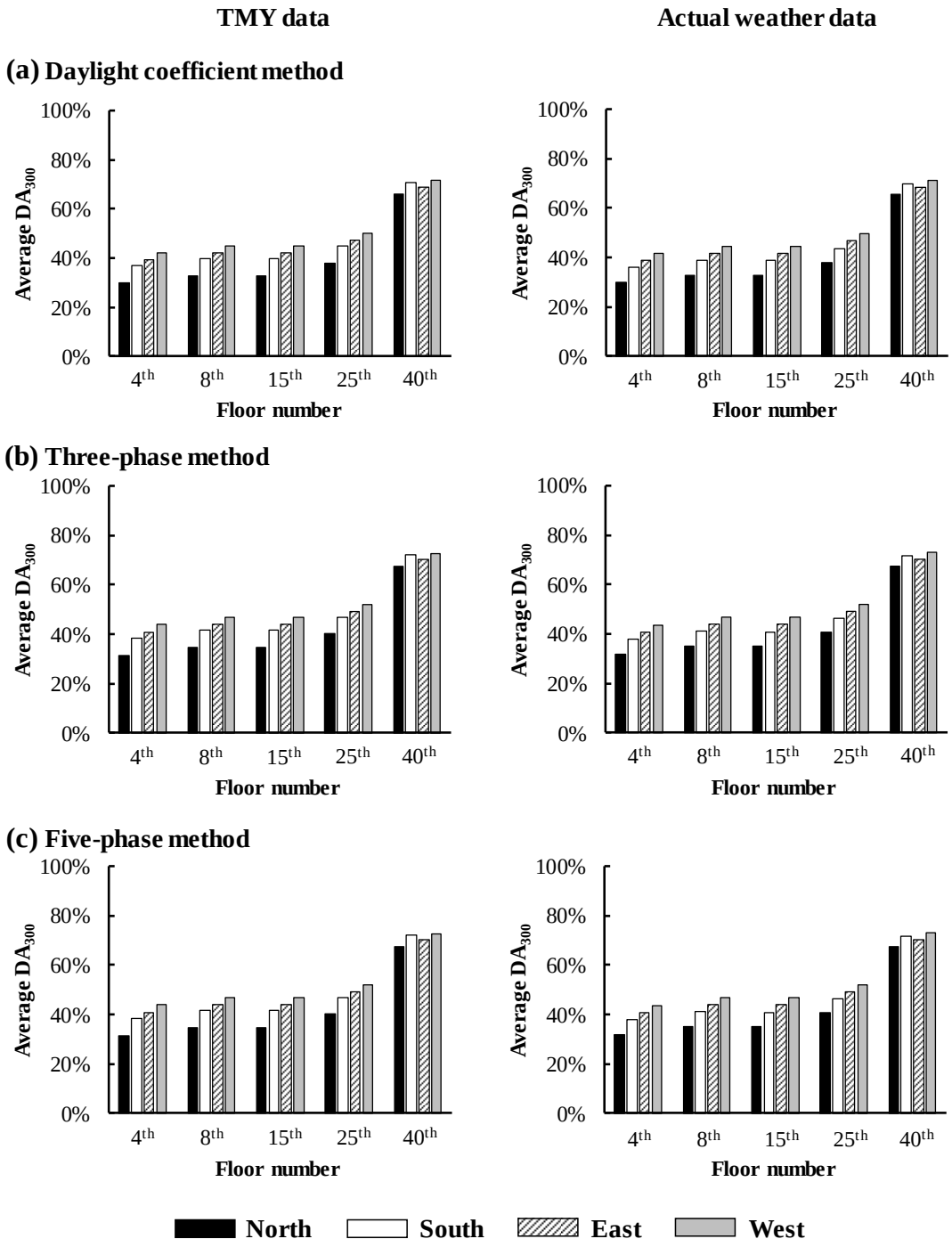

Figure 6.7 Comparisons of the average DA_{300} that were derived using the three simulation methods and the two weather data throughout the entire year.

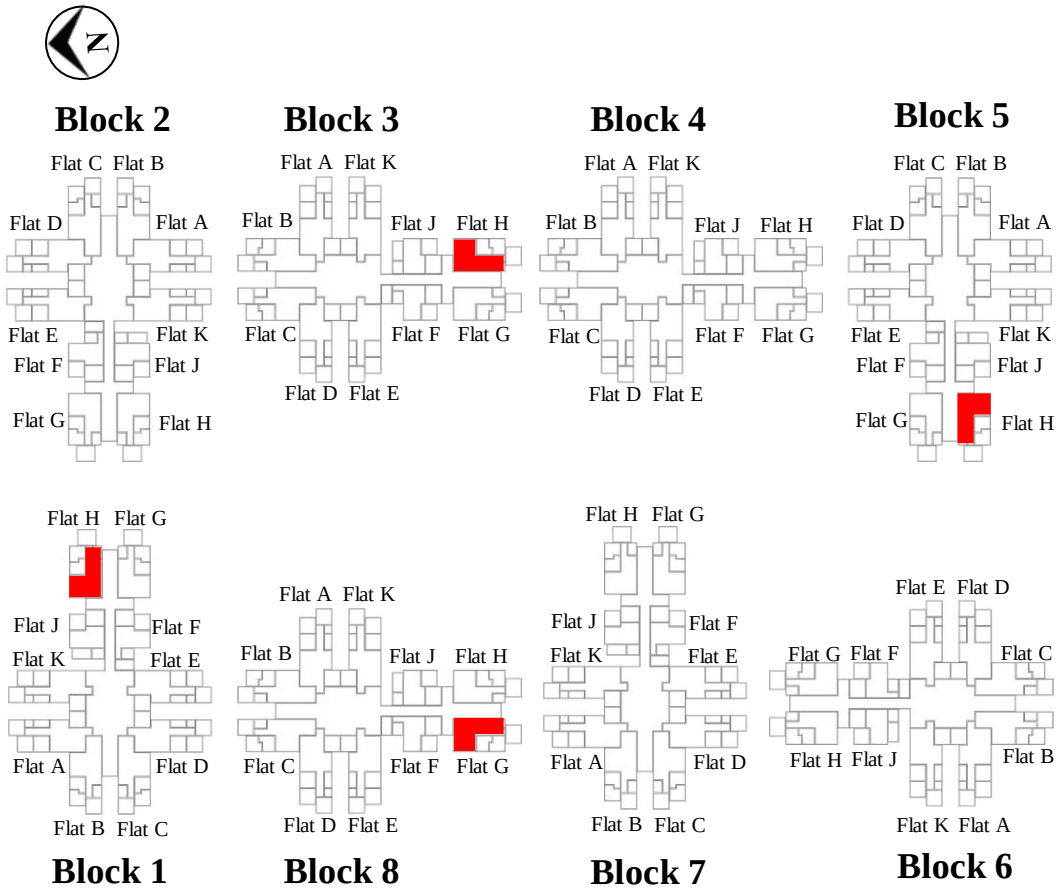

Figure 6.8 Layout of the eight blocks in Bauhinia Garden. The flats highlighted in red are the four identical living rooms selected for characterizing the spatial distribution of the UDI values throughout the entire year.

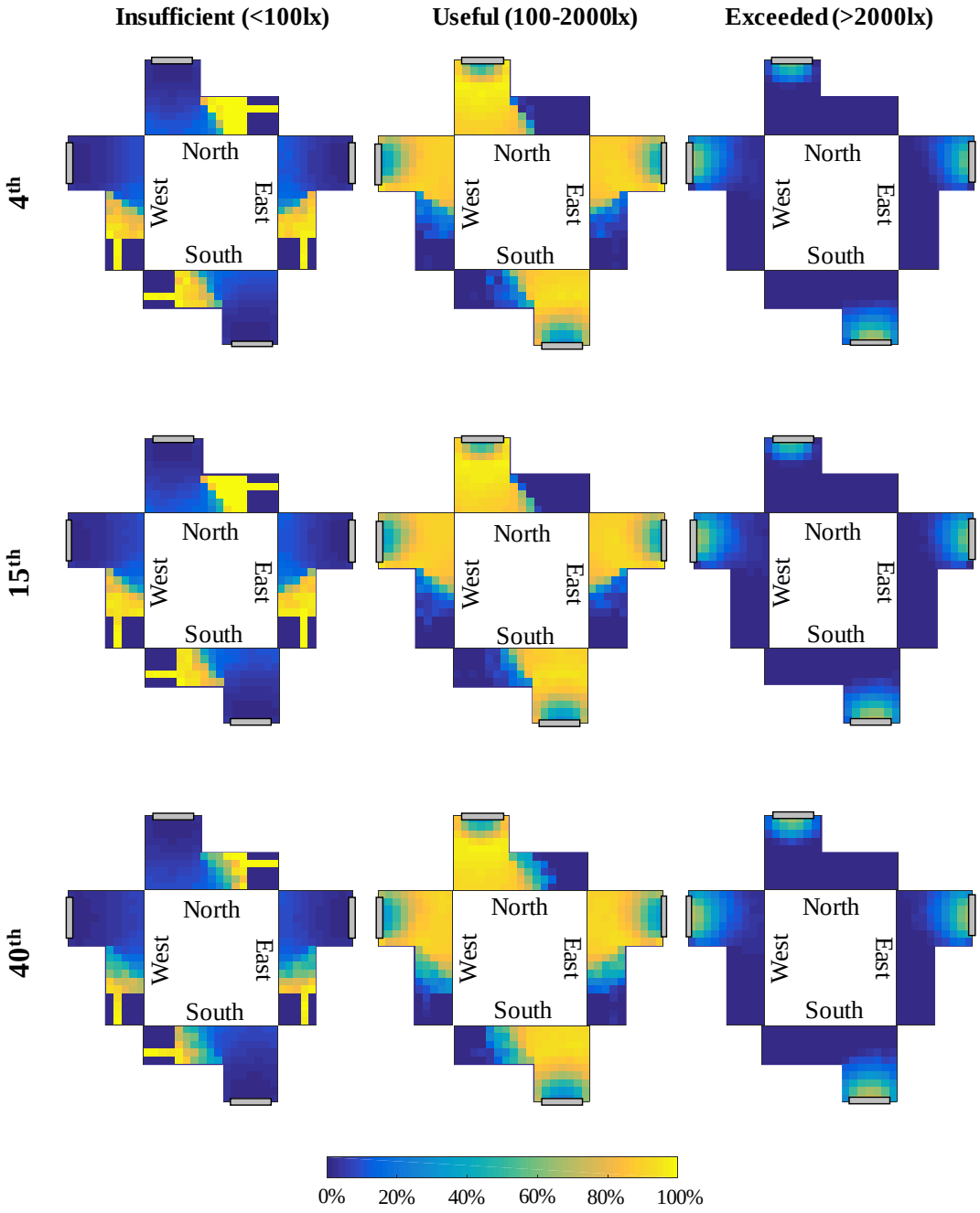

Figure 6.9 Spatial distribution of the UDI values that are classified in three categories calculated using the five-phase method and the actual weather data throughout the entire year in the four identical living rooms on the three selected floors.

- **Average Daylight Illuminance**

Fig 6.10 shows the average daylight illuminance values in the flats throughout the entire year. It can be seen that the average daylight illuminance values calculated using the three- and five-phase methods were generally higher than those calculated using

the daylight coefficient method, which was the reason for producing higher average $sDA_{300/50\%}$ and UDI values. Moreover, the actual weather data were found to result in higher average daylight illuminance than the TMY data, with the largest difference of 16% for the east-facing flats. Thus, the subjective evaluations on the daylight quantity and quality in the flats should be correlated to the measures derived using the actual weather data.

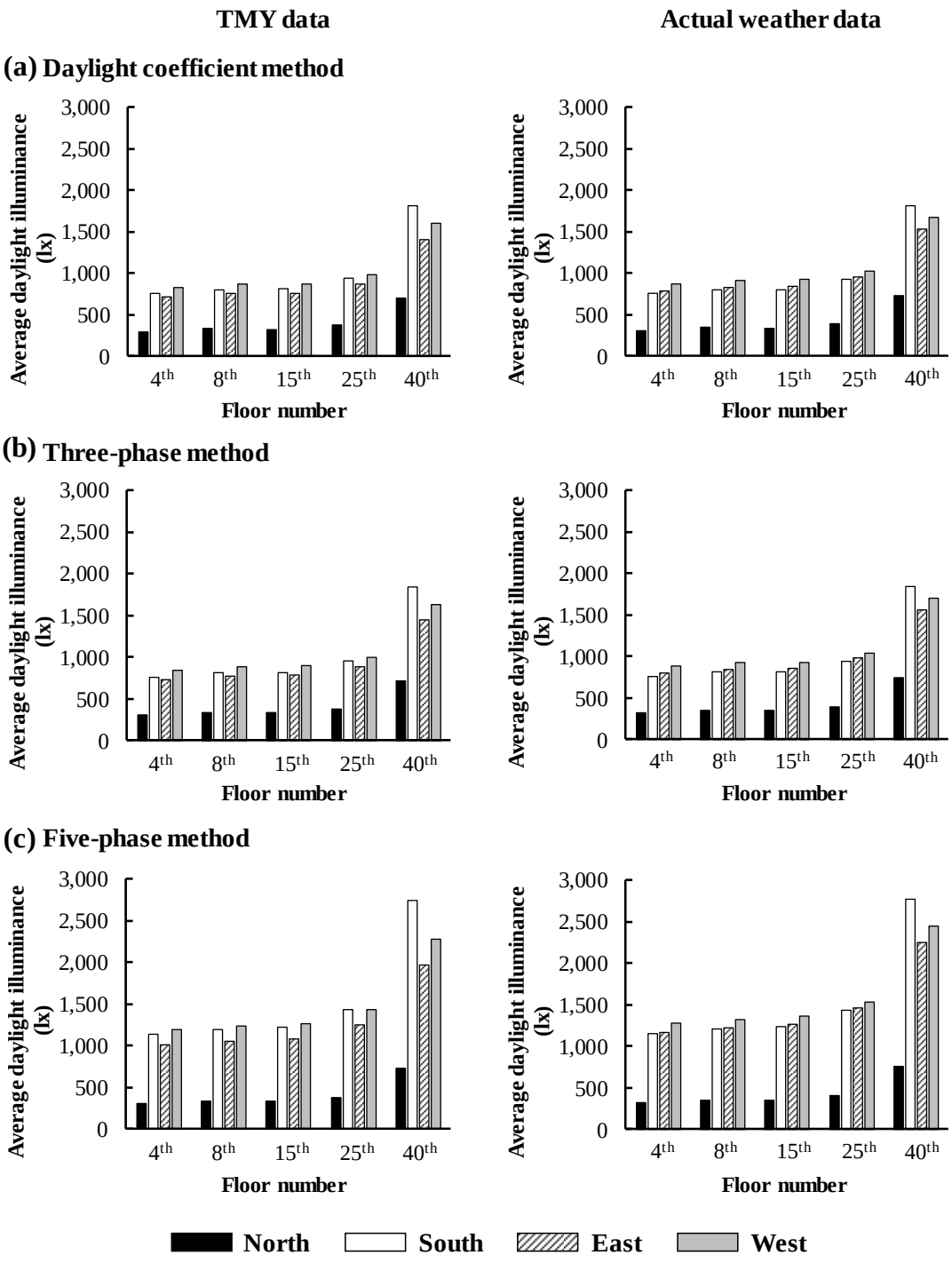

Figure 6.10 Comparisons of the average daylight illuminance that was derived using the three simulation methods and the two weather data throughout the entire year.

6.2.2 Statistical Analysis of the Survey Data

The internal consistency of two categories of questions, including "feelings towards daylight" and "human adaptive behaviours", was calculated using the Cronbach's

alpha, with the value being equal to 0.7 and 0.23 respectively. Since the acceptable Cronbach's alpha was suggested to be higher than 0.6 (Yildirim et al., 2007; Tavakol et al., 2011), the survey data in the category of the "feelings towards daylight" were believed to be reliable.

The correlations between the different potential factors affecting residents' evaluations on the daylight environment and their satisfaction with daylighting were investigated using the Spearman's rank correlation. As summarized in Tables 6.1 and 6.2, for the category of the "façade features", the external obstruction, with a correlation coefficient of 0.35, was found to have a higher correlation to the residents' satisfaction with daylighting compared to the other factors, such as floor level, orientation, and area of window. For the category of the "feelings towards daylight", the perception of uniformity was significantly correlated to the residents' satisfaction with daylighting, with a correlation coefficient of 0.61. The other factors, such as abundant daylight hours, the hours of solar access in winter and summer, expected hours of solar access in summer, and thermal discomfort were found to have weak correlations to the residents' satisfaction with daylighting.

Table 6.1 Spearman's rank correlation coefficients between the residents' satisfaction with daylighting and the items in the category of façade features.

	Spearman's rank correlation coefficient				
	Façade features				
	Floor level	Orientation	Area of living room	Area of window	External obstruction
Satisfaction with daylighting	0.14*	0.13*	0.1	0.12*	0.35**

*. Correlation is significant at the 0.05 level (2-tailed)

**. Correlation is significant at the 0.01 level (2-tailed)

Table 6.2 Spearman's rank correlation coefficients between the residents' satisfaction with daylighting and the items in the category of feelings towards daylight.

	Spearman's rank correlation coefficient								
	Feelings towards daylight								
	Abundant daylight hours	Uniformity	Hours of solar access		Expected hours of solar access		Potential daylight problems		
			Summer	Winter	Summer	Winter	Thermal discomfort	Glare	Fading objects
Satisfaction with daylighting	0.38**	0.61**	0.27**	0.21**	0.22**	0.04	0.18**	0.09	0.11

**. Correlation is significant at the 0.01 level (2-tailed)

A total of 10 factors were then selected as independent variables to derive a regression model for better characterizing residents' satisfaction with daylighting. As shown in Table 6.3, four factors and a constant were found to fit the best regression model, with an adjusted R-square value of 0.45. Moreover, the perception of uniformity was found to have a good correlation to the residents' satisfaction with daylighting due to the highest value of the standard coefficient.

Table 6.3 Coefficients between a set of predictors and the residents' satisfaction with daylighting in the best regression model.

	Regression coefficient*		
	Standardized coefficient beta	**t**	**P-value**
(Constant)		7.632	< 0.001
Uniformity	0.464	9.332	< 0.001
Thermal	0.246	5.322	< 0.001
Obstruction	0.184	3.856	< 0.001
Solar access	0.168	3.544	< 0.001

*. Dependent Variable: Satisfaction with daylighting

In addition, a strong correlation was also found between the residents' satisfaction with daylighting and their satisfaction with luminous environment, with a Spearman's rank correlation coefficient of 0.64. Such a finding was supported by the results of the Kruskal-Wallis test, which was adopted to investigate how the residents' satisfaction with daylighting influenced their satisfaction with luminous environment. As shown in Figure 6.11, the residents' satisfaction with daylighting had a positive correlation to their satisfaction with luminous environment. The higher the satisfaction towards the daylight, the higher the satisfaction towards the overall luminous environment. This suggested that the daylight quality was critically important to the residents' satisfaction with the luminous environment.

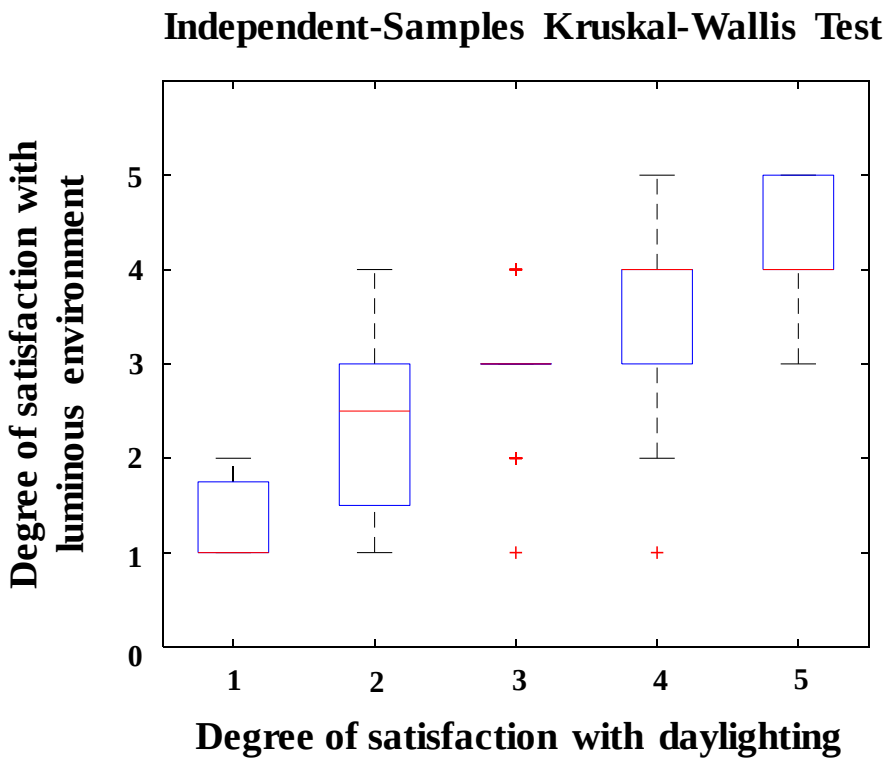

Total N	**340**
Test Statistic	**138.699**
Degree of Freedom	**4**
Asymptotic Sig. (2-sided test)	**< .001**

Figure 6.11 Result of the Kruskal-Wallis test for investigating the correlation between the residents' satisfaction with daylighting and their satisfaction with luminous environment.

6.2.3 Correlation between Subjective Evaluations and Objective Daylight Measures

Since the three different simulation methods significantly affected the simulation results and a validation suggested the effectiveness in using the five-phase method to characterize the direct sunlight contribution (Lee et al., 2018), the simulation results derived using the five-phase method and the actual weather data and the residents' subjective satisfaction with daylighting were expected to be correlated.

Similarly, both the Spearman's rank correlation and the stepwise regression were used to investigate the relationships between the residents' subjective satisfaction with daylighting and the objective daylight measures, including the various CBDM-based measures, average daylight uniformity, and maximum average daylight illuminance, for the corresponding flats. It is worthwhile to mention that the maximum average daylight illuminance is defined as the highest value of the average daylight illuminance derived at each calculation point during the occupied time throughout the entire year.

Table 6.4 Spearman's rank correlation coefficients between the residents' subjective satisfaction with daylighting and the objective daylight measures.

Spearman's rank correlation coefficient							
	Dynamic daylight measures						
	Average uniformity	DA_{300}	$sDA_{300/50\%}$	$ASE_{1000,250h}$	UDI (100-2000lx)	Average daylight illuminance	Maximum average daylight illuminance
Satisfaction with daylighting	0.12	0.44**	0.46**	0.40**	0.21*	0.49**	0.50**

*. Correlation is significant at the 0.05 level (2-tailed)
**. Correlation is significant at the 0.01 level (2-tailed)

Table 6.4 summarizes the Spearman's rank correlation coefficients between the objective daylight measures and the residents' satisfaction with daylighting. It can be observed that all the measures, except the average uniformity, were highly correlated to the residents' satisfaction with daylighting. The stepwise regression was then calculated to characterize the best correlation between the residents' satisfaction with daylighting and the objective daylight measures. As shown in Table 6.5, the best regression model was only found between the residents' satisfaction with daylighting and the average $sDA_{300/50\%}$ and the maximum average daylight illuminance. In addition, the standard coefficients, which revealed the strength of the correlation between two variables, suggested that both the average $sDA_{300/50\%}$ and the maximum average daylight illuminance had similar effects on the subjective evaluations.

Table 6.5 Coefficients between the two objective daylight measures and the residents' satisfaction with daylighting in the best regression model.

	Regression coefficient*		
	Standardized coefficient beta	**t**	**P-value**
(Constant)		5.443	< 0.001
$sDA_{300/50\%}$	0.324	2.914	0.004
Maximum average daylight illuminance	0.302	2.718	0.008

*. Dependent Variable: Satisfaction with daylighting

The scatter plots of the residents' subjective satisfaction with daylighting versus these two objective daylight measures are shown in Figure 6.12. It was found that each measure had a positive correlation to the residents' satisfaction with daylight environment in the flats. When the residents were satisfied with the daylight environment at the highest or the lowest degree, the values of these two measures in the flats were very high or low. In contrast, the values were dispersed when the residents had a neutral opinion about the daylight environment. Such findings suggested that the flats with higher values of the average $sDA_{300/50\%}$ and the maximum average daylight illuminance were more likely to provide a satisfactory daylight environment.

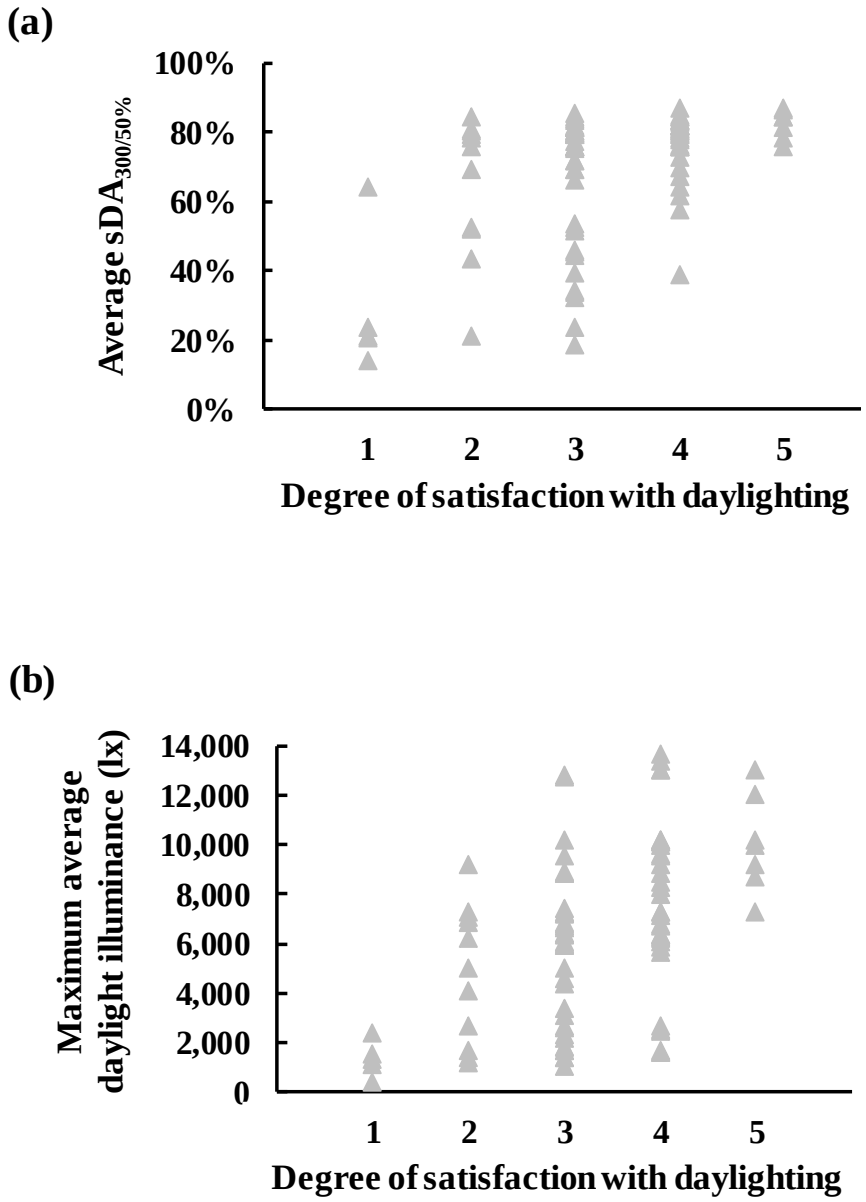

Figure 6.12 Scatter plots of the residents' subjective satisfaction with daylighting versus (a) Average $sDA_{300/50\%}$ and (b) Maximum average daylight illuminance.

6.2.4 Criteria for Characterizing the Acceptable Daylight Quality in the Residential Buildings

Given the correlations and regression models derived between the subjective evaluations and objective daylight measures, we proposed a criterion to characterize the acceptable daylight quality for the residential buildings in Hong Kong using the average $sDA_{300/50\%}$ and the maximum average daylight illuminance. The values for

each rating were averaged and plotted in Figure 6.13. It can be observed that both the average $sDA_{300/50\%}$ and the maximum average daylight illuminance had positive correlations to the resident' satisfaction with daylighting, which suggested the effectiveness in using these two measures to characterize daylight quality of the flats. Since the rating 3 represented a neutral opinion about the daylight environment, the lower boundaries of the criteria were set at the rating 3 for characterizing an acceptable daylight quality. Therefore, the flats with the average $sDA_{300/50\%}$ above 66% and the maximum average daylight illuminance above 5624 lx were considered to have an acceptable daylight quality in Hong Kong.

It should be noted that the residents did not complain about the glare in the survey, though the flats were found to have "excessive" amount of daylight. This can also be found in Figure 6.13. It was likely due to the obstruction caused by the adjacent buildings, which commonly happens in Hong Kong. Therefore, there is no need to have upper boundaries for the two measures.

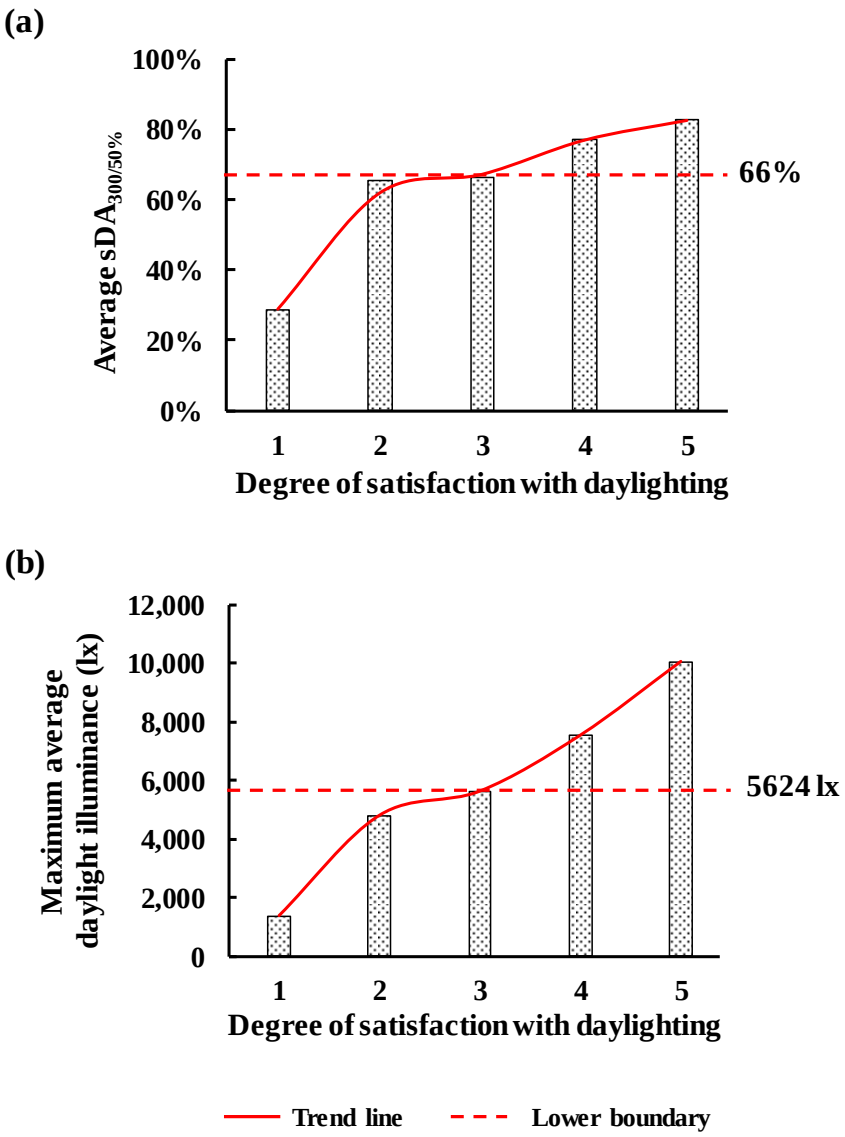

Figure 6.13 Criteria of (a) Average sDA$_{300/50\%}$ and (b) Maximum average daylight illuminance for characterizing the acceptable daylight quality in the flats.

6.3 Discussion

Based on the proposed criteria, the daylight quality of the 400 flats, as characterized using the two measures, in the eight blocks are shown in Figures 6.14 and 6.15. It was found that both the average sDA$_{300/50\%}$ and the maximum average daylight illuminance generally increased at the higher floors. In addition, all the flats on the highest floor (i.e., the 40th floor) in each block met the criterion of the average sDA$_{300/50\%}$ regardless

of the orientations, but the north-facing flats did not meet the criterion of the maximum average daylight illuminance.

Both the measures had different values at the lower floors due to the different orientations. For example, only the east-facing flats met the criteria in the four blocks on the east side (i.e., Blocks 2, 3, 4, and 5 as shown in Figure 6.1), with the value being around 80% for the average $sDA_{300/50\%}$ and 7000 lx for the maximum average daylight illuminance respectively. This may be due to the lack of external obstructions. Such a condition was also applicable to the west-facing flats in the four blocks on the west side (i.e., Blocks 2, 3, 4, and 5 as shown in Figure 6.1). Similarly, the north-facing flats took an advantage of the unobstructed environment in blocks 1 and 2 on the north side, with the average $sDA_{300/50\%}$ values increasing with the floors. This may be due to the geographical location of Hong Kong. Since Hong Kong is just located in the south of the tropic of cancer, the solar altitude angle is always large during the sun movement. Such a benefit of the geographical location was more obvious to the south-facing flats on the highest floors, with the maximum average daylight illuminance being higher than 12000 lx.

In addition, although the subjective evaluations showed a strong correlation between the perception of uniformity and the residents' satisfaction with daylighting, the objective measure of the average uniformity was not correlated to the residents' subjective satisfaction with the daylight quality. Such a finding did not corroborate the finding produced in a previous study (Xue et al., 2016), which was likely because the daylight quality was not derived using the actual weather data and the subjective and objective evaluations did not focus on the same period.

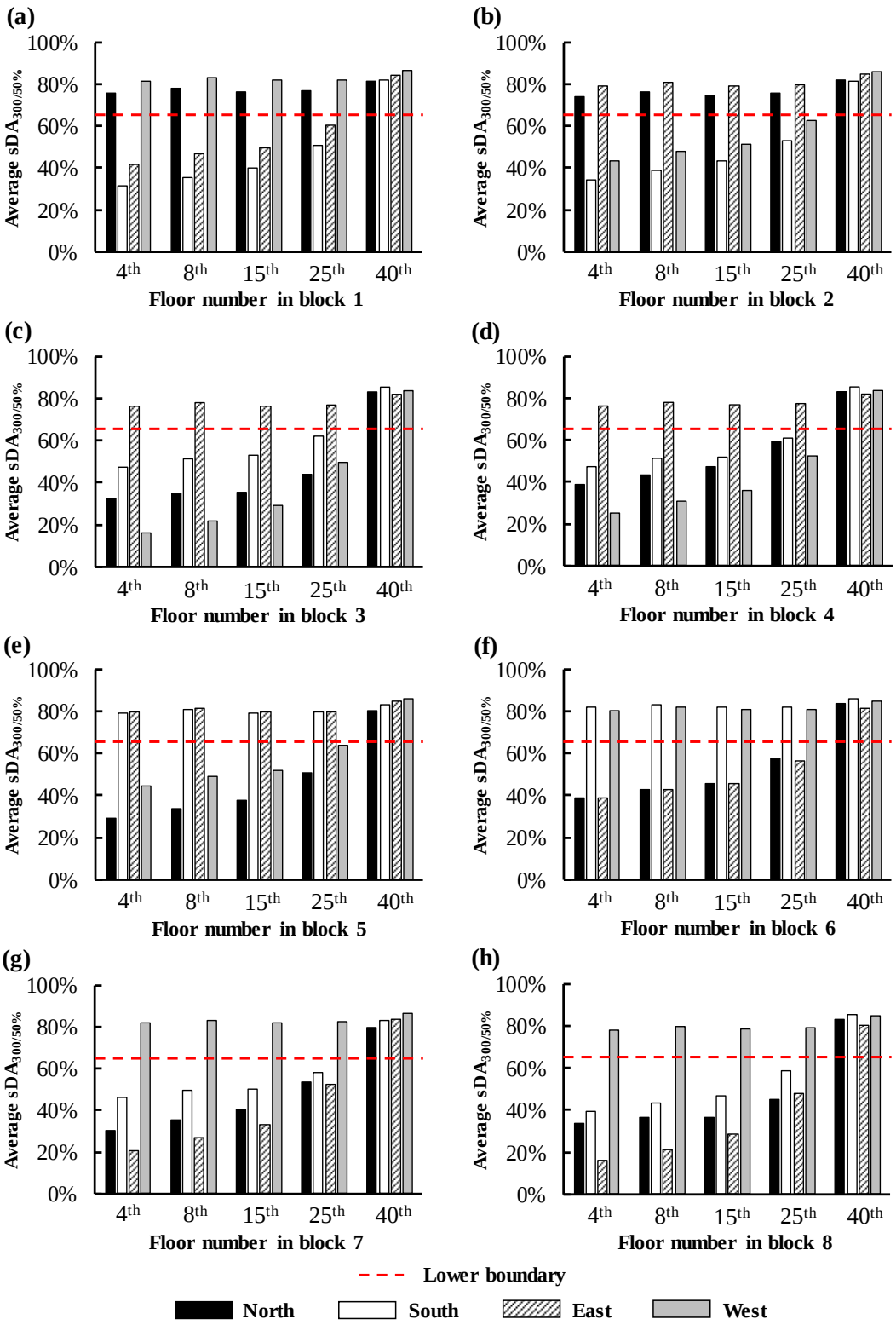

Figure 6.14 Summary of the average sDA$_{300/50\%}$ of the 400 flats in the residential buildings and the proposed criterion.

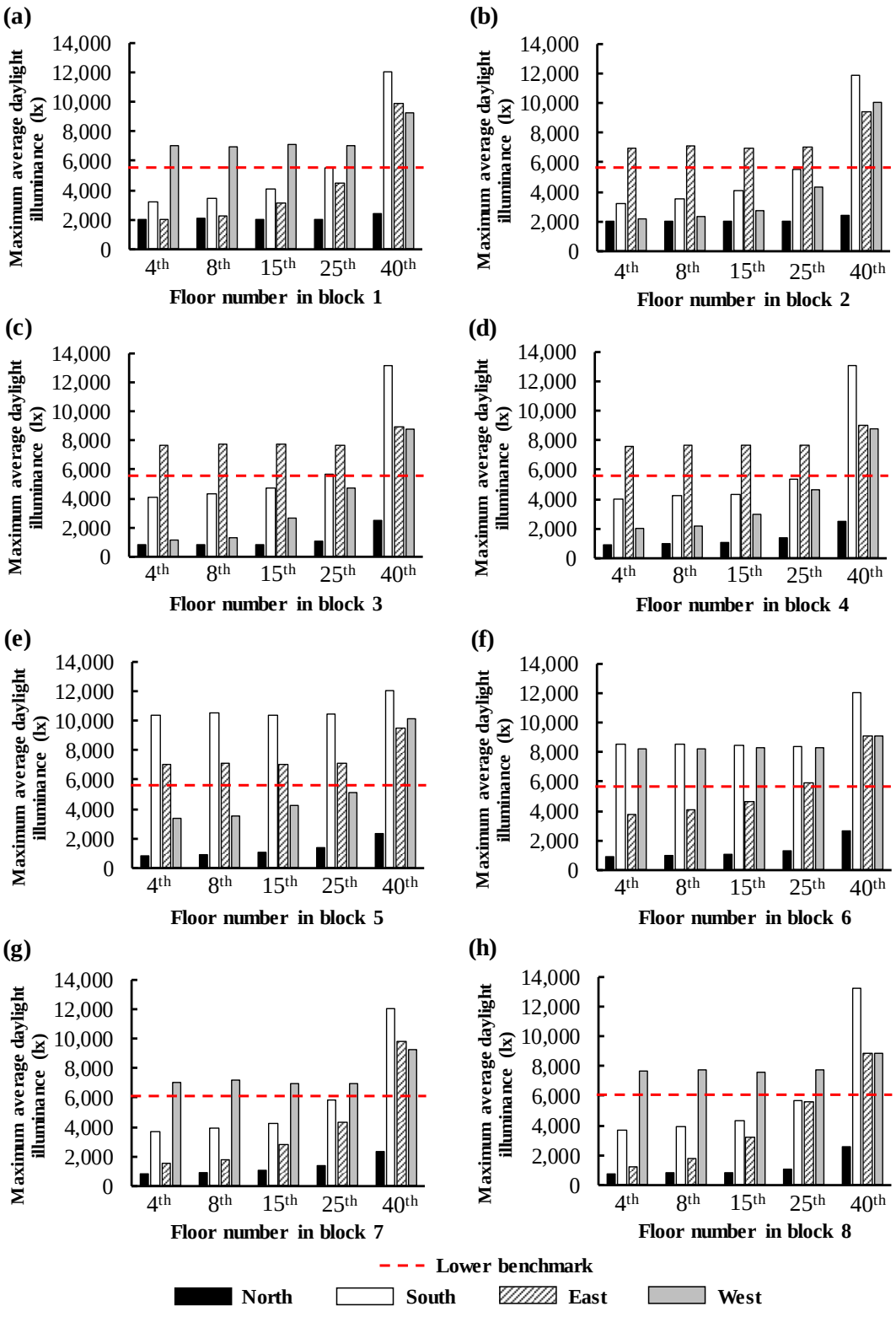

Figure 6.15 Summary of the maximum average daylight illuminance of the 400 flats in the residential buildings and the proposed criterion.

6.4 Summary

This study aimed to characterize the acceptable daylight quality by correlating the subjective evaluations and the objective calculations for the high-rise and dense residential buildings in Hong Kong. The objective daylight measures, such as average $sDA_{300/50\%}$, average $ASE_{1000,\ 250h}$, average UDI, average DA_{300}, average daylight illuminance, and average uniformity, were derived from the daylight simulation results of 400 flats in eight blocks of residential buildings, which were calculated using three different simulation methods (i.e., the daylight coefficient, three- and five-phase methods) and two weather data (i.e., the TMY data and the actual weather data) throughout an entire year. Significant differences were introduced to the average $ASE_{1000,\ 250h}$ and the average daylight illuminance by the two weather data, with the former as large as 16% for the south-facing flats and the latter as large as 16% for the east-facing flats.

A questionnaire survey was carried out in the residential buildings, collecting the residents' long-term opinions about the overall luminous environment in their flats from 340 residents. The survey focused on the same period as the daylight simulation. It was found that the residents' satisfaction with daylighting had the most significant impact on their satisfaction with luminous environment in their flats. In addition, the residents seldom complained about the thermal and glare problems, which was likely due to the obstructions between the residential buildings.

The relationship between the subjective evaluations on the daylight quality and the objective calculations on the daylight quality were investigated through correlation and stepwise regression analyses. It was found that both the average $sDA_{300/50\%}$ and the maximum average daylight had strong correlations to the residents' satisfaction

with daylighting. It was proposed to adopt the criteria that a flat with the average $sDA_{300/50\%}$ above 66% and the maximum average daylight illuminance above 5624 lx can provide an acceptable daylight quality.

The findings can not only help designers and architects to improve the daylight quality when designing high-rise and dense residential buildings in Hong Kong, but also help policy makers to evaluate the daylight quality in various residential buildings in Hong Kong.

Chapter 7

Study 3: Comparison of Daylight Simulation Methods for Reflected Sunlight From Curtain Walls

7.1 Methodology

7.1.1 Building Information and Modelling

The Jockey Club Innovation Tower (JCIT), with a height of around 76 meters, in The Hong Kong Polytechnic University was selected for the investigation. The building façade comprises the main body and the curtain wall, with the former referring to the white frame structures and the latter referring to the reflective surfaces. Figure 7.1 shows the building and also highlights the serious reflected sunlight caused by the curtain wall at different directions.

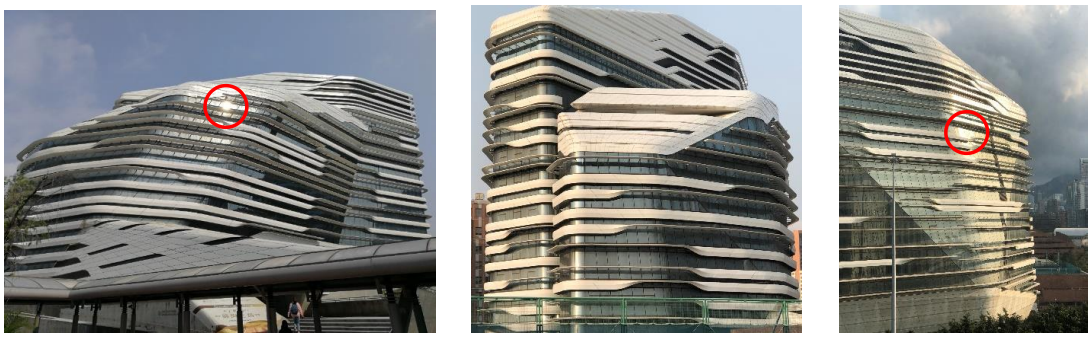

Figure 7.1 Photograph of the Jockey Club Innovation Tower in The Hong Kong Polytechnic University, with the red circles highlighting the reflected sunlight from the curtain wall.

Both the main body and the curtain wall were modelled in Rhino and exported to Radiance. Specifically, the main body was directly exported as one geometry file, with a ground patch being modelled in an individual layer. The curtain wall was separated into 2915 individual planar patches, with each patch being put on an individual layer in a geometry file. Such a division allows the identification of the locations on the

ground and curtain wall patches that receive and introduce serious reflected sunlight. Figure 7.2 shows the rendering of the building.

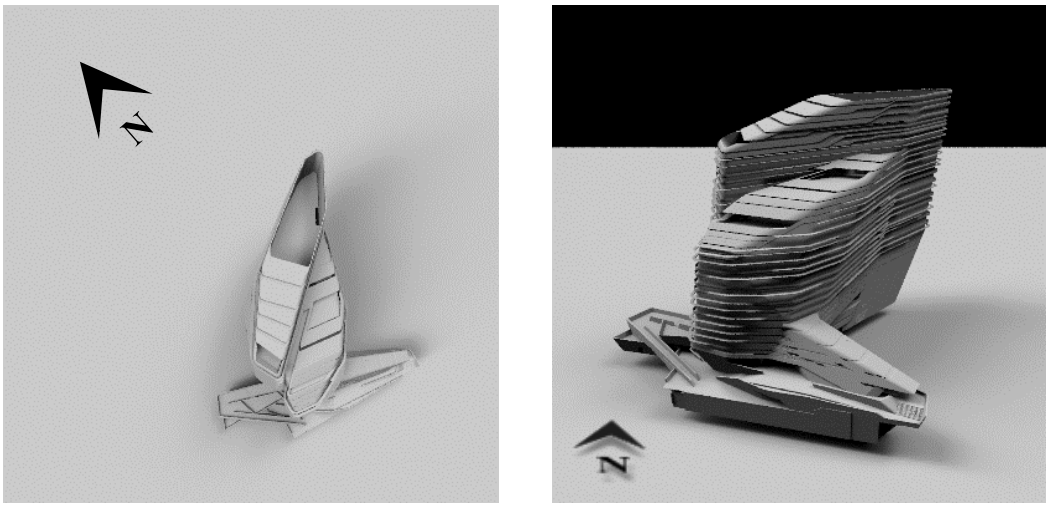

(a) **(b)**

Figure 7.2 Rendering of the building produced by Radiance. (a) Plan view; (b) Projected view.

To highlight the effect of the reflected sunlight from the curtain wall, each of the 2915 curtain wall patches was assigned a *mirror* material with a specular reflectance of 100%, which was able to generate a secondary source in Radiance. Both the main body and the ground were assigned a black material with a reflectance of zero, so that the reflections caused by the main body and the ground were ignored.

7.1.2 Simulation Methods for Characterizing the Illuminance of the Reflected Sunlight

The effect of the reflected sunlight from the curtain wall, in terms of illuminance, was characterized using a single point-in-time backward ray-tracing and three matrix-based methods (i.e., the two-phase, three-phase, and sun coefficient methods), with the hourly contributions of the reflected sunlight during a period of time being combined. A point-in-time sun vector or a time-series of sun-only matrix used in different

simulation methods was derived from the TMY data of Hong Kong, which were downloaded from the EnergyPlus website (NREL, 2007). Table. 7.1 summarizes the parameters used for modelling the sky and the sun in the different simulation methods.

Table 7.1 Summary of the parameters used for modelling the sky and the sun in each simulation method. MF: 1 implies that the sky is divided into 145 patches or generated with 145 sun patches based on the Reinhart sky subdivision scheme.

	Sky definition	Sky subdivision	Sun position	Sky/Sun patches
Single point-in-time backward ray-tracing method	Perez sky model	—	based on geographical locations, time, and instantaneous irradiance data	solar discs in the continuous sky
Two-phase method	Reinhart sky model	MF: 1	3 adjacent sky patches	145 sky patches
Three-phase method	Reinhart sky model	MF: 1	3 adjacent sky patches	145 sky patches
Sun coefficient method	Reinhart sky model	MF: 1	a sun patch	145 sun patches

The effects of the different simulation methods on characterizing the reflected sunlight were compared from two perspectives. Firstly, the comparisons were made on the illuminance caused by the reflected sunlight at the areas around the building during a short period of time (i.e., from 9:30 AM to 5:30 PM on June 21st). The impact of the curtain wall was characterized using a ratio of the reflected sunlight illuminance to the direct sunlight illuminance. Secondly, the comparisons were made on the illuminance caused by the reflected sunlight at the areas around the building throughout the entire year (i.e., 8760 hours for the 365 days) using the three matrix-based methods. Since the curtain wall patches were assigned a perfect *mirror* material with a specular reflectance of 100%, the effect of the reflected sunlight on the surrounding areas, in terms of illuminance, was considered as a relative measure for characterizing the reflected sunlight from the curtain wall. Table 7.2 summarizes the parameter settings used for each simulation method in Radiance and Figure 7.3 shows the workflow of each simulation method.

Table 7.2 Summary of the parameter settings used for each simulation method in Radiance.

Parameter	-ab	-ad	-lw	-dr	-ar	-aa
Description	ambient bounces	ambient divisions	maximum weight of rays	maximum generation of secondary sources	ambient resolution	ambient accuracy
Single point-in-time backward ray-tracing method	1	1000	0.001	1 (0)	256	0.1
Two-phase method	1	1000	0.001	1 (0)	0	0
Three-phase method	1 (0)	1000	0.001	1	0	0
Sun coefficient method	1	1000	0.001	1 (0)	0	0

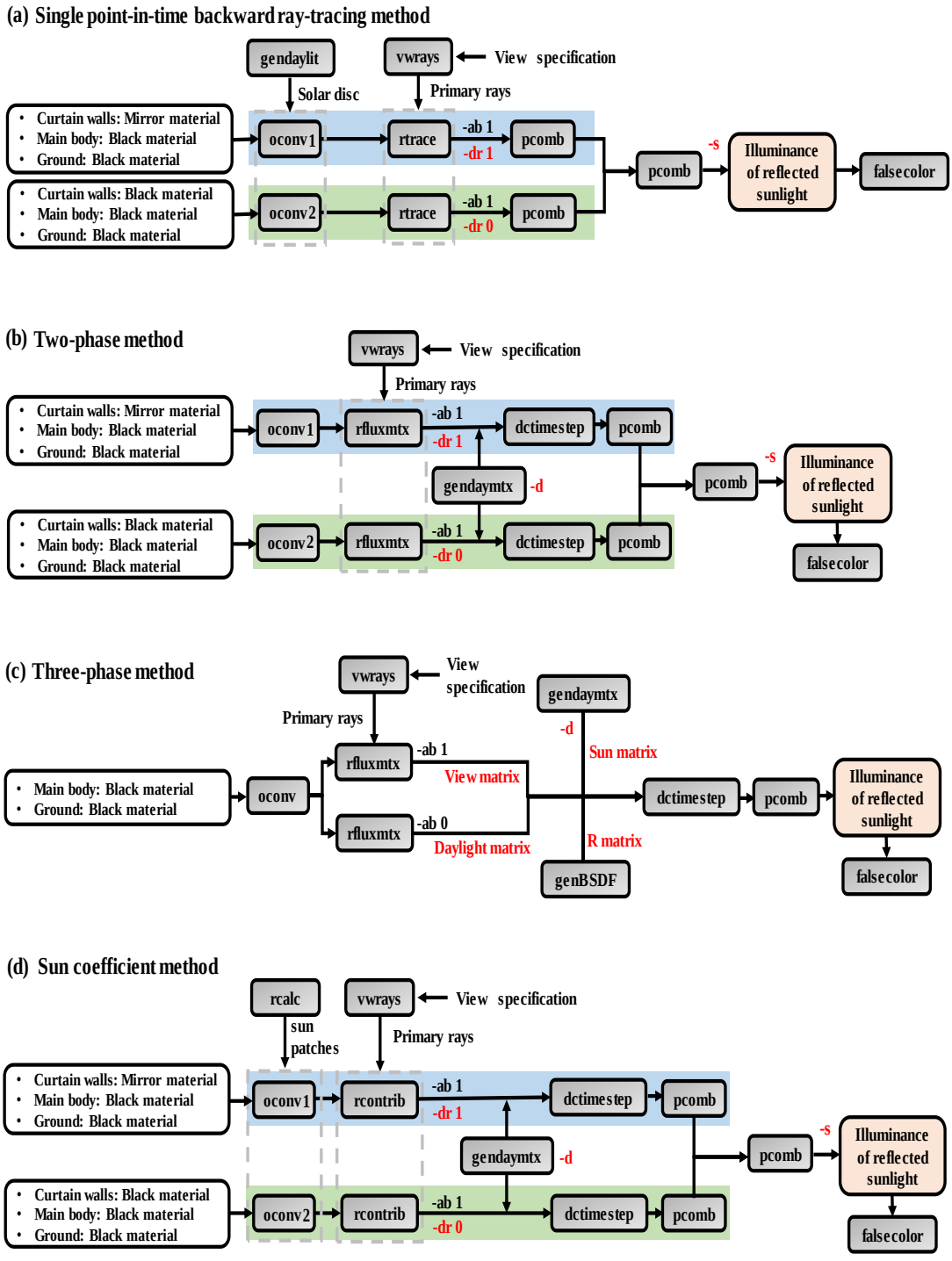

Figure 7.3 Workflows of the simulation methods employed in the study. The steps shaded in light blue consider both the direct and reflected sunlight, while those shaded in light green only consider the direct sunlight. (a) Single point-in-time backward ray-tracing method; (b) Two-phase method; (c) Three-phase method; (d) Sun coefficient method.

- **Single Point-in-time Backward Ray-tracing Method**

This method is generally similar to a backward ray-tracing algorithm. A scene viewed from a specified position along a specified viewing direction can be rendered using this method by the *rtrace* program in Radiance. It can show either the luminance or the illuminance value at each pixel. Thus, the reflected sunlight from the curtain wall, in terms of the illuminance, can be characterized by taking the difference between two images using the *pcomb* program. In other words, the illuminance caused by both the direct sunlight and reflected sunlight from the curtain wall were considered in the first image, with only the curtain wall patches being assigned a perfect *mirror* material with a specular reflectance of 100%. By setting the number of relays for secondary sources (i.e., *-dr*) to 1, the curtain wall patches became the first generation of secondary sources. In contrast, only the illuminance caused by the direct sunlight was considered in the second image, with all the curtain wall patches being assigned a black material with the reflectance of zero. In addition, the optical properties of the main body and ground, as described in Section 7.1.1, kept the same in the two images. Both images were rendered by only considering the sun in the sky, with the sum luminance being derived using the continuous Perez sky model, as shown in Table 7.1. The total illuminance were then derived by combing the images at different times (i.e., the short period of time or the entire year) using the *pcomb* program. The workflow of this method is shown in Figure 7.3(a).

- **Two-phase Method**

The workflow of the two-phase method was similar to that using the single point-in-time backward ray-tracing method, as illustrated in Figures 7.3(a) and 7.3(b). However, the two-phase method distributed the sun luminance to the three closest sky patches,

and correlated the illuminance at each pixel to the average luminance of each sky patch using a coefficient. The illuminance at any point was derived by multiplying the coefficient matrix of the point with the luminance of the sun-only matrix. Both the material specifications and the calculation procedures were the same as those used in the single point-in-time backward ray-tracing method.

- **Three-phase Method**

As mentioned before, the front transmission component of the BSDF is generally used as the T matrix when using the three-phase method. For example, for a perfect transmitting surface, a light ray hitting the exterior of the fenestration from the 7^{th} direction (the yellow patch) will transmit through the fenestration towards the interior along the 7^{th} direction (the red patch), as shown in Figure 7.4(a). In order to calculate the reflected sunlight caused by the exterior of the fenestration, the values in the front transmission matrix need to be replaced with those in the reflection matrix (R), with the patch numbers being reordered to consider the symmetrical distributions of the patches in the reflection and transmission matrices. For example, the 7^{th} direction in transmission (i.e., the red patch in Figure 7.4(a)) needs to be changed to the 9^{th} direction in reflection (i.e., the red patch in Figure 7.4(b)). Therefore, the calculation of V×T×D×S in the three-phase method was actually revised to the calculation of V×R×D×S.

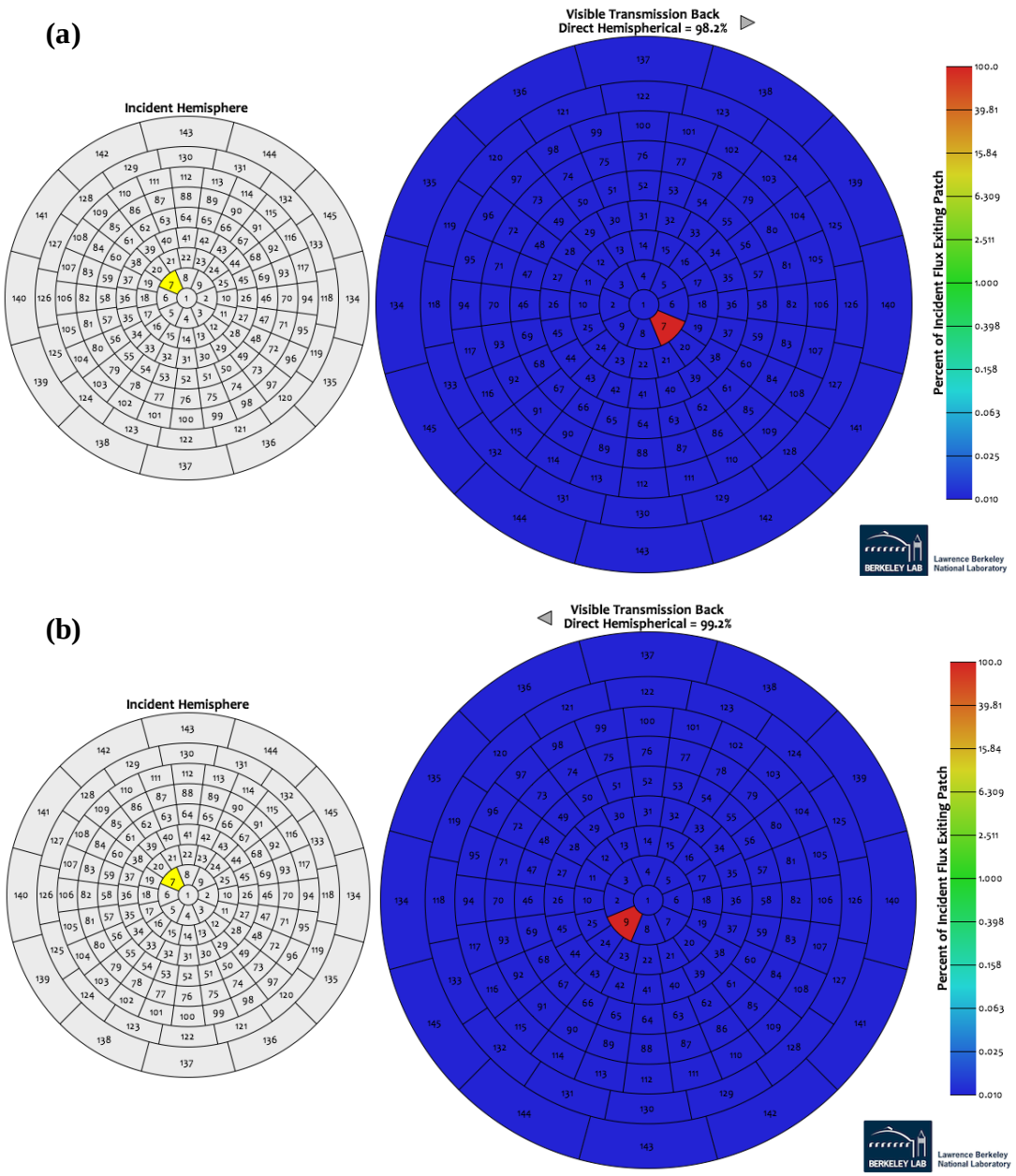

Figure 7.4 Screenshot of the BSDF generated based on the standard Klems scheme with 145 × 145 patches. The left figure refers to the incident hemisphere, the right figure refers to (a) the transmission and (b) the reflection hemisphere. (a) Transmission for sunlight coming from the incident hemisphere that is used in the three-phase calculation; (b) Revised transmission for sunlight coming from the incident hemisphere that can be used in the three-phase calculation, which is actually showing the back reflection of the material.

To improve the efficiency of the simulation, the view and daylight matrices were derived for a group of curtain wall patches rather than for each individual curtain wall patch. Thus, the 2915 curtain wall patches were classified into 47 and 94 groups, with each group containing about 60 and 30 patches. The patches in each group were

coplanar and had the same orientations. Due to the same optical property, the curtain wall patches in each group were represented by a shared BSDF. The shared BSDF was generated using the *genBSDF* program based on a standard Klems scheme with 145 × 145 patches, with each patch having an angular diameter of around 13.5°. In addition, the geometry of the shared BSDF was modelled large enough to ensure that the probability of the rays leaving through the edge of the grouped coplanar patches was insignificant.

The images of a scene showing the reflected sunlight illuminance at different times at each pixel were produced by multiplying the matrices VRDS using the *dctimestep* program, as shown in Figure 7.3(c). The reflected sunlight illuminance during the short period and the entire year was then derived by combining these images using the *pcomb* program.

- **Sun Coefficient Method**

The workflow of the sun coefficient method was similar to that of the two-phase method, as illustrated in Figures 7.3(b) and 7.3(d). However, the sun coefficient method generated 145 sun patches, with each having an angular diameter of around 0.533°, rather than distributing the sun luminance to the three closest sky patches. It is worthwhile to mention that the insertion of a high resolution tensor tree BSDF characterizing the optical property of the curtain wall patches was not considered in this study. The material specifications and the calculation procedures, as shown in Figure 7.3 (d), were the same as those used in the single point-in-time backward ray-tracing and the two-phase methods.

7.1.3 Proof of Concept Using A Simple Model

The feasibility of using the four methods to calculate the reflected sunlight illuminance was tested using a simple model. The model comprised a south-facing mirror and a ground plane. The mirror had a dimension of 3 m (height) × 4 m (width), with a specular reflectance of 100%; the ground was modelled with the reflectance of zero. Based on the ambient parameter settings and the sun and sky modelling summarized in Tables 7.1 and 7.2, the illuminance caused by the reflected sunlight from the mirror was calculated using the above four simulation methods during the period from 9:30 AM to 5:30 PM on December 21st. Figure 7.5 shows the combined reflected sunlight contributions with illuminance values at different times. It can be observed that the four simulation methods produced similar illuminance distributions. In addition, the average illuminance levels due to the reflected sunlight derived using the four simulation methods were also similar, as shown in Figure 7.6. Such findings suggested the feasibilities of using these four simulation methods to quantitatively characterize the effect of the reflected sunlight from a curtain wall.

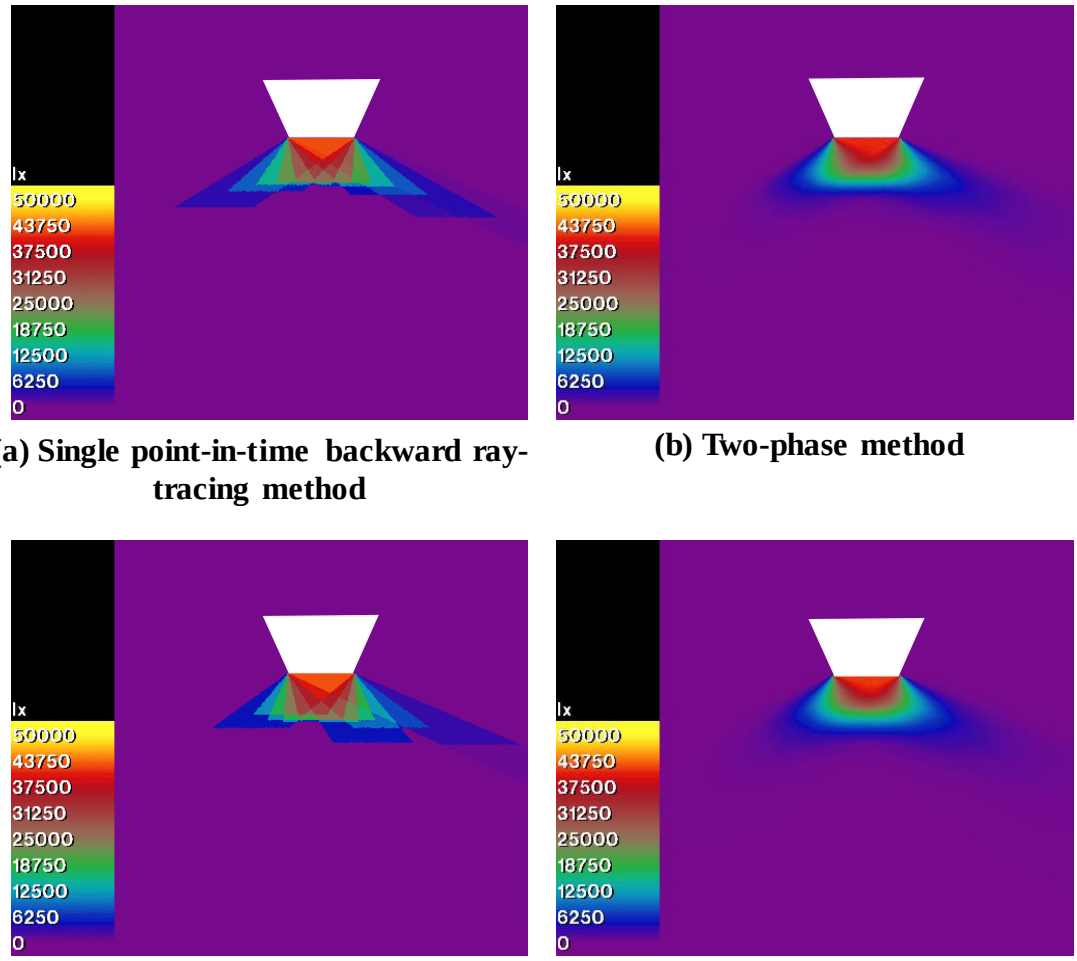

(a) Single point-in-time backward ray-tracing method

(b) Two-phase method

(c) Sun coefficient method

(d) Three-phase method

Figure 7.5 Results of the reflected sunlight illuminance from the simple model from 9:30 AM to 5:30 PM on December 21st using the four simulation methods. The white area represents the mirror which is a perfect specular reflector. (a) Single point-in-time backward ray-tracing method; (b) Two-phase method; (c) Sun coefficient method; (d) Three-phase method.

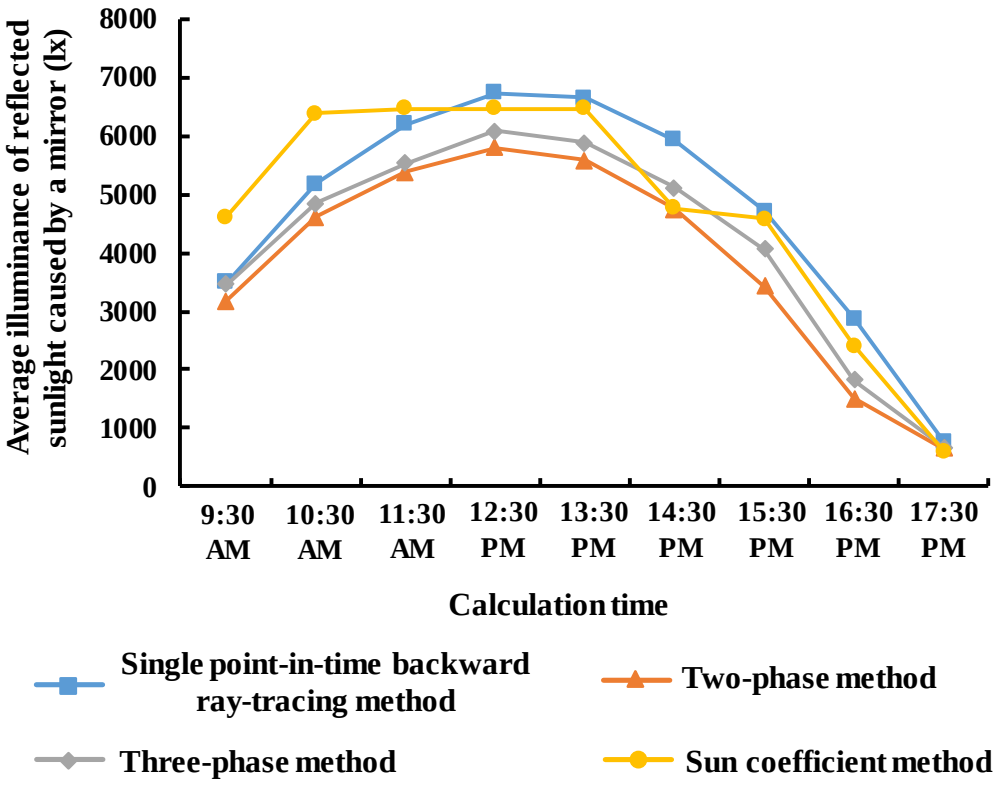

Figure 7.6 Comparison of the average illuminance of the reflected sunlight from the simple model from 9:30 AM to 5:30 PM on December 21st.

7.1.4 Simulation Method for Identifying Curtain Wall Patches Introducing and Locations Receiving Reflected Sunlight

Though the above four methods can calculate the reflected sunlight illuminance at the locations on or above the ground, they cannot be used to identify the locations on the curtain wall that introduce the reflected sunlight.

A forward ray-tracing method, which was developed based on a previous work (Walker, 2012), was used to simultaneously identify the locations on the curtain wall that introduced the reflected sunlight and those on the ground that received the reflected sunlight. By setting the *MF* to 5, the 3601 sun patches were generated and uniformly distributed in the sky dome, with each patch having an angular diameter of around 0.533°. Based on the geographical location of Hong Kong and the local TMY data, only 524 sun patches had non-zero luminance values throughout the entire year.

A single light ray was then sent from the centre of each of the 524 sun patches along the vector of the solar direction to the curtain wall patches. The propagation of the light rays was traced based on the forward ray-tracing algorithm. The locations where the light rays intersected with the curtain wall patches were recorded, which were the locations that introduced the reflected sunlight from the curtain wall.

In order to identify the locations that received the reflected sunlight, a virtual hemisphere was modelled as a receiver with a radius of 100 m, as shown in Figure 7.7. During the ray-tracing process, only one reflection from the curtain wall was allowed. The locations where the reflected light rays intersected with the ground or the hemisphere were recorded. The locations on the ground that received the reflected sunlight were identified by the coordinates where the rays reached the ground, while those on the hemisphere were identified by the directions based on the radius of 100 m.

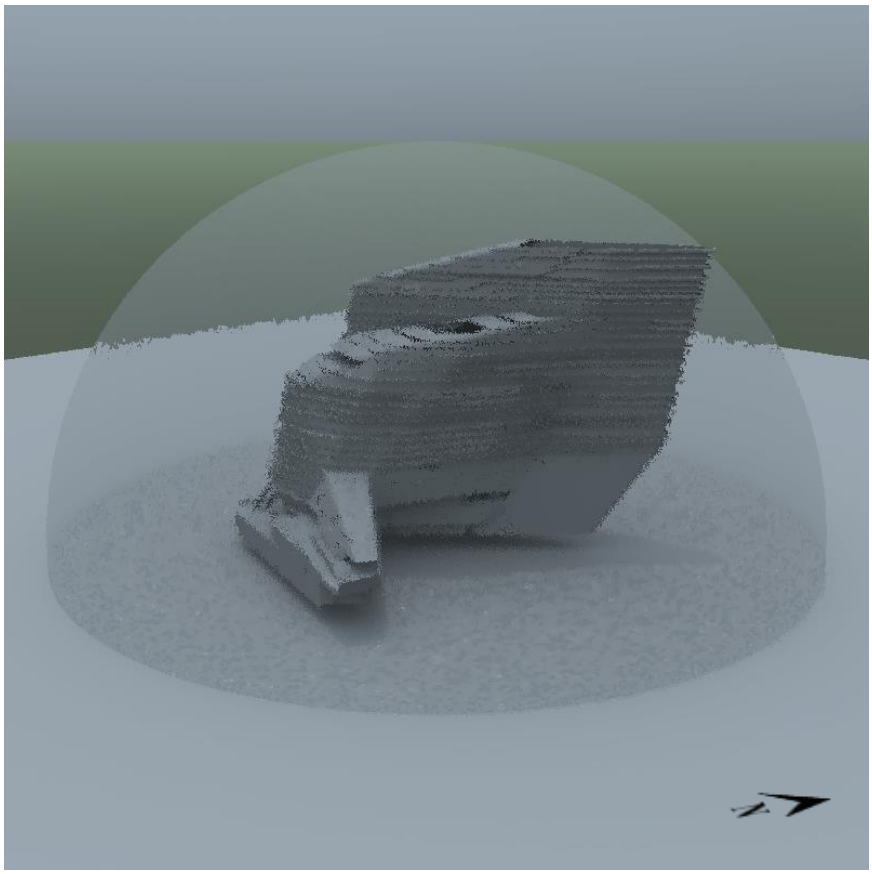

Figure 7.7 Illustration of the virtual hemisphere with a radius of 100 m that was built to identify the directions that received the reflected sunlight. The rendering was produced with the viewing position being specified as (190, -190, 100) and the viewing direction being specified as (-0.5, 0.5, -0.2).

The horizontal illuminance of the reflected sunlight at the identified locations were also calculated in this study using the two-phase, sun coefficient, and three-phase methods throughout the entire year, with the ambient parameter settings and the sun and sky modelling being summarized in Tables 7.3 and 7.4. In reality, these locations were only used to identify the direction of the reflected sunlight, which can be used to investigate whether the adjacent buildings or windows would receive reflected sunlight. Therefore, the illuminance of the reflected sunlight should be calculated based on the orientations of these adjacent buildings or windows.

Table 7.3 Summary of the modelling of the sky and the sun for calculating the horizontal illuminance at the identified locations that received reflected sunlight using each simulation methods. MF: 5 implies that the sky is subdivided into 3601 patches or generated with 3601 sun patches according to the Reinhart sky subdivision scheme.

	Sky definition	Sky subdivision	Sun position	Sky/Sun patches
Two-phase method	Reinhart sky model	MF: 5	3 adjacent sky patches	3601 sky patches
Three-phase method	Reinhart sky model	MF: 5	3 adjacent sky patches	3601 sky patches
Sun coefficient method	Reinhart sky model	MF: 5	a sun patch	3601 sun patches

Table 7.4 Summary of the parameter settings for calculating the horizontal illuminance at the identified locations that received reflected sunlight using each simulation method in Radiance.

Parameter	-ab	-ad	-lw	-dr
Description	ambient bounces	ambient divisions	maximum weight of rays	maximum generation of secondary sources
Two-phase method	5	10000	0.0001	1 (0)
Three-phase method	5	10000	0.0001	1
Sun coefficient method	5	10000	0.0001	1 (0)

7.2 Results and Discussion

7.2.1 Illuminance of the Reflected Sunlight on A Single Day

The illuminance distributions at the ground areas around the building due to the reflected sunlight is shown in Figure 7.8, with the values being calculated from 9:30 AM to 5:30 PM on June 21st using the four simulation methods. It can be observed that the illuminance distributions were similar regardless of the simulation methods. However, significant differences were introduced to the illuminance levels. The single-point-in-time backward ray-tracing and the sun coefficient methods produced much higher illuminance levels than the two- and three-phase methods, with the highest levels being around 117066, 114202, 15707, and 18222 lx for the single point-in-time backward ray-tracing, sun coefficient, two-phase, and three-phase methods.

There were two reasons for such significant differences using the different methods. Firstly, the methods used different source types to model the sun. For example, the sun was modelled using the *light* material in the single point-in-time backward ray-tracing and the sun coefficient methods, so that the direct sunlight contribution was calculated in a deterministic way. In contrast, the sun was modelled using the *glow* material in the two- and three-phase methods, so that the direct sunlight contribution was calculated in a stochastic way. Since the identical division sampling rays (i.e., *-ad* 1000) were used for all the methods, the reflected sunlight illuminance calculated using the single point-in-time backward ray-tracing and the sun coefficient methods would be higher. Such a result indicated that the 1000 sampling rays were not enough to model the sun when it was modelled using the *glow* material. Secondly, the sun luminance distribution was characterized in different ways (i.e., whether using individual sun patches or distributing the sun luminance to the three closest sky patches). For example, since the two- and three-phase methods distributed the sun luminance to the three closest sky patches, the density of sky patches would affect the calculation of the direct sunlight. Thus, the calculation results were expected to produce large errors when only the 145 sky patches were used in the two- and three-phase methods. This was likely due to the underestimated sun luminance, which was caused by the solar radiation from a patch of 0.533° angular diameter being distributed to three 13.5° sky patches. Moreover, though the sun coefficient method used 145 sun patches to model the sun contribution, these 145 sun patches did not completely cover the all possible sun locations.

It can be also observed that the results derived using the two- and three-phase methods had a significant difference, though the two methods modelled the sun in the same way. As shown in Figure 7.8(b), the results derived using the two-phase method had higher

noises, which were likely due to the insufficient sampling. Though both the two- and three-phase methods used the identical division sampling rays (i.e., *-ad* 1000), the same value had different meanings to the methods. This was likely because the three-phase method used the BSDF to characterize the reflected sunlight from the curtain wall patches. Thus, the 1000 sampling rays were not only distributed from each pixel of the image but also from the 145 Klems patches. Such a difference may be subtle to simple geometries, such as the model shown in Figures 7.5(b) and 7.5(d), but may be significant to complicated geometries.

Furthermore, the calculation results may be also affected by the Klems BSDF patches and sky patches. When using the three-phase method, the shared BSDF was generated based on a standard Klems scheme with 145 × 145 patches, with each patch of the transmitted and reflection hemispheres having an angular diameter of around 13.5°, and the sky was divided into 145 patches, with each sky patch also having around 13.5° angular diameter. Since the solar distribution from a patch of 0.533° angular diameter was distributed to the three closest sky patches, the sun luminance was averaged and distributed to more than six Klems patches, which reduced the intensities of the reflected sunlight on the reflection hemisphere.

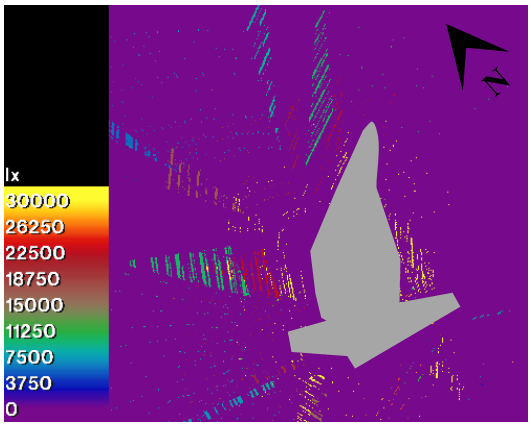

(a) Single point-in-time backward ray-tracing method

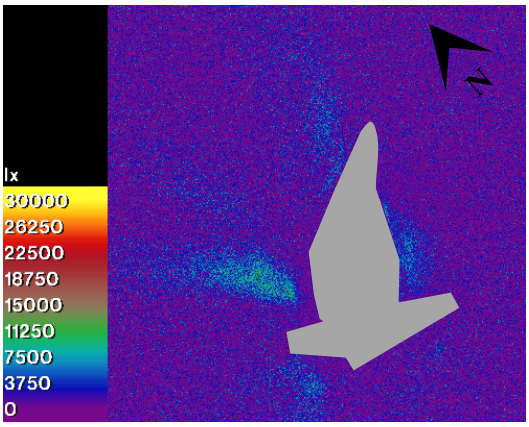

(b) Two-phase method

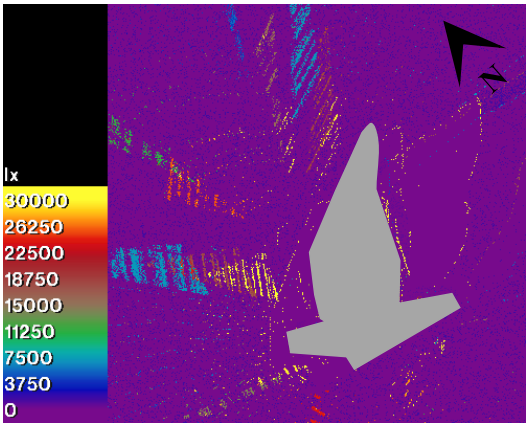

(c) Sun coefficient method

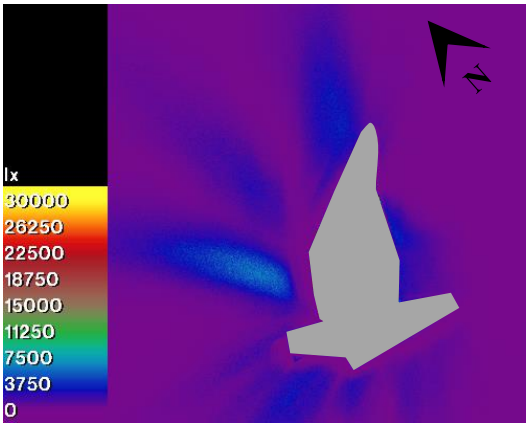

(d) Three-phase method

Figure 7.8 Comparisons of the illuminance of the reflected sunlight from the curtain wall from 9:30 AM to 5:30 PM on June 21st using the four simulation methods. The grey area represents the building. (a) Single point-in-time backward ray-tracing method; (b) Two-phase method; (c) Sun coefficient method; (d) Three-phase method. The images were produced with the viewing position being specified as (-10, 0, 300) and the viewing direction being specified as (0.1, 0.1, -1).

In addition, the grouping of the curtain wall patches would affect the calculation results derived using the three-phase method, since the view and daylight matrices were calculated for each group. The calculation results derived using a large number of groups in the three-phase method were expected to be similar to those produced using the other methods. Figures 7.9(a) and 7.9(b) show different distributions of the reflected sunlight around the building calculated using the different groupings of the curtain wall patches using the three-phase method. The 94 groups produced the highest

illuminance of 18222 lx, while the 47 groups produced the highest illuminance of 16423 lx. Thus, the 94 groups were used to calculate the reflected sunlight illuminance throughout the entire year.

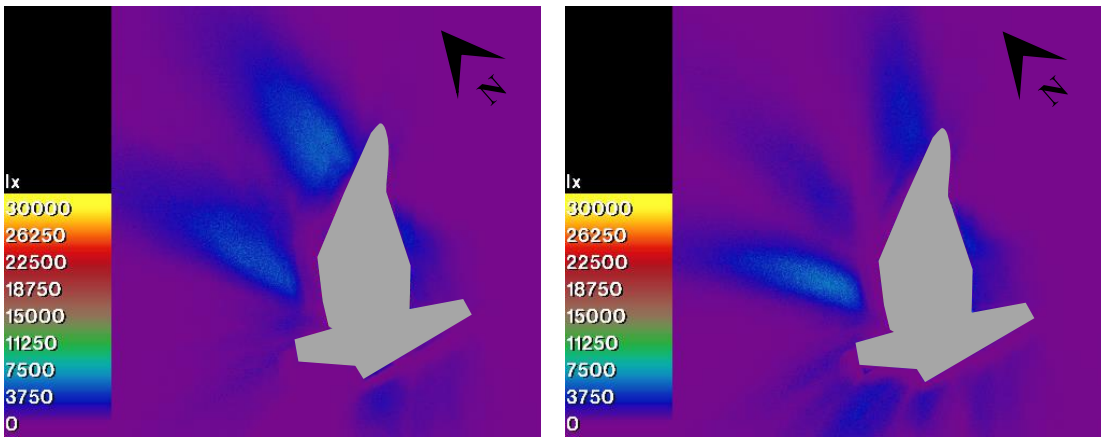

(a) **(b)**

Figure 7.9 Comparisons of the illuminance of the reflected sunlight calculated using the three-phase method with the different groupings of the curtain wall patches on the building façade. The calculations were from 9:30 AM to 5:30 PM on June 21st. The grey area represents the building. (a) 47 groups with each containing about 60 curtain wall patches; (b) 94 groups with each containing about 30 curtain wall patches.

Figure 7.10 shows the ratios of the reflected sunlight illuminance to the direct sunlight illuminance from 9:30 AM to 5:30 PM on June 21st, which were derived from the calculation results derived using the single point-in-time backward ray-tracing, two-phase, and sun coefficient methods (note: the reflected sunlight illuminance was directly calculated when using the three-phase method, as explained in Figure 7.3(c)). Though the average direct sunlight illuminance was 229836, 225540, and 222676 lx for the single-point-in-time backward ray-tracing, two-phase, and the sun coefficient methods, the ratios were 0.10, 0.015, and 0.035 respectively.

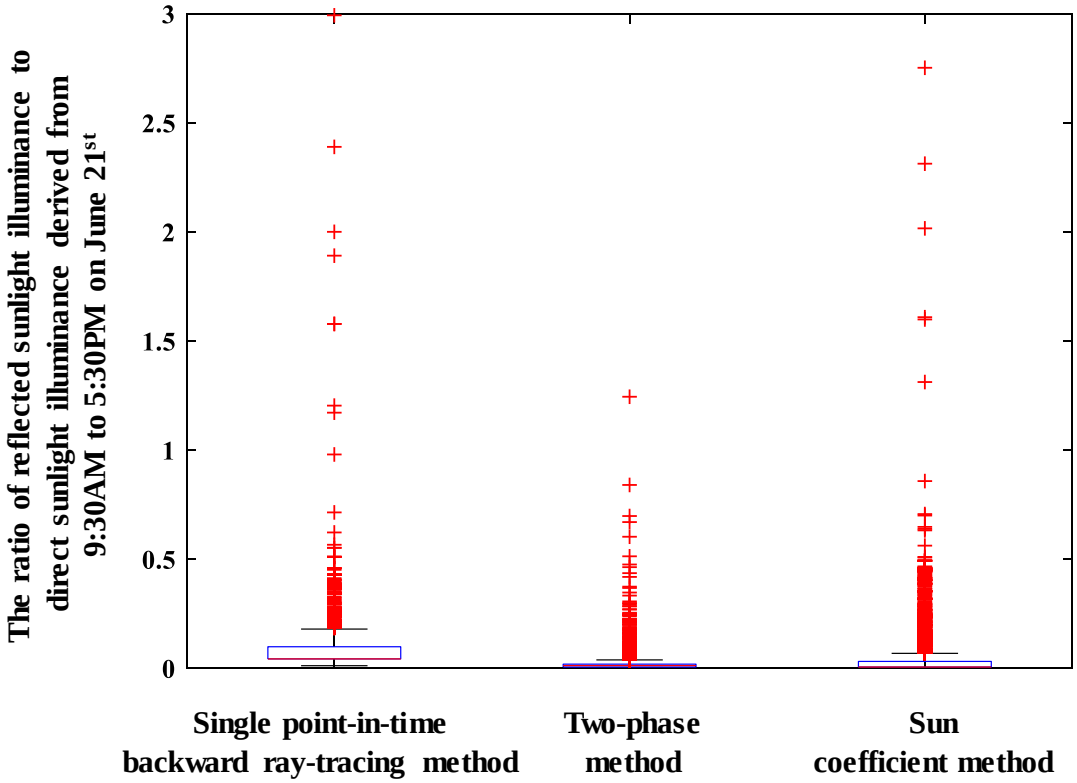

Figure 7.10 Comparison of the ratio of the illuminance of the reflected sunlight to that of the direct sunlight from 9:30 AM to 5:30 PM on June 21st when the three different simulation methods were used.

7.2.2 Average Illuminance of the Reflected Sunlight throughout the Entire Year

Figure 7.11 shows the average illuminance of the reflected sunlight calculated using the three matrix-based simulation methods (i.e., two-phase, sun coefficient, and three-phase methods) throughout the entire year. The calculation results can be used to identify the potential ground locations receiving serious reflected sunlight from the curtain wall throughout the entire year. It can be observed that all the three methods consistently identified the ground locations in the southeast of the building that would have the highest frequency to receive serious reflected sunlight. The highest average illuminance of the reflected sunlight calculated using the sun coefficient method was 46003 lx, while those calculated using the two- and three-phase methods were around 8166 and 12754 lx respectively. Similar to the results of a single day, the two-phase

method produced higher noises, while the three-phase method produced smoother illuminance distributions.

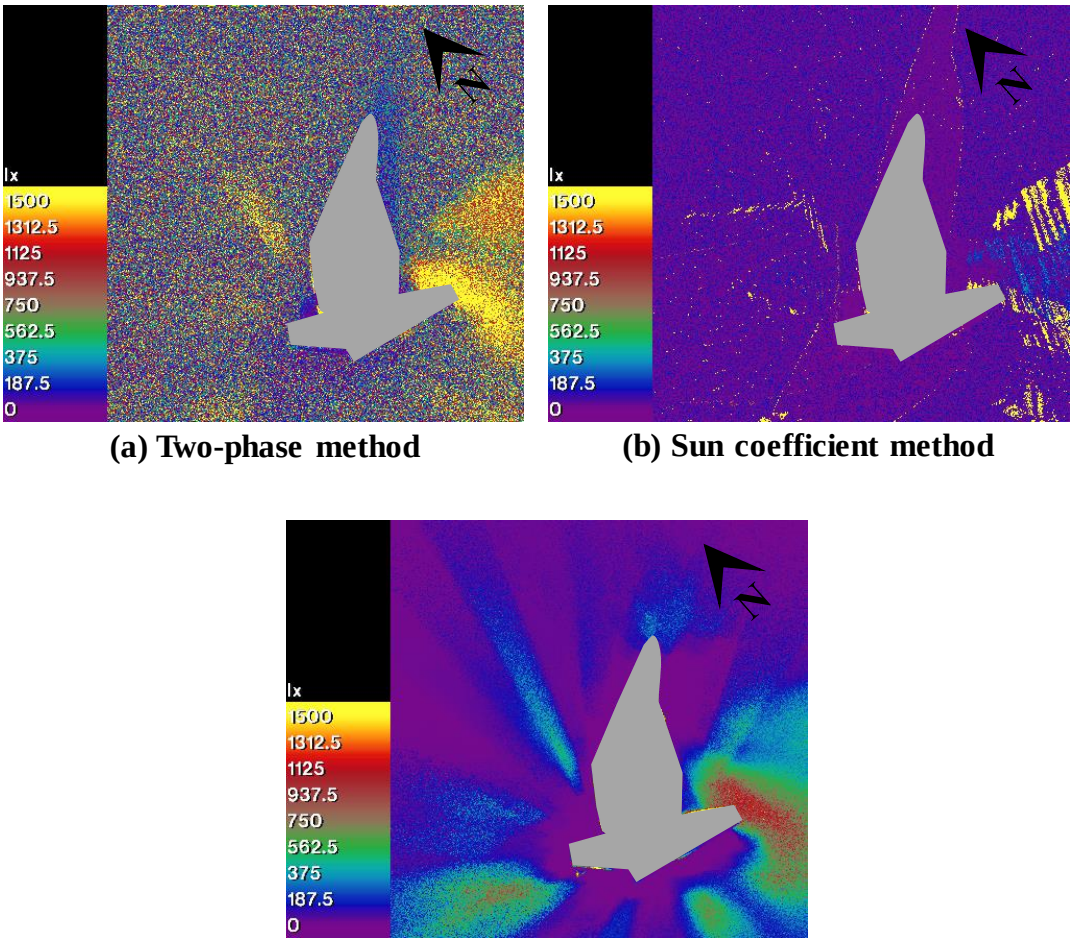

(a) Two-phase method **(b) Sun coefficient method**

(c) Three-phase method

Figure 7.11 Comparisons of the average illuminance of the reflected sunlight in the entire year calculated using the three simulation methods. The grey area represents the building. (a) Two-phase method; (b) Sun coefficient method; (c) Three-phase method.

7.2.3 Identification of Curtain Wall Patches Introducing and Locations Receiving Reflected Sunlight

The forward ray-tracing method identified eight locations that received serious reflected sunlight in a year, with three on the ground and five on the virtual hemisphere, as shown in Figure 7.12. The corresponding eight curtain wall patches that introduced

serious reflected sunlight to these eight locations were also identified, as shown in Figure 7.13.

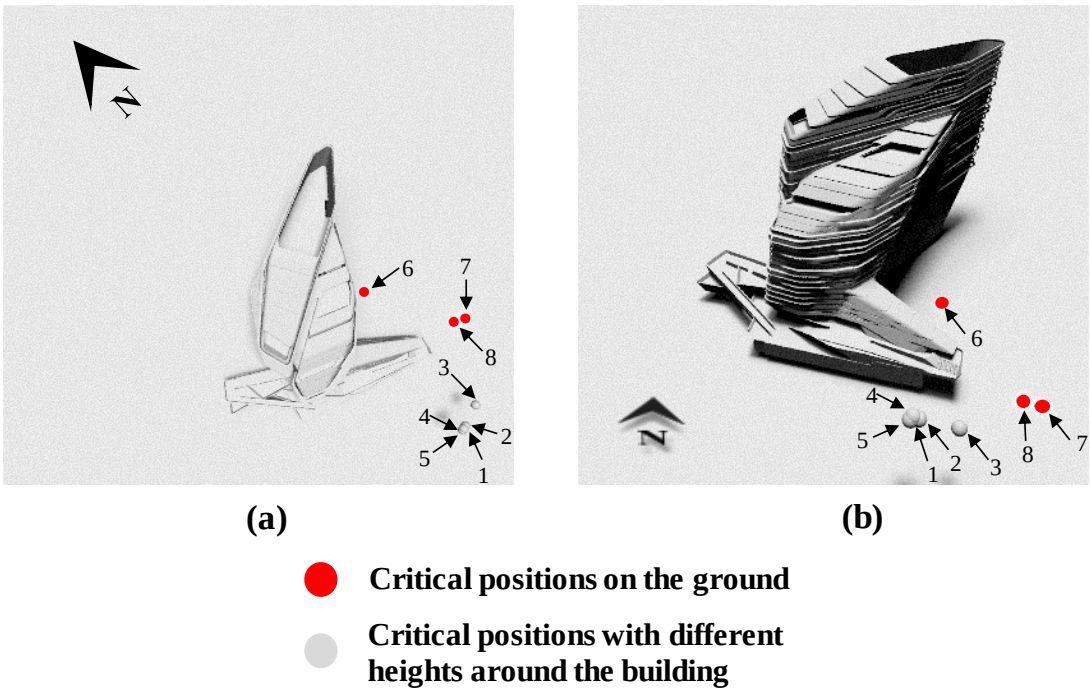

Figure 7.12 Illustration of the eight locations that were identified to receive serious reflected sunlight using the forward ray-tracing method. Locations 1 to 5 were not on the ground (around 30 meters above the ground); locations 6 to 8 were on the ground. (a) Plan view; (b) Perspective view.

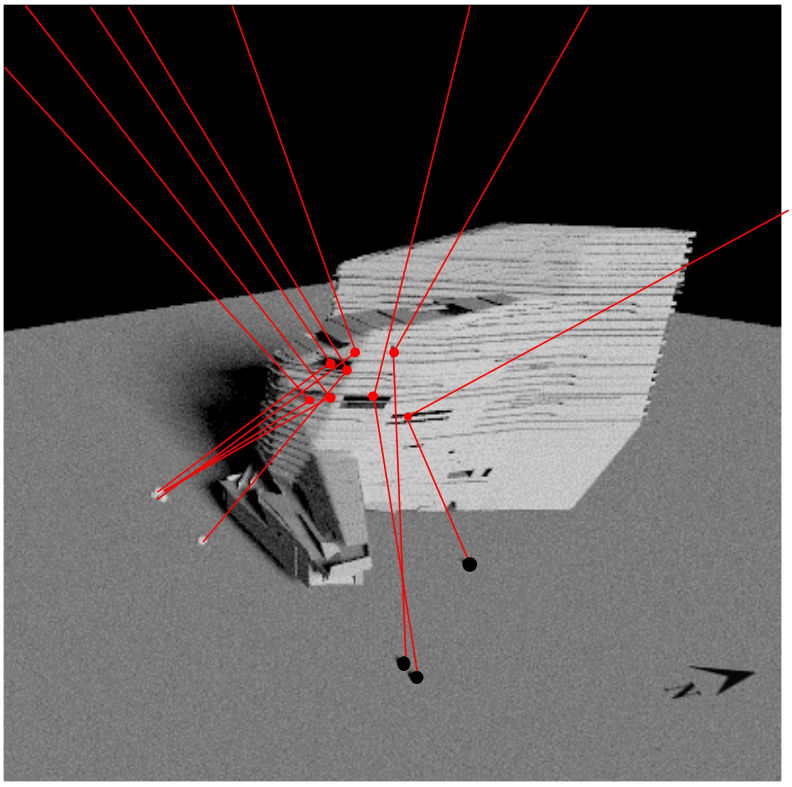

Figure 7.13 Illustration of using the forward ray-tracing method to identify the curtain wall patches introducing the serious reflected sunlight and the locations receiving the serious reflected sunlight. Each red line represents a sun ray that was sent from a sun patch and reflected by the curtain wall. The red points represent the origins of the reflected sunlight on the curtain walls. The grey and black points are those shown in Figure 7.12.

The horizontal illuminance of the reflected sunlight received at these eight locations was then calculated using the two-phase, sun coefficient, and three-phase methods with an interval of one hour throughout the entire year. The calculation results derived at four locations (i.e., position 1, 3, 6, and 7 shown in Figure 7.12) were selected and shown in Figures 7.14-7.17. It was found that the different simulation methods produced significant differences to the reflected sunlight illuminance. Again, this was likely due to the different source types used for modelling the sun and the different ways used for characterizing the sun luminance contributions.

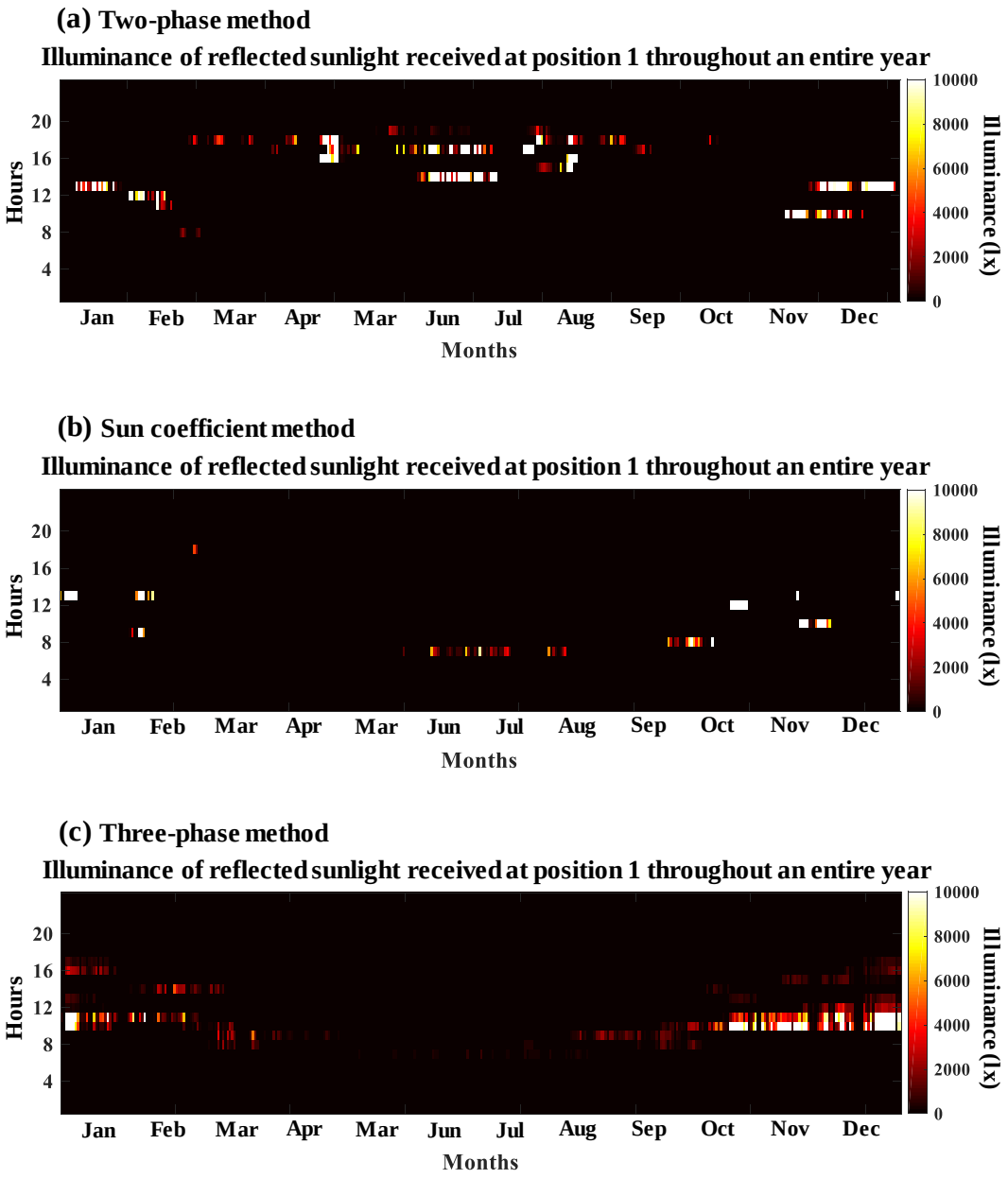

Figure 7.14 Summary of the horizontal illuminance of the reflected sunlight at position 1 throughout the entire year calculated using the different matrix-based methods. (a) Two-phase method; (b) Sun coefficient method; (c) Three-phase method.

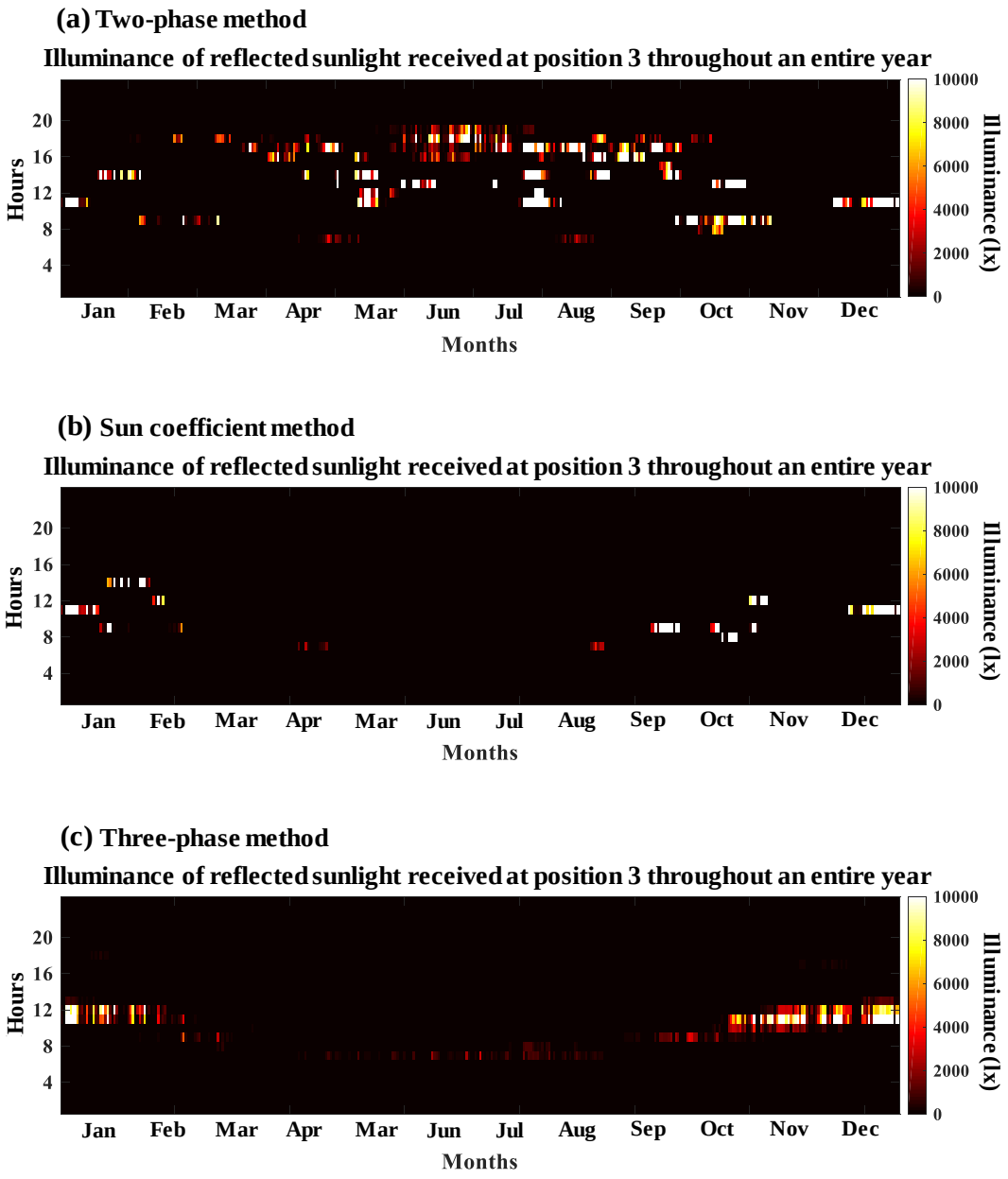

Figure 7.15 Summary of the horizontal illuminance of the reflected sunlight at position 3 throughout the entire year calculated using the different matrix-based methods. (a) Two-phase method; (b) Sun coefficient method; (c) Three-phase method.

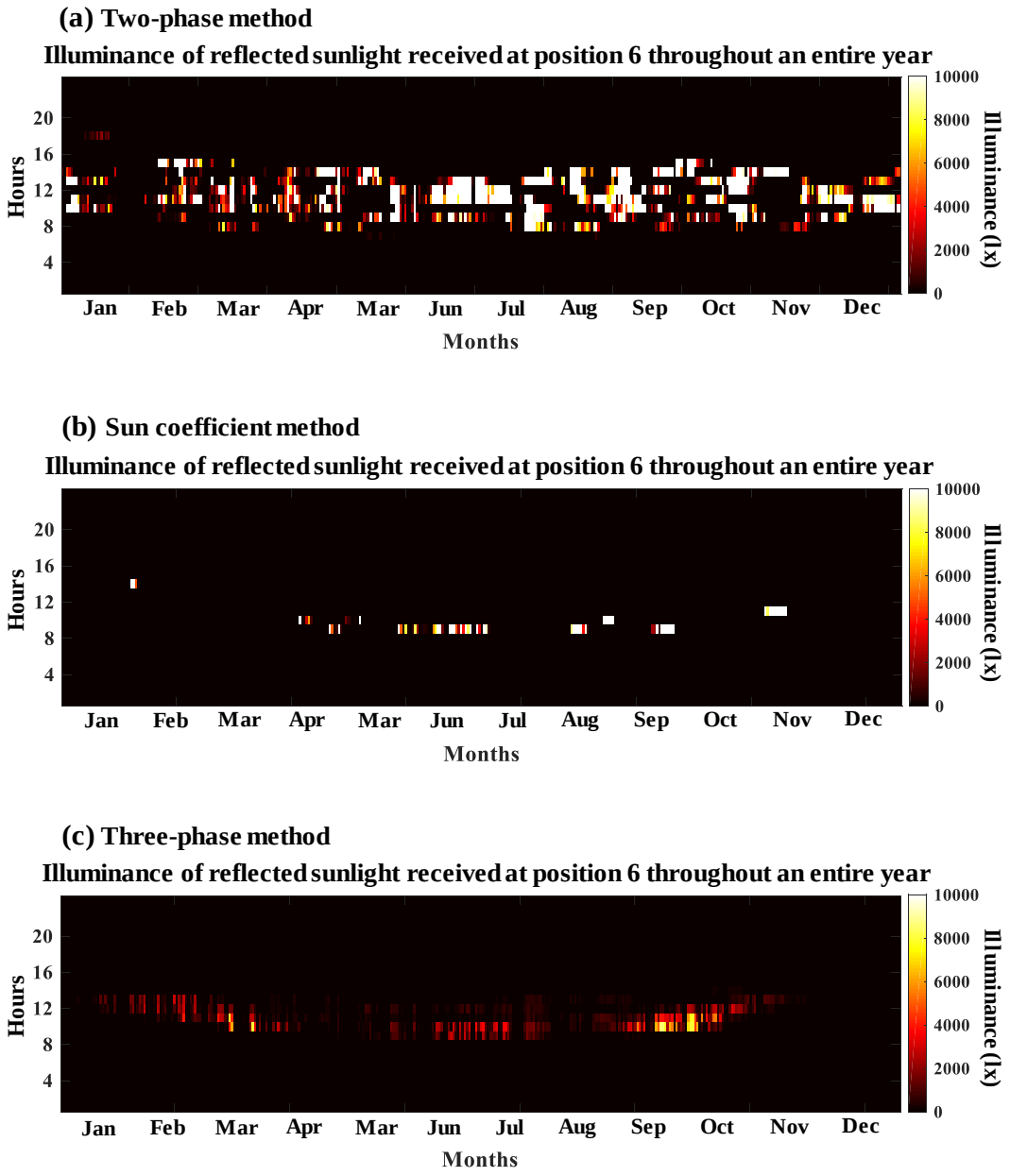

Figure 7.16 Summary of the horizontal illuminance of the reflected sunlight at position 6 throughout the entire year calculated using the different matrix-based methods. (a) Two-phase method; (b) Sun coefficient method; (c) Three-phase method.

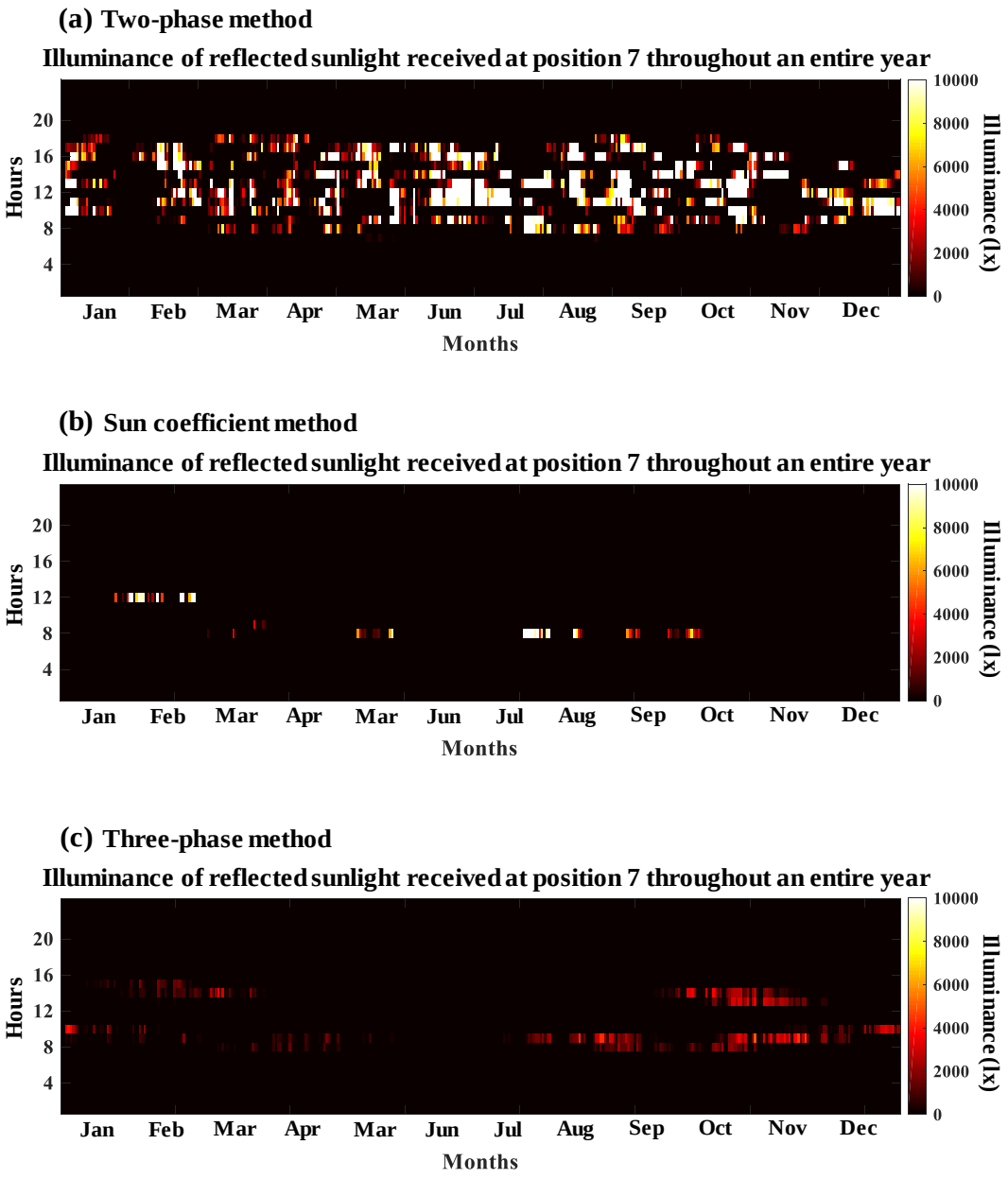

Figure 7.17 Summary of the horizontal illuminance of the reflected sunlight at position 7 throughout the entire year calculated using the different matrix-based methods. (a) Two-phase method; (b) Sun coefficient method; (c) Three-phase method.

The above results clearly revealed how different simulation methods characterized the effect of reflected sunlight from the curtain wall. Specifically, the backward ray-tracing methods (i.e., two-phase, sun coefficient, and three-phase methods) can be used to identify the potential ground areas receiving serious reflected sunlight and to characterize the effect of the reflected sunlight with illuminance levels on the ground areas throughout the entire year.

In contrast, the forward ray-tracing method can be more efficient and effective to identify the exact locations receiving serious reflected sunlight. Furthermore, the backward ray-tracing methods (i.e., two-phase, sun coefficient, and three-phase methods) can then be used to calculate the reflected sunlight illuminance at these locations. If the locations receiving the serious reflected sunlight are not on the ground, the light rays can be used to trace the directions where the serious reflected sunlight may happen in surrounding buildings. More importantly, the forward ray-tracing method can also be used to identify the locations (e.g., curtain wall patches) that introduce the serious reflected sunlight, which is useful for geometry design and material selection of the building façade.

7.3 Limitations and Future Work

The study was designed to compare how different daylight simulation methods can be used to characterize reflected sunlight from a curtain wall throughout an entire year. A future work is believed necessary to address the following limitations.

1. The ambient calculation parameters were set identical when using the different simulation methods in this study. The results clearly suggested that the same parameter settings would have different meanings to the different methods. A follow-up work is planned to compare how different ambient parameter settings would affect the characterization of reflected sunlight. The simulation results will be validated with the field measurement.

2. A limited number of the sun and sky patches were used to model the sun in this study. It would be interesting to further investigate how the numbers of the sun and sky patches, in conjunction with the resolution of the BSDF for the curtain wall patches, affect the simulation results for the reflected sunlight. It is necessary to ensure that the

sun luminance can be characterized using the Klems patches without missing the peak intensity.

3. The simulation only considered the JCIT building without any surrounding buildings. Since the Radiance simulation is based on the far-field assumption, the effects of the surrounding environment on simulation results should be considered when comparing the results to the field measurement.

4. The simulation results derived using the three-phase method are believed to be affected by the groupings of the curtain wall patches. It is necessary to further investigate how the accuracy and efficiency of the simulation should be balanced by optimizing the grouping of the curtain wall patches, especially for complicated fenestration systems.

5. Last but not least, thermal effect is also important when characterizing reflected sunlight from the curtain wall. Both the horizontal and vertical irradiance levels need to be calculated for characterizing the thermal effects.

7.4 Summary

The study comprehensively compared how different daylight simulation methods, including four backward ray-tracing methods (i.e., the single point-in-time backward ray-tracing, two-phase, sun coefficient, and three-phase methods) and a forward ray-tracing method, can be used to characterize reflected sunlight from a curtain wall. It was found that the simulation results derived using the different backward ray-tracing methods were significantly affected by the material specification and the luminance characterization of the sun, the ambient calculation, and the resolutions of the BSDF and sky patches. The results suggested that a higher value of the ambient sampling

rays and a higher density of the sky patches were needed for the two- and three-phase methods, especially for the three-phase method using the Klems BSDF for fenestration systems.

In addition, the forward ray-tracing method was recommended to effectively and efficiently identify the locations and directions receiving the serious reflected sunlight and the curtain wall patches introducing the reflected sunlight, with a backward ray-tracing method being followed to calculate the illuminance at the identified locations receiving the serious reflected sunlight.

In short, this study provides the daylight simulation community with a guidance to characterize reflected sunlight from a curtain wall, and future work is necessary to further investigate how different ambient parameters should be set for different simulation methods by comparing the simulation results with the field measurements.

Chapter 8

Conclusions

This dissertation included three studies, all of which were conducted to investigate how the daylight simulation can be used to characterize different daylight-related issues for buildings in Hong Kong.

It starts with the investigation of the difference between the predicted and actual daylight quantity and quality and the performance of a daylight-responsive dimming control system in a classroom. Specifically, the predictions were made based on the TMY data and the actual performance was characterized using a real weather data. The investigation was performed for four different fenestration systems (i.e., clear glazing, 0°, and ±45° venetian blinds) using three different simulation methods (i.e., the daylight coefficient, three-phase, and five-phase methods) throughout an entire year. The TMY data was found to result in lower average daylight illuminance than the actual weather data, with the largest difference of 30% for the space. Larger variations due to the weather conditions in the actual weather data suggested the necessity to perform the system calibration under the weather conditions that were similar to those at the selected calibration hours in the TMY data. Otherwise, the system would cause lower energy savings and a more frequent occurrence of the over-dimming conditions than the predictions, with the differences as high as 15% and 86% respectively. In addition, performing the system calibration under the weather conditions that had high S/E ratios may be helpful to reduce the occurrence of the over-dimming conditions. An additional study was carried out to investigate the effect of a prismatic film on the performance of the daylight-responsive dimming system in a south-facing classroom. The prismatic film attached to the clear glazings was found to cause the over-dimming

conditions to happen more frequently throughout the entire year, regardless of the daytime calibration hours.

Then, the characterizations of the daylight quantity and quality in residential buildings in Hong Kong were investigated through the subjective evaluations and the objective calculations. Specifically, the subjective evaluations were carried out by collecting the residents' long-term opinions about the luminous environment in their flats using a questionnaire survey; the objective calculations were performed in 400 flats using three different simulation methods (i.e., the daylight coefficient, three-phase, and five-phase methods) and the actual weather data. Both the subjective evaluations and the objective calculations focused on the same period of time. The results of the subjective evaluations suggested that the residents' satisfaction with daylighting was highly correlated to their satisfaction with the luminous environment. The results of two measures—the average $sDA_{300/50\%}$ and the maximum average daylight illuminance—were found to have strong correlations to the residents' satisfaction with daylighting. It was proposed to adopt the average $sDA_{300/50\%}$ above 66% and the maximum average daylight illuminance above 5624 lx as criteria to define the acceptable daylight quality for the residential buildings in Hong Kong.

Finally, the effects of different simulation methods on the characterization of reflected sunlight from curtain walls were investigated. The investigation was performed on a real building in Hong Kong using four backward ray-tracing methods (i.e., a single point-in-time, two-phase, three-phase, and sun coefficient methods) and a forward ray-tracing method throughout an entire year. Specifically, the backward ray-tracing methods were used to quantify the illuminance caused by the reflected sunlight at the areas around the building; the forward ray-tracing method was used to identify the locations introducing and receiving the reflected sunlight. It was found that the

illuminance caused by the reflected sunlight was significantly affected by the material specification and the luminance characterization of the sun, the ambient calculation, and the resolutions of the BSDF and sky patches. Such findings suggested that a higher value of the ambient sampling rays and a higher density of the sky patches were needed for the two- and three-phase methods. A combination of the forward and backward ray-tracing methods was recommended to identify the areas of the curtain wall introducing the reflected sunlight and the exact locations and directions receiving the reflected sunlight, and to quantify the illuminance caused by the reflected sunlight at these locations.

In short, the findings of these three studies provided useful guidance to the building designers to design the building elements for better daylight quality in Hong Kong. It also allows policy makers to better evaluate the performance of daylighting in buildings in Hong Kong. Future work is needed to further investigate how the different parameters affect the calculation results in comparison to field measurements.

Publication Arising from Dissertation

Journal Articles:

1. Wang, J., Wei, M., Chen, L. Does typical weather data allow accurate predictions of daylight quality and daylight-responsive control system performance. Energy and Buildings, 2019, 184, 72-87.

2. Wang, J., Wei, M., Ruan, X. Characterization of the acceptable daylight quality in typical residential buildings in Hong Kong. Building and Environment, 2020, 182, 107094.

3. Wang, J., Wei, M., Ruan, X. Comparison of daylight simulation methods for reflected sunlight from curtain walls. Building Simulation, 2020.

Conference Articles:

1. Wang, J., Wei, M. Difference between predicted and actual performance of a daylight-responsive dimming control system. Proceedings of the 4th Asia conference of international building performance simulation association, Hong Kong, 2018.

References

Abu Hanieh, A.M. Orientation of solar photovoltaic panels in desert regions. International Review of Automatic Control, 2008, 1 (3), 347-354.

Acosta, I, Campano, M.A., Molina, J. F. Window design in architecture: analysis of energy savings for lighting and visual comfort in residential spaces. Applied Energy, 2016, 168, 493-506.

ASHRAE. Weather year for energy calculations. American Society of Heating, Refrigerating and Air-conditioning Engineers (ASHRAE), Atlanta (GA), USA, 1985.

ASHRAE. WYEC2 weather year for energy calculations 2, toolkit and data. American Society of Heating, Refrigerating and Air-conditioning Engineers (ASHRAE), Atlanta (GA), USA, 1997a.

ASHRAE. International weather for energy calculations (IWEC weather files) user's manual. American Society of Heating, Refrigerating and Air-conditioning Engineers (ASHRAE), Atlanta (GA), USA, 2002.

Bartzokas, A., Kambezidis, H.D., Darula, S., Kittler, R. Comparison between winter and summer sky-luminance distribution in Central Europe and in the Eastern Mediterranean. Journal of Atmospheric and Solar-Terrestrial, 2005, 67 (7), 709-718.

Building and Construction Authority (BCA). Regulation on daylight reflectance of materials used on exterior of buildings. Singapore, 2016. Available from: https://www.corenet.gov.sg/media/2013555/circular-on-regulation-on-daylight-reflectance-of-materials-used-on-exterior-of-buildings.pdf (Accessed: Feb 26th 2019).

Billy, Y. Wikimedia commons, 2012. Available from: https://zh.wikipedia.org/wiki/%E5%AF%B6%E7%9B%88%E8%8A%B1%E5%9C%92 (Accessed: Mar 27th 2020).

Bourgeois, D., Reinhart, C.F., Ward, G. Standard daylight coefficient model for dynamic daylighting simulation. Building Research and Information, 2008, 36 (1), 68-82.

Building Energy Code (BEC). Code of practice for energy efficiency of building services installation, 2015 edition. Electrical and Mechanical Services Department (EMSD), Hong Kong, 2015.

Boerstra, A., Beuker, T., Loomans, M., Hensen, J. Impact of available and perceived control on comfort and health in European offices. Architectural Science Review, 2013, 56 (1), 30-41.

Bryan, H.J. A simplified procedure for calculating the effects of daylight from clear skies. Journal of the Illuminating Engineering Society, 1980, 9 (3), 142-151.

Brzezicki, M. The influence of reflected solar glare caused by the glass cladding of a building: application of caustic curve analysis. Computer-Aided Civil and Infrastructure Engineering, 2012, 27, 347-357.

Brembilla, E., Mardaljevic, J. Climate-based daylight modelling for compliance verification: benchmarking multiple state-of-the-art methods, Building and Environment, 2019, 158, 151-164.

Chan, A.L.S. Generation of typical meteorological years using genetic algorithm for different energy systems. Renewable Energy, 2016, 90, 1-13.

Chen, L. Sensor performance of advanced photocontrol systems. Master Thesis. The Pennsylvania State University, USA, 2013.

Chirarattananon, S., Chaiwiwatworakul, P. Distributions of sky luminance and radiance of North Bangkok under standard distributions. Renewable Energy, 2007, 32 (8), 1328-1345.

Choi, A.S., Song, K.D., Kim, Y.S. The characteristics of photosensors and electronic dimming ballasts in daylight responsive dimming systems. Building and Environment, 2005, 40 (1), 39-50.

Choi, A.S. and Mistrick, R.G. On the prediction of energy savings for a daylight dimming system. Journal of the Illuminating Engineering Society, 1997, 26 (2), 77-90.

Choi, A.S., Mistrick, R.G. Analysis of daylight responsive dimming system performance. Building and Environment, 1998, 34 (3), 231-243.

Choi, H.Y., Hong, S.K., Choi, A.S., Sung, M.K. Toward the accuracy of prediction for energy savings potential and system performance using the daylight responsive dimming system. Energy and Buildings, 2016, 133, 271-280.

Chow, S.K.H., Li, D.H.W., Lee, E.W.M., Lam, J.C. Analysis and prediction of daylighting and energy performance in atrium spaces using daylight-linked lighting controls. Applied Energy, 2013, 112, 1016-1024.

Chow, T.T., Li, C.Y., Lin, Z. Innovative solar windows for cooling-demand climate. Solar Energy Materials and Solar Cells, 2010, 94 (2), 212-220.

Christoffersen, J., Johnsen, K., Petersen, E., Valbjorn, O., Hygge, S. Windows and daylight-a post-occupancy evaluation of Danish offices. Proceedings of lighting 2000 ILE/CIBSE joint conference, University of York, UK, 2000.

Chung, T.M., Burnett, J., Wu, M.K.T. Office lighting retrofit using dimmable electronic ballasts and occupancy controls. HKIE Transactions, 2001, 8 (3) 8-15.

Chung, T.M. Daylighting in Hong Kong: potential and problems. Lighting Research and Technology, 2003, 35 (1), 39-41.

Crawley, D.B. Which weather data should you use for energy simulations of commercial buildings?. ASHRAE Transactions, 1998, 104 (2), 498-515.

Crow, L.W. Summary description of typical year weather data, Chicago midway airport. ASHRAE research project RP-100. American Society of Heating, Refrigerating and Air conditioning Engineers (ASHRAE), 1970.

Crow, L.W. Development of hourly data for weather year for energy calculations (WYEC), including solar data, at 29 stations throughout the United States and 5 stations in Canada. ASHRAE research project 364, Final Report. American Society of Heating, Refrigerating and Air-conditioning Engineers (ASHRAE), 1983.

Danks, R. Applications of large scales solar modelling in the built environment. Proceedings of the eSim 2014 conference on building simulation, Ottawa (ON), CA, 2014.

Danks, R., Good, J. Urban solar reflection identification, simulation, analysis and mitigation: learning from case studies. Proceedings of the eSim 2016 building performance simulation conference. McMaster University, Hamilton (ON), CA, 2016.

Danks, R., Good, J., Sinclair, R. Assessing reflected sunlight from building facades: A literature review and proposed criteria. Building and Environment, 2016, 103, 193-202.

Darula, S., Kittler, R. CIE general sky standard defining luminance distributions. Proceedings of the eSim 2002 building energy simulation conference, Montreal (QC), CA, 2002.

DiLaura, D.L. and Houser, G.A. On calculating the effects of daylighting in interior spaces. Journal of the Illuminating Engineering Society, 1978, 8 (1), 2-14.

DiLaura, D.L., Houser, K.W., Mistrick, R.G., Steffy, G.R. The Lighting Handbook, 10th edition. The Illuminating Engineering Society of North America, New York (NY), USA, 2011.

Doulos, L., Tsangrassoulis, A., Topalis, F.V. Multi-criteria decision analysis to select the optimum position and proper field of view of a photosensor. Energy Conversion and Management, 2014, 86, 1069-1077.

EC&M. Field study sheds light on photocontrol system performance, 2007. Available from: https://www.ecmweb.com/content/field-study-sheds-light-photocontrol-system-performance (Accessed: Mar 12nd 2020).

Electrical and Mechanical Services Department (EMSD). Hong Kong energy end-use data 2019. Available from: https://www.emsd.gov.hk/filemanager/en/content_762/HKEEUD2019.pdf (Accessed: Mar 12nd 2020).

Enarun, D., Littlefair, P. Luminance models for overcast skies: assessment using measured data. Lighting Research and Technology, 1995, 27 (1), 53-58.

Finkelstein, J.M. and Schafer, R.E. Improved goodness-of-fit tests, Biometrika, 1971, 58 (3), 641-645.

Garfield, L. The 'death ray hotel' burning Las Vegas visitors came up with a simple fix. Business Insider, 2016. Available from: https://www.businessinsider.com/the-vdara-death-ray-hotel-is-still-burning-people-in-las-vegas-2016-6 (Accessed: Mar 13th 2020).

Geisler-Moroder, D., Lee, E.S., Ward, G.J. Validation of the five-phase method for simulating complex fenestration systems with Radiance against field measurements. Proceedings of the 15th international conference of the international building performance simulation association, California, USA, 2017.

Gibson, T. and Krarti, M. Comparative analysis of prediction accuracy from daylighting simulation tools. The Journal of the Illuminating Engineering Society, 2015, 11 (2), 49-60.

Gillette, G., Pierpoint, W., Treado, S. A general daylight illuminance model for daylight availability. The Journal of the Illuminating Engineering Society, 1984, 13 (4), 330-340.

Gobakis, K., Kolokotsa, D., Maravelaki-Kalaitzaki, N., Perdikatsis, V., Santamouris, M. Development and analysis of advanced inorganic coatings for buildings and urban structures. Energy and Buildings, 2015, 89, 196-205.

Grobe, L.O., Noback, A., Wittkopf, S., Kazanasmaz, T. Comparison of measured and computed BSDF of a daylight redirecting component. Proceedings of International Conference CISBAT, Lausanne, Switzerland, 2015.

Hall, I.J., Prairie, R.R., Anderson, H.E., Boes, E.C. Generation of a typical meteorological year. Proceedings of the annual meeting of the American section of the international solar energy society, San Diego (CA), USA, 1978.

Hensen, J.L.M. and Lamberts, R. Building performance simulation for design and operation, 2nd edition. Routledge, London, UK, 2019.

Heschong Mahone Group. Daylight metrics-PIER daylighting plus research program, Final Report to the California Energy Commission, CA, USA, 2012.

Herrera, M., Natarajan, S., Coley, D.A., Kershaw, T., Ramallo-Gonzalez, A.P., Eames, M., Fosas, D., Wood, M. A review of current and future weather data for building simulation. Building Services Engineering Research and Technology, 2017, 38 (5), 602-627.

Heydarian, A., Pantazis, E., Carneiro, J.P., Gerber, D., Becerik-Gerber, B. Lights, buildings, action: Impacts of default lighting setting on occupant behaviour. Journal of Environmental Psychology, 2016, 48, 212-223.

Ichinose, M., Inoue, T., Nagahama, T. Effect of retro-reflecting transparent window on anthropogenic urban heat balance. Energy and Buildings, 2017, 157, 157-165.

IES LM-83-12. Approved method: IES spatial daylight autonomy (sDA) and annual sunlight exposure (ASE). Illuminating Engineering Society, New York (NY), USA, 2013.

ISO 15469:1997. CIE S003 Spatial distribution of daylight-CIE standard overcast sky and clear sky. Commission Internationale de l'Eclairage (CIE), 1997.

ISO 15469:2004. CIE S003 Spatial distribution of daylight-CIE standard overcast sky and clear sky, 2nd edition. Commission Internationale de l'Eclairage (CIE), 2004.

Igawa, N., Matsuzawa, T., Nakamura, H., Koga, Y., Goto, K., Kojo, S. Sky luminance distribution between two CIE standard skies. Proceedings of Lux Pacifica, Nagoya, Japan, 1997.

Inanici, M., Hashemloo, A. An investigation of the daylighting simulation techniques and sky modeling practices for occupant centric evaluations. Building and Environment, 2017, 113, 220-231.

Inanici, M., Liu, Y. Robust sky modelling practices in daylighting simulations. Proceedings of the 32nd international conference on passive and low energy architecture, Los Angeles (CA), USA, 2016.

Iversen, A., Svendsen, S., Nielsen, T. R. The effects of different weather data sets and their resolution on climate-based daylight modelling. Lighting Research and Technology, 2013, 45, 305-316.

Jennings, J.D, Rubinstein, F.M., DiBartolomeo, D., Blanc, S.L. Comparison of control options in private offices in an advanced lighting controls testbed. Journal of the Illuminating Engineering Society, 2000, 29 (2), 39-60.

Kennelly, P.J., Stewart, A.J. General sky models for illuminating terrains. International Journal of Geographical Information Science, 2014, 28 (2), 383-406.

Keyvanfar, A., Shafaghat, A., Abd Majid, M.Z., Lamit, H.B., Hussin, M.W., Binti Ali, K.N., Saad, A.D. User satisfaction adaptive behaviours for assessing energy efficient building indoor cooling and lighting environment. Renewable and Sustainable Energy Reviews, 2014, 39, 277-295.

Kimball, H.H. and Hand, I.F. Daylight illumination on horizontal, vertical, and sloping surfaces. Monthly Weather Review, 1922, 50 (12), 615-628.

Kittler, R. Standardisation of the outdoor conditions for the calculation of the daylight factor with clear skies. Proceedings of conference on sunlight in buildings, Bouwcentrum, Rotterdam, Netherlands, 273-286, 1967.

Kittler, R., Perez, R., Darula S. US-SK 92 052 Final Report: A set of standard skies characterizing daylight conditions for computer and energy conscious design. Polygrafia SAV, Bratislava, Slovakia, 1998.

Kim, S.Y., Kim, J.J. The impact of daylight fluctuation on a daylight dimming control system in a small office. Energy and Buildings, 2007, 39 (8), 935-944.

Kim, S.Y., Mistrick, R.G. Recommended daylight conditions for photosensor system calibration in a small office. Journal of the Illuminating Engineering Society, 2001, 30 (2), 176-188.

Kim, S.H., Kim, I.T., Choi, A.S., Sung, M.K. Evaluation of optimized PV power generation and electrical lighting energy savings from the PV blind-integrated daylight responsive dimming system using LED lighting. Solar Energy, 2014, 107, 746-757.

Klems, J.H. A new method for predicting the solar heat gain of complex fenestration systems: I. Overview and derivation of the matrix layer calculation. ASHRAE Transactions, 1994a, 100 (1), 1065-1072.

Klems, J.H. A new method for predicting the solar heat gain of complex fenestration systems: II. Detailed description of the matrix layer calculation. ASHRAE Transactions, 1994b, 100 (1), 1073-1086.

Klepeis, N.E., Nelson, W.C., Ott, W.R., Robinson, J.P., Tsang, A.M., Switzer, P., Behar, J.V., Hern, S.C., Engelmann, W.H. The national human activity pattern survey (NHAPS): a resource for assessing exposure to environmental pollutants. Journal of Exposure Analysis and Environmental Epidemiology, 2001, 11 (3), 231-252.

Krarti, M., Erickson, P.M., Hillman, T.C. A simplified method to estimate energy savings of artificial lighting use from daylighting. Building and Environment, 2005, 40 (6), 747-754.

Lau, K.L., Ng, E., He, Z.J. Residents' preference of solar access in high-density sub-tropical cities. Solar Energy, 2010, 85 (9), 1878-1890.

Larson, G.W., Shakespeare, R., Mardaljevic, J., Ehrlich, C., Phillips, E., Apian-Bennewitz, P. Rendering with Radiance: The art and science of lighting visualization, Morgan Kaufmann, San Francisco, USA, 1998.

Lee, E.S., Geisler-Moroder, D., Ward, G. Modelling the direct sun component in buildings using matrix algebraic approaches: Methods and validation. Solar Energy, 2018, 160, 380-395.

Li, D.H.W., Cheung, K.L., Wong, S.L., Lam, T.N.T. An analysis of energy-efficient light fittings and lighting controls. Applied Energy, 2010, 87 (2), 558-567.

Li, D.H.W., Lam, J.C. An analysis of lighting energy savings and switching frequency for a daylit corridor under various indoor design illuminance levels. Applied Energy, 2003, 76, 363-378.

Li, D.H.W., Lau, C.C.S., Lam, J.C. A study of 15 sky luminance patterns against Hong Kong data. Architectural Science Review, 2003, 46 (1), 61-68.

Li, D.H.W., Lau, C.C.S., Lam, J.C. Overcast sky conditions and luminance distribution in Hong Kong. Building and Environment, 2004, 39 (1), 101-108.

Li, D.H.W., Wong, S.L., Tsang, C.L. Cheung, G.H.W. A study of the daylighting performance and energy use in heavily obstructed residential buildings via computer simulation techniques. Energy and Buildings, 2006, 38 (11), 1343-1348.

Li, D.H.W., Lam, T.N.T., Wong, S.L. Lighting and energy performance for an office using high frequency dimming controls. Energy Conversion and Management, 2006, 47 (9-10), 1133-1145.

Li, D.H.W., Tsang, E.K.W. An analysis of measured and simulated daylight illuminance and lighting savings in a daylit corridor. Building and Environment, 2005, 40 (7), 973-982.

Littlefair, P.J. and Motin, A. Lighting controls in areas with innovative daylighting systems: a study of sensor type. Lighting Research and Technology, 2001, 33 (1), 59-73.

Lynes, J.A. A sequence for daylighting design. Lighting Research and Technology, 1979, 11 (2), 102-106.

Mardaljevic, J. Validation of a lighting simulation program under real sky conditions. Lighting Research and Technology, 1995, 27 (4), 181-188.

Mardaljevic, J. Validation of a lighting simulation program: a study using measured sky brightness distributions. Proceedings of the 8th European lighting conference, Amsterdam, Netherland, 1997.

Mardaljevic, J. Daylight simulation: validation, sky models and daylight coefficients. Ph.D thesis, De Montfort University, Leicester, UK, 2000.

Mardaljevic, J. Simulation of annual daylighting profiles for internal illuminance. Lighting Research and Technology, 2000, 32 (3), 111-118.

Mardaljevic, J. Verification of program accuracy for illuminance modelling: assumptions, methodology and an examination of conflicting findings. Lighting Research and Technology, 2004, 36 (3), 217-239.

Mardaljevic, J. The BRE-IDMP dataset: a new benchmark for the validation of illuminance prediction techniques. Lighting Research and Technology, 2001, 33 (2), 117-134.

Mardaljevic, J. Examples of climate-based daylight modelling. Proceedings of CIBSE national conference 2006: Engineering and Future, London, UK, 2006.

Mardaljevic, J. Sky model blends for predicting internal illuminance: a comparison founded on the BRE-IDMP dataset. Journal of Building Performance Simulation, 2008, 1 (3), 163-173.

Mardaljevic, J. Climate-based daylight modelling and its discontents. CIBSE Technical Symposium, London, UK, 2015.

Marion, W. and Urban, K. Technical report: user's manual for TMY2s derived from the 1961-1990 national solar radiation data base. National Renewable Energy Laboratory, Golden (CO), USA, 1995.

Martirano, L. A smart lighting control to save energy. Proceedings of the 6th IEEE international conference on intelligent data acquisition and advanced computing systems, Prague, Czech Republic, 2011.

Masters, G.N. A comparison of latent trait and latent class analyses of Likert-type data. Psychometrika, 1985, 50 (1), 69-82.

Maxwell, E.L, Marion, W., Myers, D., Rymes, M., Wilcox, S. National solar radiation data base, vol.2 – final technical report (1961-1990). National Renewable Energy Laboratory, Golden (CO), USA, 1990.

McNeil, A. The three-phase method for simulating complex fenestration with Radiance. Lawrence Berkeley National Laboratory (LBNL), Berkeley (CA), USA, 2013.

McNeil, A. The five-phase method for simulating complex fenestration with Radiance. Lawrence Berkeley National Laboratory (LBNL), Berkeley (CA), USA, 2013.

McNeil, A., Jonsson, C.J., Appelfeld, D., Ward, G., Lee, E.S. A validation of a ray-tracing tool used to generate bi-directional scattering distribution functions for complex fenestration systems. Solar Energy, 2013, 98, 404-414.

McNeil, A., Lee, E.S. A validation of the radiance three-phase simulation method for modelling annual daylight performance of optically complex fenestration systems. Journal of Building Performance Simulation, 2013, 6 (1), 24-37.

McNeil, A. genBSDF tutorial. Lawrence Berkeley National Laboratory (LBNL), 2015.

Mistrick, R.G., Chen, C.H., Bierman, A., Felts, D. A comparison of photosensor-controlled electronic dimming systems in a small office. Journal of the Illuminating Engineering Society, 2000, 29 (1), 66-80.

Mistrick, R.G. and Thongtipaya, J. Analysis of daylight photocell placement and view in a small office. Journal of the Illuminating Engineering Society, 1997, 26 (2), 150-160.

Mistrick, R.G. and Sarkar, A. A study of daylight responsive photosensor control in five daylighted classrooms. Journal of the Illuminating Engineering Society, 2005, 1, 51-74.

Mistrick, R.G., Casay, C., Chen, L. Subramaniam, S. Computer modelling of daylight-integrated photocontrol of electric lighting systems. Buildings, 2015, 5 (2), 449-466.

Mitchell, R., Kohler, C., Klems, J.H., Rubin, M.D., Arasteh, D.K., Huizenga, C., Yu, T.F., Curcjia, D.C. WINDOW 6.2/THERM 6.2 Research version user manual, Report, Lawrence Berkeley National Laboratory (LBNL), 2008.

Modest, M.F. A general model for the calculation of daylighting in interior spaces. Energy and Buildings, 1982, 5 (1), 69-79.

Moon, P., Spencer, D.E. Illumination from a non-uniform sky. Illuminating Engineering, 1942, 37 (10), 707-726.

Nabil, A., Mardaljevic, J. Useful daylight illuminances: a replacement for daylight factors. Energy and Buildings, 2006, 38 (7), 905-913.

Nakamura, H., Oki, M., Hayashi, Y. Luminance distribution of intermediate sky. Journal of Light and Visual Environment, 1985, 9 (1), 6-13.

Navvab, M., Perez, R., Hosobuchi, H. The estimated frequencies of CIE luminance distributions and the impact of circumsolar region using TMY weather files. Proceedings of the 39th national passive solar conference and the 2nd meeting of young and emerging professionals in renewable energy, San Francisco (CA), USA, 2014.

NCDC. Tape reference manual-Test Reference Year (TRY). National Climatic Data Centre, Asheville (NC), USA, 1976.

Ng, E. A study on the accuracy of daylighting simulation of heavily obstructed buildings in Hong Kong. Proceedings of the 7th international IBPSA conference, Rio de Janeiro, Brazil, 2001.

Ng, E. Studies on daylight design and regulation of high-density residential housing in Hong Kong. Lighting Research and Technology, 2003, 35 (2), 127-139.

National Renewable Energy Laboratory (NREL). Typical Meteorological Year 3 (TMY3). EnergyPlus. Available from: https://energyplus.net/weather. (Accessed: Jul 20th 2020).

Pandharipande, A., Caicedo, D. Daylight integrated illumination control of LED systems based on enhanced presence sensing. Energy and Buildings, 2011, 43 (4), 944-950.

Park, B.C., Choi, A.S., Jeong, J.W., Lee, E.S. A preliminary study on the performance of daylight responsive dimming systems with improved closed-loop

control algorithm. Journal of the Illuminating Engineering Society, 2011, 8 (1), 41-59.

Perez, R., Seals, R., Michalsky, J. All-weather model for sky luminance distribution-preliminary configuration and validation. Solar Energy, 1993, 50 (3), 235-245.

Perez, R., Ineichen, P., Seals, R., Michalsky, J., Stewart, R. Modelling daylight availability and irradiance components from direct and global irradiance. Solar Energy, 1990, 44 (5), 271-289.

Ranasinghe, S. and Mistrick, R.G. A study of photosensor configuration and performance in a daylighted classroom space. Journal of the Illuminating Engineering Society, 2003, 32 (2), 3-20.

Reinhart, C.F., Herkel, S. The simulation of annual daylight illuminance distributions-a state-of-the-art comparison of six Radiance-based methods. Energy and Buildings, 2000, 32 (2), 167-187.

Reinhart, C.F., Walkenhorst, O. Validation of dynamic RADIANCE-based daylight simulations for a full-scale test office with external blinds. Energy and Buildings, 2001, 33 (7), 683-697.

Reinhart, C.F., Andersen, M. Development and validation of a Radiance model for a translucent panel. Energy and Buildings, 2006, 38 (7), 890-904.

Reinhart, C.F., Voss, K. Monitoring manual control of electric lighting and blinds. Lighting Research and Technology, 2003, 35 (3), 243-260.

Reinhart, C.F., Weissman, D.A. The daylit area-correlating architectural student assessments with current and emerging daylight availability metrics, Building and Environment, 2012, 50, 155-164.

Roisin, B., Bodart, M., Deneyer, A., D'Herdt, P. Lighting energy savings in offices using different control systems and their real consumption. Energy and Buildings, 2008, 40 (4), 514-523.

Rogers, Z. Daylighting metric development using daylight autonomy calculations in the sensor placement optimization tool. Architectural Energy Corporation, Boulder (CO), USA, 2006.

Rubinstein, F., Ward, G.J., Verderber, R. Improving the performance of photo-electrically controlled lighting systems. Journal of the Illuminating Engineering Society, 1989, 18 (1) 70-94.

Samant, S. A critical review of articles published on atrium geometry and surface reflectances on daylighting in an atrium and its adjoining spaces. Architectural Science Review, 2010, 53 (2), 145-156.

Santamouris, M., Synnefa, A., Karlessi, T. Using advanced cool materials in the urban built environment to mitigate heat islands and improve thermal comfort conditions. Solar Energy, 2011, 85 (12), 3085-3102.

Saxena, M., Ward, G.J., Perry, T., Heschong, L., Higa, R. Dynamic Radiance–predicting annual daylighting with variable fenestration optics using BSDFs. Proceedings of the 4th national conference of international building performance simulation association, New York (NY), USA, 2010.

Schregle, R., Renken, C., Wittkopf, S. Spatio-temporal visualization of reflections from buildings integrated photovoltaic. Buildings, 2018, 8 (101), 1-28.

Schweiker, M., Brasche, S., Bischof, W., Hawighorst, M., Voss, K., Wagner, A. Development and validation of a methodology to challenge the adaptive comfort model. Building and Environment, 2012, 49, 336-347.

Shih, N.J., Huang, Y.S. An analysis and simulation of curtain wall reflection glare. Building and Environment, 2001, 36 (5), 619-626.

Subramaniam, S., Chen, L., Mistrick, R.G. Annual performance metrics for photosensor-controlled daylight-responsive lighting control system. Proceedings of the 2013 IES annual conference, Huntington Beach (CA), USA, 2013.

Subramaniam, S. Daylighting simulations with radiance using matrix-based methods. Lawrence Berkeley National Laboratory (LBNL), Berkeley (CA), USA, 2017.

Sun, Y.Y., Liang, R.Q., Wu, Y.P., Wilson, R., Rutherford, P. Development of a comprehensive method to analyse glazing systems with parallel slat transparent insulation material (PS-TIM). Applied Energy, 2017, 25, 951-963.

Suk, J.Y., Schiler, M., Kensek, K. Reflectivity and specularity of building envelopes: how materiality in architecture affects human visual comfort. Architectural Science Review, 2017, 60 (4), 256-265.

Tavakol, M., Dennick, R. Making sense of Cronbach's alpha. International Journal of Medical Education, 2011, 2, 53-55.

Tregenza, P.R., Waters, I.W. Daylight coefficients. Lighting Research and Technology, 1983, 15 (2), 65-71.

Tregenza, P.R. Subdivision of the sky hemisphere for luminance measurements. Lighting Research and Technology, 1987, 19 (1), 13-14.

Tregenza, P.R., Perez, R., Michalsky, J., Seals, R., Molineaux, B., Ineichen, P. Guide to recommended practice of daylight measurement. Commission Internationale de l'Eclairage (CIE), Vienna, 1994.

Tregenza, P.R., Mardaljevic, J. Daylighting buildings: standards and the needs of the designer. Lighting Research and Technology, 2018, 50 (1), 63-79.

Tsangrassoulis. A., Bourdakis, V. Comparison of radiosity and ray-tracing techniques with a practical design procedure for the prediction of daylight levels in atria. Renewable Energy, 2003, 28 (13), 2157-2162.

USGBC. LEED v4 for building design and construction. US Green Building Council, Washington DC, USA, 2014.

Walkenhorst, O., Luther, J., Reinhart, C.F., Timmer, J. Dynamic annual daylight simulations based on one-hour and one-minute means of irradiance data. Solar Energy, 2002, 72 (5), 385-395.

Walker, T. Walkie Talkie architect 'didn't realise it was going to be so hot'. The Telegraph, 2013. Available from: https://www.telegraph.co.uk/culture/culturenews/10292147/Walkie-Talkie-architect-blames-consultants-for-buildings-failures.html (Accessed: Mar 13th 2020).

Walker, S. Complex facades in sunny climates, microclimates, reflection caustics, Radiance Workshop, 2012, https://www.radiance-online.org/community/workshops/2012-

copenhagen/Day3/Walker/Steve%20Walker%20-%20Radiance%20workshop%202012%20-%20Greg%20Ward.pdf (Accessed: Mar 20th 2020).

Walsh, J.W.T. The early years of illuminating engineering in Great Britain. Transactions of the Illuminating Engineering Society, 1951, 16 (3), 49-60.

Ward, G.J. The Radiance lighting simulation and rendering system. Proceedings of the 21st annual conference in computer graphics and interactive techniques, Orlando (FL), USA, 1994.

Ward, G.J., Mistrick, R.G., Lee, E.S., McNeil, A., Jonsson, J. Simulating the daylight performance of complex fenestration systems using bidirectional scattering distribution functions within Radiance. Journal of the Illuminating Engineering Society, 2011, 7(4), 241-261.

Ward, G.J., Rubinstein, F.M. A new technique for computer simulation of illuminated spaces. Journal of the Illuminating Engineering Society, 1988, 17 (1), 80-91.

Ward, G.J. What's new in Radiance for 2017. The 16th international Radiance workshop, Portland (OR), USA, 2017.

Wilcox, S. and Marion, W., Technical report: user's manual for TMY3 data sets. National Renewable Energy Laboratory (NREL), 2008.

Wittkopf, S.K., Soon, L.K. Analysing sky luminance scans and predicting frequent sky patterns in Singapore. Lighting Research and Technology, 2007, 39 (1), 31-51.

Xue, P., Mak, C.M., Cheung, H.D. The effects of daylighting and human behaviour on luminous comfort in residential buildings: a questionnaire survey. Building and Environment, 2014, 81, 51-59.

Xue, P, Mak, C.M., Cheung, H.D. New static lightshelf system design of clerestory windows for Hong Kong. Building and Environment, 2014, 72, 368-376.

Xue, P., Mak, C.M., Cheung, H.D., Chao, J.Y. Post-occupancy evaluation of sunshades and balconies' effects on luminous comfort through a questionnaire survey. Journal of Building Services Engineering Research and Technology, 2015, 37 (1), 51-65.

Xue, P., Mak, C.M., Huang, Y. Quantification of luminous comfort with dynamic daylight metrics in residential buildings. Energy and Buildings, 2016, 117, 99-108.

Yang, X.M., Grobe, L.O., Wittkopf, S. Simulation of reflected daylight from building envelopes. Proceeding of the 13th conference of international building performance simulation association, Chambery, France, 2013.

Yildirim, K., Akalin-Baskaya, A., Celebi, M. The effects of window proximity, partition height, and gender on perceptions of open-plan offices. Journal of Environmental Psychology, 2007, 27 (2), 154-165.

Yuan, J., Farnham, C., Emura, K. Development of a retro-reflective material as building coating and evaluation on albedo of urban canyons and building heat loads. Energy and Buildings, 2015, 103, 107-117.